VILNIUS UNIVERSITY
INSTITUTE OF CHEMISTRY OF CENTER FOR PHYSICAL SCIENCES AND TECHNOLOGY

Justė Trinkūnaitė- Felsen

INVESTIGATION OF CALCIUM HYDROXYAPATITE SYNTHESIZED USING NATURAL PRECURSORS

Doctoral dissertation
Physical sciences, chemistry (03 P)

Vilnius, 2014

Disssertation was carried out from 2010 to 2014 at Vilnius University.

Scientific supervisors:

Assoc. Prof. Dr. Artūras Žalga (Vilnius University, Physical Sciences, Chemistry, 03 P) (2010/10/01- 2013/02/24).

Prof. Dr. Habil. Aivaras Kareiva (Vilnius University, Physical Sciences, Chemistry, 03 P) (2013/02/25- 2015/05/04).

Scientific advisor:

Prof. Dr. Habil. Aivaras Kareiva (Vilnius University, Physical Sciences, Chemistry, 03 P) (2010/10/01- 2013/02/24).

Contents

LIST OF ABBREVIATIONS

BCP- biphasic calcium phosphate

BSM- bone substitute materials

CaP- calcium phosphates

CHAp- calcium hydroxyapatite ($Ca_{10}(PO_4)_6(OH)_2$)

CO_3-CHAp- carbonate hydroxyapatite

CTAB- cetyltrimethylamonium bromide

DCP- dairy calcium powder

DCPA- dicalcium phosphate anhydrous

DCPD- dicalcium phosphate dehydrate

DE- Germany

DK- Denmark

DSC- differential scanning calorimetry

EDTA- ethylenediaminetetraacetic acid

EDX- energy dispersive X-ray spectrometry

EE- Estonia

Fe(x)/CHAp- iron substituted calcium hydroxyapatite, where x is iron molar concentration (%)

FIN- Finland

FTIR- Fourier transform infrared spectroscopy

HIV- human immunodeficiency virus

ICP-OES- inductively coupled plasma optical emission spectrometry

ICSD- inorganic crystal structure database

IR- infrared spectroscopy

LT- Lithuania

LV- Latvia

MCH-Cal- microcrystalline hydroxyapatite calcium

MNPs- magnetic nanoparticles

MRI- magnetic resonance imaging

NCPs- noncollagenous proteins

NIH- national institutes of health

NO- Norway

OCP- octacalcium phosphate

OSP- oyster shell powder

PAM- polyacrylamide

PAMAM- poly(amido-amine)

PEG- polyethylene glycol

PL- Poland

PVA- polyvinyl alcohol

RDA- recommended dietary allowance

SAXS- small-angle X-ray scattering

SE- Sweden

SEM- scanning electron microscopy

TCP- tricalcium phosphate

β-TCP- β-tricalcium phosphate

α- TCP- α-tricalcium phosphate

TEM- transmission electron microscopy

TG- thermogravimetric analysis

TG/DSC- thermogravimetric and differential scanning calorimetric analysis

TG/DTG-DSC- thermogravimetric (TG), derivative thermogravimetric (DTG) and differential scanning calorimetric (DSC) analysis

XRD- X-ray diffraction

1. INTRODUCTION

Health benefits of calcium compounds are widely acknowledged [1-6]. An adequate intake of both calcium and vitamin D is important for bone health and it is recognized as an important component of any osteoporosis prescription-drug regimen. The risk of one or another health condition arises when people do not consume the Recommend Dietary Allowance of calcium through their daily diet and recent studies revealed that calcium intake is inadequate in both children and elderly people [7-9] . Calcium supplements and calcium-fortified foods are additional sources of calcium for people unable to consume sufficient dietary calcium or unable to absorb calcium from foods [10, 11]. To date calcium supplements are available in a variety of different calcium salts. Apparently, our society is becoming increasingly aware of the importance of dietary calcium due to the vital role of this element in human body.

Calcium is a major structural element in bones and teeth. The mineral component of bone consists mainly of calcium hydroxyapatite ($Ca_{10}(PO_4)_6(OH)_2$; CHAp). As seen, CHAp is composed primarily of calcium and phosphorous with hydroxide ions. Synthetic CHAp and other related calcium phosphate minerals have been utilized extensively as implant materials for many years due to its excellent biocompatibility and bone bonding ability and also due to its structural and compositional similarity to that of the mineral phase of hard tissue in human bones.

Bone is a dynamic system consisting of living cells embedded in a mineralized matrix, with constant desorption and deposition of calcium into new bones [12]. Balances between bones desorption and deposition changes with age. Bone formation exceeds desorption in periods of growth in children and adolescents, whereas in early and middle adulthood both processes are relatively equal. In aging adults, particularly among postmenopausal women, bone breakdown exceeds formation, resulting in bone loss that increases the risk of osteoporosis over time [13-15]. The main source of dietary calcium in a human diet is milk

and dairy products, mainly cheese in adults [16]. Promotion of consumption of dairy products does not necessarily increase total calcium intake [17].

Obviously, to maintain proper composition of mineral in the bone, there must be adequate absorption and delivery of all bone minerals to bone sites in the human body. The scientific literature is lacking substantial information concerning maintenance of appropriate dietary mineral balances, particularly in relation to bone health. Some people have health issues that impair the absorption of calcium and may lead to poor calcium status [16]. Such factors include hypochlorhydria, a condition characterized by insufficient secretion of stomach acid. This condition affects many people and is especially common in the elderly. Due to the reasons (insufficient bioavailability of calcium from food, medical conditions, poor diet, etc.) demand of calcium fortified foods or calcium supplements arises in order to prevent calcium deficiency related diseases.

It is well known that bioavailability of different compounds depends very much on their concentration, chemical and phase composition, microstructure and morphology, crystal structure and other physical properties [18-22]. When supplementing daily diet with calcium compounds is not sufficient to solve bone health issues, the need for surgical interventions arises. An aging population, coupled with trauma injuries and bone diseases, are factors demanding for improved well- studied and analyzed therapeutics [23]. Moreover, a global demographic shift in population to the elderly side has intensified the need to provide not just replacement therapies but improved long-term cost-effective regeneration solutions [24].

There are currently a wide variety of conventional and up- to- date bone repair treatments available, each with inextricable advantages and disadvantages [25]. However, despite the vast benefits brought by nowadays technologies and methods, the need for bone repair and regeneration with minimal morbidity and mortality remains unexploited [26]. Calcium hydroxyapatite is one of the most frequently used bioceramics for bone and dental tissues reconstructions. CHAp is highly biocompatible and bioactive material. Its properties like osteoconductivity, nontoxicity, noninflammatory behaviour, and non-immunogenicity makes it well

applicable as bone implant [27]. In general, calcium phosphate (CaP) ceramics, including CHAp, β-tricalcium phosphate (β-TCP) and biphasic calcium phosphate (BCP), have been widely used as grafts for bone repair, augmentation or substitution [28].

In literature, several methods to prepare CHAp have been reported, including solid state reactions, plasma techniques, crystal growth under hydrothermal conditions, layer hydrolysis of other calcium phosphate salts, and sol-gel processing. Essentially, the synthesis of CHAp from supersaturated aqueous solutions is advantageous due to low cost and simplicity, but most of the synthetic procedures followed until now led to the formation of non-stoichiometric products. While synthetic materials have been widely used in the biomedical field with great success, natural structural materials are now providing an abundant source of novel biomedical applications [29]. During the last decade, an increased understanding of bio-mineralization has initiated improvements in biomimetic synthesis methods and production of new generation of biomaterials. The use of natural biogenic structures and materials such as corals, seashells, bones for medical purposes has been motivated by limitations in generating synthetic materials with the requisite structure and mechanical integrity [28]. Consequently, due to the ever-growing need to develop pure, clean, non-toxic and environmentally friendly techniques, CHAp powders have been also produced using biogenic materials.

In the first part of doctoral thesis chemical and phase composition, as well as morphology of naturally derived calcium compounds (from dairy, corals, sea-shells and bovine bones) used in food industry were analysed and characterized. In this research a novel approach towards dairy derived calcium by characterizing it as a possible source of CaPs for biomedical applications was proposed as well as a method of synthesis of CHAp powders using sea shells, namely *Macoma balthica (L.)*, via sol-gel route was developed.

CaP ceramics derived from coral and sea urchin spines, are also gaining more acceptance for orthopedic use in non-load bearing applications [30]. The wide availability and the low cost of sea shells, along with their biological–natural

origin are highly attractive properties in the preparation of CHAp powders for biomedical application. The mollusk shells are micro-laminate composites of mineral and biopolymers, typically consisting of 95–99% $CaCO_3$ by weight, 1–5% organic macromolecules and other minerals in trace quantities [31].

To the best of our knowledge, there is no study aimed at producing CHAp powders from raw materials derived of natural–biological sea shells using an environmentally friendly water-based sol-gel reaction. There are no scientific data suggesting of using dairy powder as a source of calcium hydroxyapatite for biomedical applications as well. Moreover, iron (Fe) substituted sea shell derived CHAp for the first time was synthesized and characterized in this study. The above mentioned information highlights the novelty and authenticity of this PhD research study.

Thus, the aim of this work was to emphasize the importance of calcium phosphates, in particular hydroxyapatite, in human nutrition as well as in bone graft applications. In the subsequent part of the study, characterized calcium compounds with natural origin were used for the synthesis of calcium hydroxyapatite. This research was undertaken in order to investigate the possibilities of transforming a widely available sea-shell as well as dairy powder resource into a viable human bone replacement biomaterial.

The main aims of the dissertation:

1. Characterization of calcium compounds derived from natural sources used for development innovative functional foods as well as food supplements. Suggest their bioavailability depending on the characterized physical and chemical properties.
2. Development of synthesis method for the preparation of crystalline calcium phosphate (CaP) ceramics from dairy powders.
3. Development of an aqueous sol-gel synthesis route for production of pure and highly crystalline calcium hydroxyapatite ($Ca_{10}(PO_4)_6(OH)_{2;}$ CHAp) using sea-shells as a precursor of calcium.

4. Investigation the influence of geographical location of sea-shells collected from different coast of the Baltic Sea on the chemical and phase composition and morphological properties of resulting CHAp product.
5. Synthesis and investigation of iron substitution effects on the formation of iron-substituted calcium hydroxyapatite $(Ca_{10-x}Fe_x)(PO_4)_6(OH)_2$.

Statements for defence

1. Dairy derived calcium phosphates are the optimal compounds to be used for functional food/ food supplement applications.
2. It is possible to produce crystalline calcium phosphates (calcium hydroxyapatite and whitlockite mixture) for biomedical applications when heating dairy powder at elevated temperatures.
3. Sea-shell derived calcium hydroxyapatite could be produced using environmentally friendly and sustainable aqueous sol-gel synthesis route.
4. The geographical origin of sea-shells collected at the coast of the Baltic Sea does not highly influence chemical composition and phase purity of resulting calcium hydroxyapatite powders. However, the particle size, shape as well as surface morphology varies significantly.
5. Sea-shell derived Fe-substituted calcium hydroxyapatite $(Ca_{10-x}Fe_x)(PO_4)_6(OH)_2$ can be produced via the same sol-gel chemistry approach.

2. LITERATURE REVIEW

2.1 IMPORTANCE OF CALCIUM IN HUMAN NUTRITION

Calcium is the most common mineral in the human body and is required for muscle contraction, blood vessel contraction and expansion, the secretion of hormones and enzymes, and transmission of messages through the nervous system. However only less than 1% of total body calcium is needed to support these critical metabolic functions [13, 14]. Several clinical trials have demonstrated a relationship between increased calcium intakes and both lower blood pressure and risk of hypertension [32, 33], although the reductions are inconsistent. Serum calcium is very tightly regulated and does not fluctuate with changes in dietary intakes; the body uses bone tissue as a reservoir for, and source of calcium, to maintain constant concentrations of calcium in blood, muscle, and intercellular fluids [13, 15].

The remaining 99% of the body's calcium supply is stored in the bones and teeth where it supports their structure and function [13]. Calcium is a major structural element in bones and teeth.

2.1.1 Recommended daily intake and groups of people at risk

Depending on age, gender, and medical conditions the Recommended Dietary Allowance (RDA) of calcium slightly varies; the detailed information is provided in the Table 1. Recommended Dietary Allowance is an average daily level of intake sufficient to meet the nutrient requirements of nearly all (97%–98%) healthy individuals.

The size and mass of bones increase during periods of growth in childhood and adolescence, reaching peak bone mass between the ages of 18 and 25. The greater the peak bone mass, the longer the serious bone loss with increasing age could be delayed. Therefore consumption of adequate amounts of calcium and vitamin D throughout childhood, adolescence, and early adulthood is of great importance. Osteoporosis, a disorder characterized by porous and fragile bones, is a serious public health problem.

Table 1. Recommend Dietary Allowance (mg/day) of Calcium [13].

Life Stage Group	Calcium Recommended Dietary Allowance (mg/day)
Infants 0 to 6 months	Adequate intake is 200 mg/day
Infants 6 to 12 months	Adequate intake is 260 mg/day
1 - 3 years old	700
4 - 8 years old	1000
9 - 13 years old	1300
14 - 18 years old	1300
19 - 30 years old	1000
31 - 50 years old	1000
51 - 70 years old	1000
51 - 70 years old females	1200
71 + years old	1200
14 - 18 years old, pregnant/lactating	1300
19 - 50 years old, pregnant/lactating	1000

Osteoporosis has been recognized as an established and well-defined disease that affects more than 75 million people in the United States, Europe and Japan [34]. Osteoporosis causes more than 8.9 million fractures annually worldwide, of which more than 4.5 million occur in the Americas and Europe [35]. The lifetime risk for a wrist, hip or vertebral fracture has been estimated to be in the order of 30% to 40% in developed countries – in other words, very close to that for coronary heart disease. Osteoporosis is not only a major cause of fractures, it also ranks high among diseases that cause people to become bedridden with serious complications [34]. These complications may be life threatening in elderly people. In the Americas and Europe osteoporotic fractures account for 2.8 million disability-adjusted life years annually [35]. Supplementation with calcium plus vitamin D has been demonstrated to be effective in reducing fractures and falls (which can cause fractures) in institutionalized older adults [36].

When calcium intake is low or ingested calcium is poorly absorbed, bone breakdown occurs. Bone loss also occurs as part of the normal aging process,

particularly in postmenopausal women due to decreased amounts of estrogen [35]. Many factors increase the risk of developing osteoporosis, including being female, race, thin, inactive, or of advanced age; smoking cigarettes; drinking excessive amounts of alcohol; and having a family history of osteoporosis [36]. That makes the following groups to be at risk: postmenopausal women, amenorrheic women and the female athlete triad, individuals with lactose intolerance or cow's milk allergy (due to low dairy consumption), vegetarians as well as pregnant and lactating females [13-15].

2.1.2 Sources of calcium: food and food supplements

To ensure the sufficient consumption of calcium, it is suggested to consume enough of calcium rich food products because calcium from food sources is better absorbed by the body than calcium in a supplement form. Milk, yogurt, and cheese are rich natural sources of calcium and are the major food contributors (approx. 70%) of this nutrient to the general population [16]. The additional compounds in dairy products act with calcium to promote its benefits. Non-dairy sources include vegetables, such as Chinese cabbage, kale, and broccoli (16% of intake) [13, 16]. Drinking water, including mineral water, provides 6-7% of dietary calcium [16]. The detailed list is provided in Table 2.

Table 2. List of calcium- rich foods [37].

Food	Serving Size (average)	Calcium (mg)
Milk		
Milk, semi-skimmed	glass, 200 ml	240
Milk skimmed	glass, 200 ml	244
Milk whole	glass, 200 ml	236
Yoghurt and Cream		
Yoghurt, low-fat, fruit	pot, 150 g	210
Yoghurt, low-fat, plain	pot, 150 g	243
Cream, double, whipped	portion, 45 g	26
Cream single	tablespoon, 15 g	13

Food	Serving Size (average)	Calcium (mg)
Cheeses		
Danish blue	portion, 40 g	195
Edam	portion, 40 g	318
Feta	portion, 40 g	144
Camembert	portion, 40 g	94
Cheddar	medium chunk, 40 g	296
Cottage	small pot, 112 g	142
Mozzarella, fresh	portion, 56 g	203
Parmesan, fresh	portion, 30 g	308
Vegetables		
Broccoli, boiled	serving, 85 g	34
Watercress, raw	small bunch, 20 g	34
Curly Kale	serving, 95 g	143
Red kidney beans, canned	3 tablespoons, 105 g	75
Chick peas, boiled	3 tablespoons, 90 g	41
Green/French beans	serving, 90 g	50
Baked beans	serving, 135 g	72
Nuts		
Almonds	12 whole, 26 g	62
Brazil Nuts	6 whole, 20 g	34
Hazlenuts	20 whole, 20 g	28
Sesame seeds	1 tablespoon, 12 g	80
Walnuts	12 halves, 40 g	38
Fish		
Sardines in oil, tinned	portion, 100 g	500
Whitebait, fried	portion, 80 g	688
Salmon, tinned	average portion, 100 g	91
Fish paste	small jar, 35 g	98
Breads and grains		
Pasta, plain, cooked	portion, 230 g	85

Food	Serving Size (average)	Calcium (mg)
Rice, white, boiled	portion, 180 g	32
White bread	slice, 30 g	53
Wholemeal bread	slice, 30 g	32
Muesli, Swiss style	portion, 50 g	55
Fruits		
Apricots, raw, no stone	4 fruit, 160 g	117
Figs, ready to eat	4 fruit, 220 g	506
Currants	2 tablespoons, 50 g	47
Orange	peeled, 160 g	75

Although there is a significant amount of various foods containing calcium, for the most part, people are still not meeting the recommended intake. Studies indicate that dietary calcium intakes fall far short of both the Recommended Dietary Allowance (RDA) and National Institutes of Health (NIH) recommendations. Intakes have declined over time, with age, and appear to be related to a decline in fluid milk consumption [38].

Dairy consumption and calcium intake remain low in most countries with large populations examined as compared with recommended amounts of dairy products and calcium. Promotion of consumption of dairy products does not necessarily increase total calcium intake [17]. Thus, calcium supplementation and fortification has become increasingly important and calcium is being incorporated into food products around the world (see Fig. 1).

In the situations, when people have medical conditions or are at risk of osteoporosis or other calcium deficiency related diseases, the demand of calcium supplements emerges. Calcium supplements come in different forms and contain varying amounts of elemental calcium. Two main forms of calcium in supplements are carbonate and citrate.

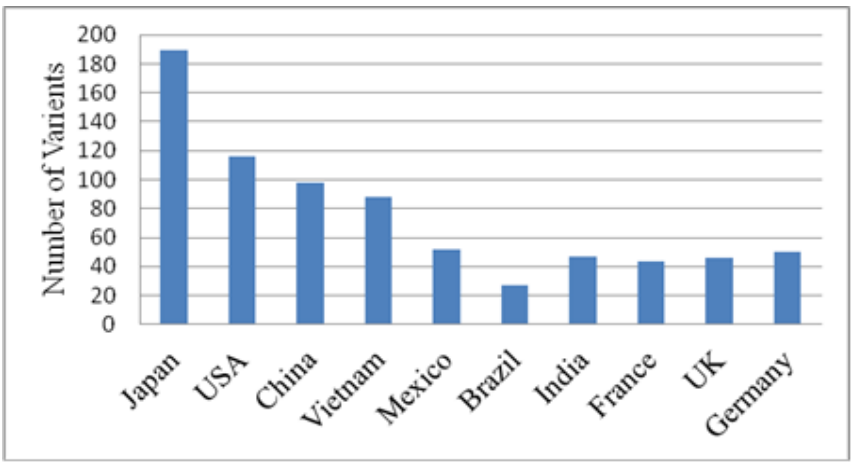

Figure 1. Calcium fortified food production in 2010 by country (*Mintel GNPD data*).

Calcium carbonate is more commonly available and is both inexpensive and convenient. Due to its dependence on stomach acid for absorption, calcium carbonate is absorbed most efficiently when taken with food, whereas calcium citrate is absorbed equally well when taken with or without food [39]. Calcium citrate is also useful for people with achlorhydria, inflammatory bowel disease, or absorption disorders [13]. Other calcium forms in supplements or fortified foods include gluconate, lactate, and phosphate both naturally and synthetically derived. Calcium citrate malate is a well-absorbed form of calcium found in some fortified juices [40].

Some individuals who take calcium supplements might experience gastrointestinal side effects including gas, bloating, constipation, or a combination of these symptoms. Calcium carbonate appears to cause more of these side effects than calcium phosphate or citrate [13], so consideration of the form of calcium supplement is warranted if these side effects are reported. Other strategies to alleviate symptoms include spreading out the calcium dose throughout the day and/or taking the supplement with meals.

2.2. BIOLOGICAL APATITE

2.2.1 Natural human bone mineral

Bones are skeletal organs that allow body mobility and protect internal organs. In addition to mechanical functions, bones have an essential role in metabolic activity as mineral reservoirs that are able to absorb and release ions. From a histological point of view, bone consists of several organic and inorganic tissues such as fibrous and lamellar parts, cartilage, and marrow and contains vascularization, innervation, etc. In terms of structure, bones can be considered as a dispersion of mineral particles (biominerals) embedded in an organic matrix, which forms the contiguous phase [41]. The Ca–P solid phase in bone was first identified by De Jong in 1926 as a crystalline calcium phosphate similar to geological apatite [42, 43]. As a result of intense investigation since, nowadays, chemical composition and structure of biological apatite is well understood.

Biological apatite is the main inorganic constituent of mineralized tissue in bones. It is a calcium-phosphate-based mineral with a structure that closely resembles hydroxyapatite with variable chemical composition [44]. As the main inorganic component of both bones and teeth, it is distributed in the organic constituents with certain sequence and direction [45]. By serving as the fillers in such biological tissues, biological apatite is critical to the physicochemical properties of the bulk materials. Bioapatite is a highly accommodating mineral species that is able to store and release calcium, phosphorous, and several other ions such as Na^+, K^+, Mg^{2+}, F^-, CO_3^{2-}, and OH^-. For this reason, bioapatite acts as an important mineral reservoir for the metabolic activity of the organism [46]. Biochemical activity makes the mineral bone composition vary greatly, depending on the site of sampling, cellular metabolism, age, diet and diseases [41].

Additionally, due to the similarity in chemical compositions and structure, together with its outstanding bioactivity and biocompatibility, biological apatite has been used as bone substitutes for the reconstruction of bone defect in oral implantology, periodontology, oral and maxillofacial surgery as well as

orthopedics [47, 48]. Given the significant role of biological apatite in the structure and function of biological tissues and its clinical applications, numerous studies have been carried out in the investigation of its basic physiochemical and biological properties [45].

Natural bioapatite is a highly defective, having poorly crystallized structure with broad diffraction lines in the XRD patterns [49]. The general formula of bioapatite $Ca_{10-x+h}X_y(PO_4)_{6-x}(CO_3)_x(OH)_{2-x+h}$ proposed by Skinner in 2000 accounts for the possible inclusion of cations (X), the substitution of CO_3^{2-} for PO_4^{3-}, and the presence of calcium vacancies [46].

In order to understand the mechanical properties of bone material, it is important to understand the structural relationship between them at the various levels of hierarchical structural organization. This section therefore, outlines the various levels associated with the hierarchical structure of human bone, the chemical composition for the biological apatite mineral (carbonated apatite) as well as bone remodeling, and biological responses.

2.2.2 Hierarchical structures of bone

Mineralized tissues have remarkable hierarchical structures that have evolved over time to achieve great functions in a large variety of organisms [50]. Due to its organic-inorganic composite nature, bone is able to adopt different structural arrangements with singular architectures, determined by the properties required from it depending on its specific location in the skeleton [51]. To better understand the complex bone architecture, several hierarchical models have been proposed. Weiner and Wagner have identified seven discrete levels of hierarchical organization in bone, which also would be described further [52]. In the corresponding model (see Fig. 2), bone refers to family of materials that all have the mineralized collagen fiber as the initial building block for subsequent higher order architectures [50, 53, 54]. The structure of bone varies greatly among different locations in the skeleton, but the basic nanoscale structure of bone consisting of mineralized collagen remains the same throughout [52].

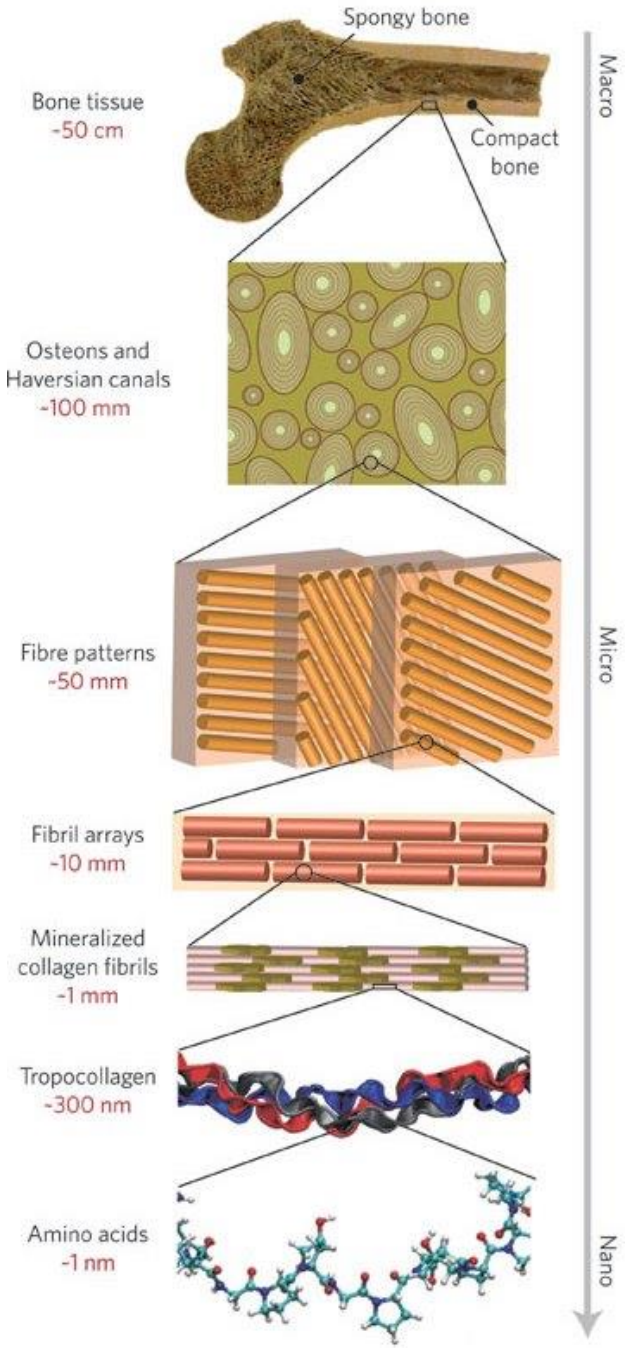

Figure 2. Hierarchical organization of human bone [54].

The first level of hierarchy consists of the molecular components: water, CHAp, collagen and other proteins. Carbonated plate-shaped CHAp crystals being in size of 50 x 25 nm of length and width, respectively, and 2-3 nm thickness are among the smallest known biological crystals [53]. In early studies, apatite needles were observed, however the results of recent studies suggest that

platelets are the dominant morphology [55, 56]. Collagen fibrils consist of triple-helix collagen chains with 1.5 nm diameter and 300 nm length. Collagen molecules are staggered, but there is a gap zone (also called a hole zone) between them in the order of 35 nm and the neighboring molecules are vertically offset by 68 nm [50]. Noncollagenous proteins (NCPs) are also present but they compose 10% or less of the total protein content in the bone matrix. The specific functions of the NCPs are still not completely understood. However, to date it is established knowledge that NCPs in addition to influencing crystal nucleation and growth, also play roles in cell signaling and ion homeostasis [57].

The second level of bone hierarchy is formed by the mineralization of collagen fibrils. This platelet-reinforced fibril conglomerate is described as containing parallel plate like shape carbonated CHAp crystals aligned along their c-axis, that eventually are embedded in a type-I collagen framework [52]. The apatite crystals are nucleated at specific regions on or within the collagen fibrils [53]. The location of these crystals in the fibril was demonstrated in a study indicating that mineralized collagen fibrils had the same banded pattern as negatively marked collagen fibrils [56]. This observation determines that mineral grows in the hole zones that exist between neighboring collagen molecules, as described in the next section. Study by Olszta *et al.* revealed that that the mineral plates are not quite as ordered as previously assumed [58]. This imperfect arrangement of nearly parallel crystals has been supported by recent small-angle X-ray scattering (SAXS) and transmission electron microscopy (TEM) data from Burger et al. [59]. Moreover, the distribution of crystals is not uniform due to bone remodeling, leading to different degrees of mineralization, with implications for crack initiation and propagation [60].

The third level of hierarchy is composed of arrays of previously described mineralized collagen fibrils. For the particular case of lamellar bone the fibrils are then arranged in parallel arrays, with crystals aligned (sub-layers) [53]. These fibrils are rarely found isolated but rather almost always associated as bundles or other arrangements. The fourth level is patterns of arrays that are formed. These include parallel arrays, woven arrangements, plywood like structures, and radial

arrays like those found in dentin [61]. As each lamella is composed of five sub-layers, the total rotation is 150°, therefore forming an asymmetric structure [53]. Moreover, the collagen fibril bundles rotate around their own axis within the five sub-layers. Both facts increase the isotropic properties of bone found at the macroscopic scale [52]. Furthermore, this type of architecture hinders crack propagation and increases toughness.

The lamellae that form cortical bone have three forms of appearance: the secondary osteons, interstitial lamellae as well as the inner and outer circumferential lamellae [53]. Secondary osteons, that are cylindrical tubes, form the fifth level. Osteons are formed with significant cellular activity and re-built by remodeling; osteoclasts destroy the bone tissue and forming a tunnel along the longitudinal axis of bone [50]. Subsequently, the tunnel is filled up by osteoblasts with circular rings of lamellae surrounding the vascular canal, both of them forming together the so called haversian channel or osteon, a cylindrical motif, formed by concentric layers of lamellae and are usually oriented in the longitudinal direction of bone [53]. These channels serve as a conduit for nerves and blood supply to the bone cells.

The sixth level of bone organization is the classification of osseous tissue as either spongy (trabecular or cancelous) or compact (cortical). Cancellous bone is highly porous (75-95% porosity), implementing space for marrow and blood vessels, but has much lower compressive strength [50]. Cortical bone is the dense outer layer (5-10% porosity) that contributes to the support functions of bone. Therefore, the mechanical properties of cortical bone represent the benchmark for synthetic bone [62]. The seventh level is simply the whole bone on the macroscopic scale, incorporating all of the lower levels of hierarchy. There are 206 bones in the adult human skeleton, the structure of which depends on the location and function.

2.2.3 Chemical composition of human bone

The bone is a heterogeneous and anisotropic material that structurally comprises two phases – mineral and organic. The mineral phase is essentially

composed of 50-74% of carbonate-substituted hydroxyapatite embedded in an organic matrix [60, 63]. The organic phase forms the remaining part of the bone tissue and is composed of collagen, glycoproteins, proteoglycans, and sialoproteins. The major component being collagen (type I) [64]. As was already mentioned, the crystals of bone apatite are mostly plate shaped, with a thickness that ranges from 2 nm (for mineralized tendon) to 7 nm (for some mature bone types) [65]. Other mineral phases that are present in bone are dicalcium heptaoxodiphosphate ($Ca_2P_2O_7$), calcium hydrogen phosphate ($CaHPO_4$), tricalcium phosphate (TCP, $Ca_3(PO_4)_2$) and some amorphous phases of calcium phosphate.

Chemical composition of apatite platelets is not constant and normally changes during mineralization and maturation. The reason for that is the structure of apatite [51]. To be more precise, the site of Ca^{2+} may be occupied by bivalent or monovalent cations such as Sr^{2+}, Ba^{2+}, Mg^{2+}, Na^{+}, and K^{+}, whereas P could be substituted by atoms such as C, As, V, S, while hydroxyl group (OH^{-}) could be replaced by the following anions OD^{-}, CO_3^{2-}, F^{-}, Cl^{-} or even be left vacant [51]. Due to that, the apatite may host carbonate in two positions: the hydroxyl sublattice producing type A carbonate apatite (CO_3-CHAp) and the phosphate (PO_4^{3-}) sublattice forming type B CO_3-CHAp [45, 51]. In physiological environment, partial dissolution of CaPs occurs in the acidic microenvironment caused by cellular activities, leading to increased supersaturation of the biological or physiological fluid. Further, precipitation of CO_3-CHAp together with other ions and organic molecules occurs [66]. There are data suggesting that biological apatite consists of a mixed substituted CO_3-CHAp, in which CO_3^{2-} ions are substituted for both PO_4^{3-} (type B, the major form) and OH^{-} (type A, the inferior form) ions [67]. In other words, biological apatite is a calcium phosphate framework incorporated by various sorts of ions. Calcium, phosphorus and oxygen are the three major elements composing the said framework. It was believed that the calcium/phosphorus (Ca/P) ratio of biological apatite was either lower than or close to that of stoichiometric CHAp, specifically, 1.67 [68, 69]. However, it was also reported that the Ca/P ratio even could be higher [70-72].

This may be attributed to the difference in the treatment methods and conditions, the raw materials, and the test methods, as well as the detection error [73, 74]. There are studies suggesting that the early-forming bone mineral is a calcium-defective deficient CHAp phase and that the calcium deficit is progressively reduced with bone mineral maturation [41]. Besides, carbon, sodium, potassium, fluorine, magnesium, aluminum, strontium, chlorine, and some trace elements are also detected as incorporated ions in the biological crystals, however their content may vary among samples and sources, and the co-presence of all these elements may not be always found [69]. Detailed ionic composition of mineral phase of human bone is presented in Table 3.

Table 3. Ionic composition of human bone mineral [75-77].

Ion	**Amount in Bone**
Ca^{2+}	36.6 (wt.%)
PO_4^{3-}	17.1 (wt.%)
CO_3^{2-}	4.8 (wt.%)
Na^{+}	1.0 (wt.%)
K^{+}	0.07 (wt.%)
Mg^{2+}	0.6 (wt.%)
Sr^{2+}	0.05 (wt.%)
Cl^{-}	0.1 (wt.%)
F^{-}	0.1 (wt.%)
Zn^{2+}	39 (ppm)
Cr^{3+}	0.33 (ppm)
$Co^{2+/3+}$	<0.025 (ppm)
Mn^{2+}	0.17 (ppm)
SiO_4^{2-}	500 (ppm)

The organic matrix of bone consists mainly of collagen type I, a triple helix of two α1 and one α2 collagen chains [78]. Collagen is composed largely of the amino acids glycine, proline and hydroxyproline. It is synthesized by osteoblasts,

assembled extracellularly into fibrils, and stabilized by cross-links [78, 79]. The matrix not only acts as a scaffold for the mineral in the composite material, but plays a decisive role in the biomechanical competence of the collagen-mineral composite itself. Characteristics of organic matrix, such as amount produced by the cell, fibril structure, and the character, number, and distribution of the fibril cross-links, are genetically determined [78].

Understanding the balanced properties of the mineral and organic phases of bone is crucial. In fact, the mineral phase confers strength and stiffness to the bone tissue, but after a certain degree of mineralization, bone becomes brittle, reducing the energy required for fracture [60]. On the other hand, the organic phase is more adaptable and defines the amount of energy that could be absorbed after the first microcracks, but before failure (fracture), therefore determining post-yield properties and the toughness of the overall bone. However, the overall picture is more complex and the differences in the degree of mineralization between different bone areas are pivotal in the process of microcrack formation and accumulation, which is a process that increases bone compliance so that it can sustain larger deformations, thus contributing to bone toughness. It is now evident that the overall bone mechanical properties are influenced by crystal size, shape, arrangement, and volume fraction, and by collagen spacing, orientation, length, and the strength of intermolecular interactions [80].

2.2.4 Bone remodeling by human bone cells

Bone differs from other tissues in that it has the ability to self-repair after fracture, without leaving a scar; bone duration and mechanical properties are restored and the resulting repaired bone is similar to the original. Fracture healing is a complex physiological process involving both biological factors and mechanical principles [78, 81]. Bone is modified either by cellular activity during growth, as a response to systemic hormones, by the response to mechanical stress applied to the skeleton or by other environmental and genetic factors [80]. During childhood and adolescence, bone remodeling contributes to linear growth and to bone mass increase. Peak bone mass is attained around 25-30 years old. After this

age bone starts slowly to change the metabolic activity, leading to progressive bone loss [80]. Remodeling is the repair mechanism of bone tissue, that helps to prevent the propagation of microcracks and their evolution into macrocracks, which can lead to complete fracture [60]. During bone remodeling, both osteoclast-mediated bone resorption of old material and osteoblast-mediated new bone matrix production occurs.

Cancellous bone is remodeled more often than the cortical bone [82]. As a consequence of bone remodeling, collagen fibers align along the direction of the load of the mature bone, which provides an increase in the mechanical strength [83]. Remodeling begins with the recruitment and differentiation of bone-resorbing osteoclasts [84]. The resorbed bone is replaced by bone forming osteoblasts. A number of these osteoblasts remain embedded within the bone matrix where they give rise to osteocytes, the third bone cell type involved in remodeling [85]. The schematic description of bone remodeling is provided in Figure 3 retrieved from reference [86].

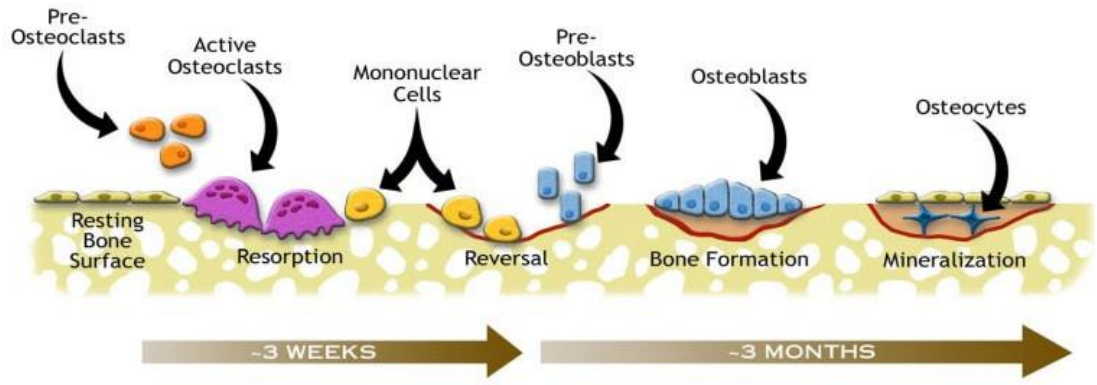

Figure 3. Bone tissue remodeling process.

Bone remodeling is regulated by a variety of systemic hormones as well as by molecules released by the central nervous system [87]. Local factors are also involved, such as cytokines, growth factors, and cell-matrix interactions [88, 89]. Up to recently, bone cells were considered of separate existence originating from distinct ancestry and having no or little connection. There is now however

extensive evidence that they communicate with each other to control bone homeostasis [85, 90]. Current data support the concept of a social network of communicating cells that differ in origin and function. Several direct and indirect links between bone cells have been identified [85]. Cells interact by releasing soluble regulatory molecules, while transmembrane molecules create cell-cell connections [91]. These network interactions play a major role in the control of bone remodeling and have a significant impact on bone homeostasis.

To sum up, during the remodeling process replacing the new woven bone with lamellar bone takes place [81]. This process, resulting in a balanced resorption of hard callus by osteoclasts and lamellar bone deposition by osteoblasts, is initiated as early as the first month and takes years to achieve a fully regenerated bone structure.

2.3 SYNTHETIC CALCIUM HYDROXYAPATITE

Among the CaP salts, calcium hydroxyapatite, as a thermodynamically most stable, most dens and most insoluble crystalline phase in body fluid, possesses the most similarity to the mineral part of bone [92, 93]. This resemblance is the origin of the excellent biocompatibility, affinity to biopolymers and high osteogenic potential [94-98].

Composition and structure of synthetic CHAp have been studied extensively in previous reports [45, 69, 99]. Two crystal forms for CHAp were reported, that is, hexagonal (space group $P6_3/m$) with the lattice parameters $a = b = 9.432$ Å, $c = 6.881$ Å, and $\gamma = 120°$ and monoclinic (space group $P2_1/b$) with the lattice parameters $a = 9.421$ Å, $b = 2\ a$, $c = 6.881$ Å, and $\gamma = 120°$ [45]. These two forms share the same elements, with a stoichiometric Ca/P ratio of 1.67. The major difference in their structure is the orientation of hydroxyl groups. In the hexagonal CHAp, two adjacent hydroxyl groups point at the reverse direction; while in the monoclinic form, hydroxyl groups have the same direction in the same column and an opposite direction among columns [100]. The monoclinic form of CHAp is more ordered and thermodynamically stable, it is formed at high temperatures, but have never had evidence of its presence in calcified tissues

[45]. Moreover only the hexagonal phase is of practical importance due to the fact that the monoclinic form is destabilized by the presence of even small amounts of foreign ions [69].

CHAp structure in hexagonal rotational symmetry is formed by a tetrahedral arrangement of phosphate (PO_4^{3-}); it can be roughly described as a phosphate assembly crossed by parallel channels filled by OH^- ions and parallel to the crystallographic *c*-axis [75] (Figure 4 [101]). Two of the oxygens are aligned with the *c* axis and the other two are in a horizontal plane. Within the unit cell, phosphates are divided into two layers, with corresponding heights of 1/4 and 3/4, respectively, resulting in the formation of two types of channels along the *c* axis, denoted as A and B [43].

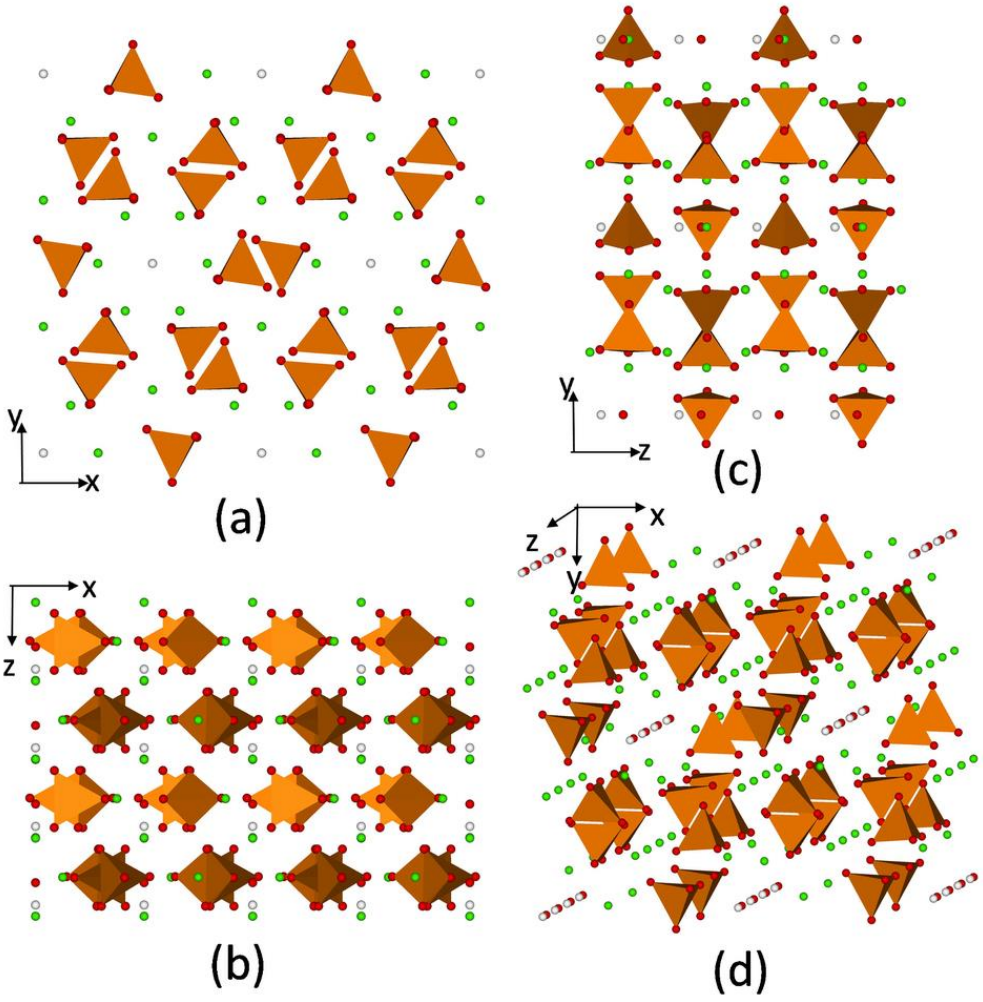

Figure 4. Projections of the supercell structure of CHAp: (a) x-y plane, (b) x-z plane, (c) y-z plane, and (d) perspective (with PO_4 tetrahedra shown as yellow-brown, Ca^{2+} as green and OH^- as red-white) [101].

The walls of channels A type are occupied by oxygen atoms of phosphate group and calcium ions, called calcium ions type II [Ca (II)], consisting of two equilateral triangles rotated 60 degrees relative to each other, at the heights of 1/4 and 3/4, respectively [102]. Type B channels are occupied by other ions of calcium, called calcium ions type I [Ca (I)]. In each cell there are two such channels, each of which contains two calcium ions at heights 0 and 1/2. In the stoichiometric CHAp, the centers of the channels type A are occupied by OH radicals, with alternating orientations.

A unit cell accommodates a formula unit $Ca_{10}(PO_4)_6(OH)_2$. Among the 10 cations, the 4 Ca(I) are tightly bonded to 6 oxygens and less strongly to the other 3 oxygens (mean Ca(I)–O distance 0.255 nm), whereas the 6 Ca(II) atoms are surrounded by 7 oxygens (mean Ca(II)–O distance 0.245 nm). Ca(I) atoms are strictly aligned in columns and any small change in the metal–oxygen interactions affects the entire lattice [103]. However, the Ca(II) atoms belonging to consecutive layers are staggered, allowing random local misplacements without compromising the whole structure. As a consequence, cations smaller than Ca or also low concentrations of slightly larger cations are preferably accommodated in site Ca(I) where stronger interactions are present, while larger cations are assumed to be accommodated in position Ca(II), even at high concentrations .

CHAp is capable of accommodating several substituents, while still maintaining its basic apatite structure. It is documented, that Ca^{2+} can be substituted by monovalent, such as, (Na^+, K^+), divalent (Mg^{2+}, Sr^{2+}, Ba^{2+}, Pb^{2+}) as well as trivalent, such as (Y^{3+}, Fe^{3+} and Cr^{3+}) cations [104]. Significant anionic substitutions, include the replacement of OH^- by CO_3^{2-}, F^-, Cl^-, and PO_4^{3-} by CO_3^{2-}, AsO_4^{3-}, VO_4^{3-} [75, 102, 105]. Some substitutions are coupled with others to maintain the charge balance in the apatite, such as, CO_3^{2-} for PO_4^{3-} coupled with Na^+ for Ca^{2+}. The trivalent anionic phosphate sites cannot accept vacancies, as the trivalent anions are quite large and vacancies are believed to destabilize the lattice. Adversely, the cationic sites can accept vacancies, up to a maximum of 2 sites out of the 10 existing in stoichiometric apatites. Some possible substitutions

as well as their influence on lattice parameters are indicated in Table 4 adapted from [106].

Table 4. Lattice parameters of aqueous and non-aqueous synthetic apatites [106].

Apatite	Major substituent	Lattice parameter, *a* , +/-0.003 nm	Lattice parameter, *c* , +/-0.003 nm
Synthetic (non-aqueous)[a]			
OH-apatite	-	9.441	6.882
F-apatite	F	9.375	6.880
Cl-apatite	Cl	9.646	6.771
CO_3-apatite	CO_3	9.544	6.859
Synthetic (aqueous)[b]			
OH-apatite (Ca-deficient)	HPO_4	9.438	6.882
F-apatite	F	9.382	6.880
(Cl, OH)-apatite	Cl	9.515	6.858
CO_3-OH apatite	CO_3	9.298	6.924
CO_3-F apatite	CO_3, F	9.268	6.924
Sr-apatite	Sr	9.739	6.913
Pb-apatite	Pb	9.894	7.422
Ba-apatite	Ba	10.162	7.722

[a] Prepared at high temperatures (1000ºC) by solid state reaction route
[b] Prepared at 100ºC either by precipitation or by hydrolysis methods

It has been demonstrated that CHAp can promote new bone ingrowth through osteoconduction mechanism without causing any local or systemic toxicity, inflammation or foreign body response [97, 98]. When a CHAp-based ceramic is implanted, a fibrous tissue-free layer containing carbonated apatite forms on its surfaces and contributes to the bonding of the implant to the living bone, resulting in earlier implant stabilization and tight fixation of the implant to the surrounding tissues [98, 107, 108]. For that reason, CHAp is commonly the material of choice for various biomedical applications. Synthetic CHAp particles are also used for coating metallic implants or bone grafts [66, 109]. Figure 5

based on the data from reference [110] indicate that usage of CHAp in implants increased significantly during the last years.

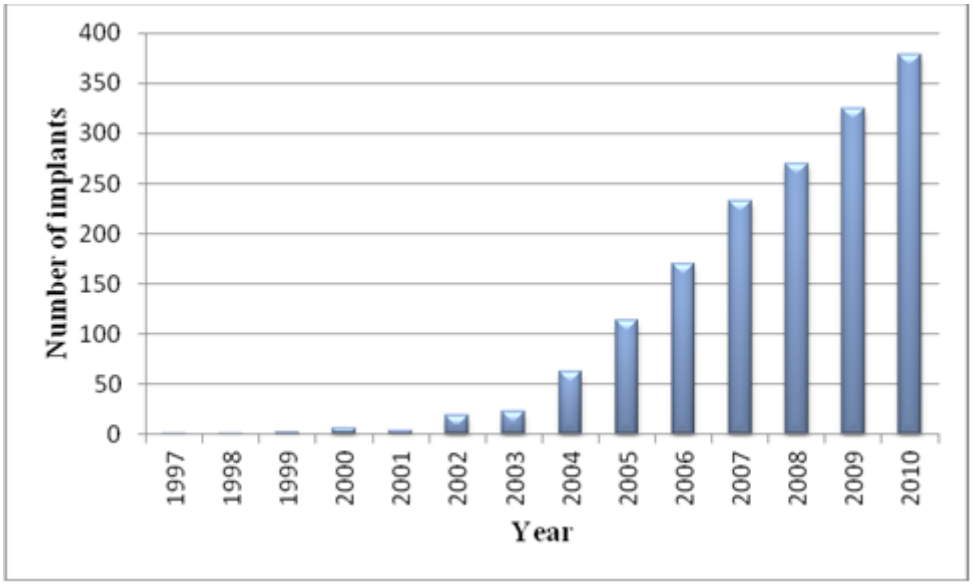

Figure 5. Distribution of CHAp implants per year.

Furthermore, recent studies have demonstrated that CHAp particles have the potential to inhibit the growth of different kinds of cancer cells [111, 112].

The general importance of CHAp and its derivatives have also led to numerous non-medical industrial and technological applications in fields such as waste water treatment and catalysis. For example, in heterogeneous catalysis, CHAp was found to be active in different reactions: oxidative dehydrogenation of light alkanes, water gas shift reaction, total oxidation of CO, photodecomposition of organic pollutants, etc. [113, 114]. CHAp also possesses high retention capacities for heavy metals or organic pollutants in aqueous effluents which confers a potential role for this calcium phosphate in environmental processes [115-117].

To suit its numerous applications, material properties such as bioactivity and mechanical strength need to be tailored accordingly. Consequently, much research has been devoted to the development of synthesis methods that enable the control of chemical and physical powder characteristics. In the following

section of dissertation, overview of the common preparation methodologies for CHAp will be presented.

2.4 SYNTHESIS METHODS USED FOR THE PREPARATION OF CALCIUM HYDROXYAPATITE

The preparation of CaP powders with a particular morphology, stoichiometry, crystallinity and crystal size distribution is important in biomedicine and materials science [118]. As mentioned in previous sections, the critical characteristics of CHAp particles, such as strength, toxicity to cells, osseointegrativity and bioresorbability, depend strongly upon their morphology, stoichiometry, crystallographic structure and phase purity [98]. In particular, for CHAp crystals, it has been demonstrated that their microscopic shape, size and size distribution can significantly influence their mechanical properties, surface properties, biocompatibility as well bioactivity [98]. Therefore, it is of significant importance to develop new synthesis procedures having precise control over the crystal geometry.

A number of different processes have been proposed to be effective to prepare CaP powders. Chemical methods used to produce synthetic CHAp could be classified in two main categories: dry methods, namely anhydrous reactions involving the solid phases, including ones at high temperatures and pressures; and wet ones, i.e., precipitation from solutions of the components and hydrolysis of calcium phosphates [119].

The dry method gives CHAp powders of stoichiometric composition (Ca/P = 1.667), which involves firing at 1000-1300°C for a mixture of substances containing Ca^{2+} and PO_4^{3-} ions (usually $Ca_3(PO_4)_2$, $Ca_2P_2O_7$, $CaHPO_4 \cdot 2H_2O$, $Ca(OH)_2$) [119]. The source of the OH^- ions, a crucial component of the apatite structure, is water vapor which is admitted during the heat treatment.

Aqueous solutions of the initial substances are used in wet chemical methods. They normally give CHAp powders with large specific surfaces and small particles. The composition deviates from stoichiometric (deficiency of Ca^{2+}),

while the structure is amorphous to an extent dependent on various factors, such as concentration, and pH of the initial solutions, dispersion hardening time, temperature, etc. Calcium sources usually used for these type of syntheses include $CaCl_2$, $Ca(NO_3)_2$, $(CH_3COO)_2Ca$, $Ca(OH)_2$, $CaCO_3$, $CaSO_4 \cdot 2H_2O$, while the phosphorus sources are $NH_4H_2PO_4$, $(NH_4)_2HPO_4$, H_3PO_4. During the synthesis, pH is maintained above 7 by the addition of NH_4OH or NaOH, in some cases with nitrogen gas passing through the mixture of solutions to remove the CO_3^{2-} [119].

Each of these methods of synthesis of CHAp has both advantages and disadvantages. Nonstoichiometric CHAp from any synthesis method tends to decompose and give rise to secondary phases, such as tricalcium phosphate or calcium oxide, during the heat treatment.

Recently there was a study conducted in order to determine the total number of the indexed scientific papers relating to each method of production of CHAp [98]. The results of the study are presented in Figure 6.

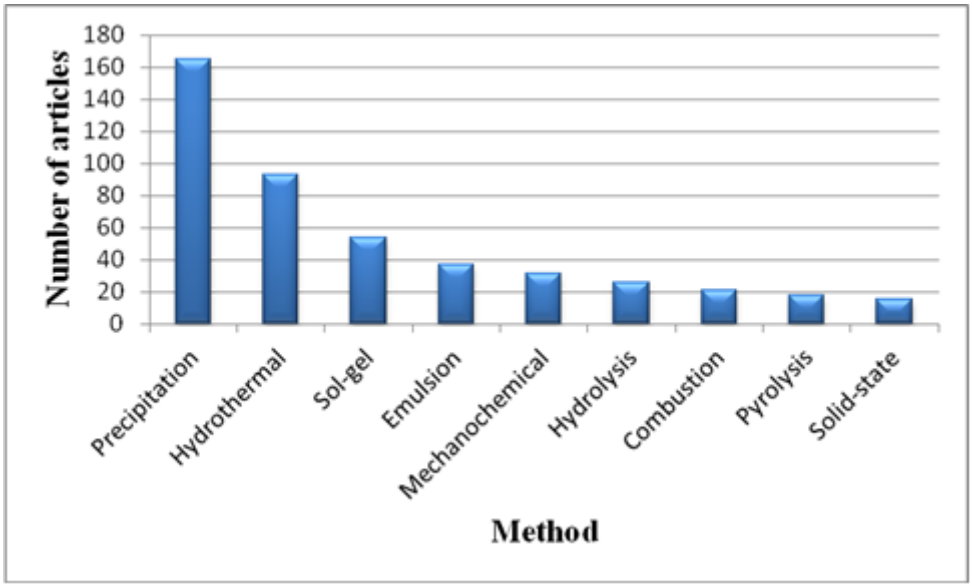

Figure 6. Total number of articles indexed in Scopus over 1999–2011 by the method of preparation of CHAp (retrieved from reference [98]).

In the further section of this chapter most recognizable techniques for CHAp production would be described in more details.

2.4.1 Sol-gel synthesis

Sol–gel synthesis of CHAp ceramics has recently received much attention [120-127] because of its well-known inherent advantages, namely homogeneous molecular mixing, low processing temperature, and ability to generate nanocrystalline powders, bulk amorphous monolithic solids as well as thin films [118]. Besides, the sol-gel approach provides significantly milder conditions for the synthesis of CHAp powders or films. Additionally, a powder obtained by a typical sol–gel method usually exhibits good stoichiometry with a large surface area and a small cluster size (ranging from 50 nm to about 1 μm, depending on the processing parameters) [98]. More to add, in vitro studies have reported that the bioresorbability of the sol–gel CHAp is higher than conventional powder and is close to biological apatite [128].

In the sol-gel synthesis of CHAp, calcium alkoxides or salts are frequently used as calcium precursors. In most cases, phosphorus compounds – oxide, triethylphosphate and triethylphosphite are employed as phosphorus precursors in water or organic solvent phase [98, 123, 129]. The schematic process for preparation of sol-gel particles is provided in Figure 7.

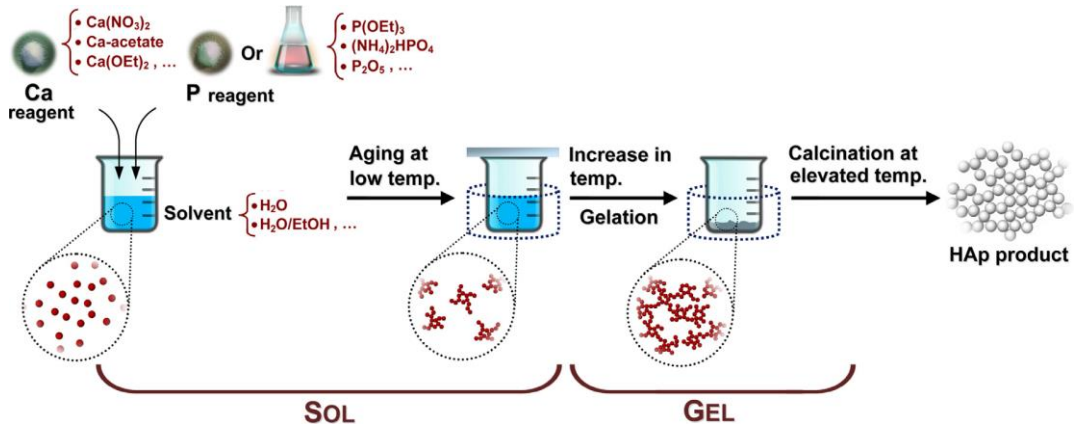

Figure 7. Preparation process of CHAp particles using sol-gel method [98].

The thermal treatment step has been found to be of great importance in the generation of pure CHAp from the porous gel [98]. Insufficient aging and/or uncontrolled gelation and heat treatment may cause the generation of various

impurities, mainly CaO, $Ca_2P_2O_7$, $Ca_3(PO_4)_2$ and $CaCO_3$ [98]. Further, the rate of gelation, the origin of the solvent, as well as the temperature and pH employed during the process significantly depend on the chemical nature of the reagents used in the sol–gel synthesis [98] .

Major disadvantages of sol-gel synthesis route include the generation of secondary phase, most often CaO, cost of starting materials (especially alkoxide based precursors) as well as a long period of the sol-gel preparation time - 24 h or longer is commonly reported in literature as required to form desirable product [123]. This is because of slow reaction between calcium and phosphorus precursors in the sol phase. As in other wet methods, a number of precursors can be exploited in a sol–gel process; the ones being employed most often are summarized in the Table 5 along with the other important factors for sol- gel synthesis.

Table 5. Overview of the most often used sol-gel methods of synthesis.

Ca precursor	**P precursor**	**Solvent**	**Chelating agent**	**Conditions (temp., pH, etc.)**	**REF**
Calcium carbonate ($CaCO_3$)	Phosphoric acid (H_3PO_4)	Water-Ethanol	-	NH_4OH solution was used to adjust pH Reaction temp.: room temperature followed by 80°C Drying temp.: 105°C	[130]
Calcium nitrate tetrahydrate ($Ca(NO_3)_2 \cdot 4H_2O$)	Triethyl phosphate ($(C_2H_5O)_3PO$)	2-metoxyethanol ($CH_3OCH_2CH_2OH$)	-	pH < 4 Aging: T = 80°C for 4 days Gelation: 90°C< T < 100°C for 16 h Drying: 180°C< T < 200°C for 4 h Annealing: 600°C< T < 1400°C, in between 12 h and 24 h.	[127]
Calcium nitrate tetrahydrate ($Ca(NO_3)_2 \cdot 4H_2O$)	Trimethyl phosphite ($(CH_3O)_3P$)	Ethanol	-	Mixing: r.t. Aging: r.t. 16 h Gelation: T= 60°C for 6 days Calcination: T= 600°C/ 800°C for 3 h	[131]
Calcium methoxide ($Ca(OCH_3)_2$)	Triethyl phosphite ($(C_2H_5O)_3P$)	Ethanol/ ethanediol	-	Hydrolysis: T= 70 °C	[121]
Calcium nitrate tetrahydrate ($Ca(NO_3)_2 \cdot 4H_2O$)	Diammonium hydrogen-phosphate ($(NH_4)_2HPO_4$)	Ethanol	-	pH = 10 (was regulated with $Ca(OH)_2$) Mixing: T = 85°C for 4 h Sintering: 400°C for 2 hours, then 750°C for 2 hours, followed by 1200°C for 2 hours	[124]
Calcium carbonate ($CaCO_3$)	$(NH_4)_2HPO_4$	Nitric acid (HNO_3) and distilled water	Alginic acid ($(C_6H_8O_6)_n$)	pH= 8.4 (adjusted with NH_4OH) Drying: T = 8°C overnight Annealing: T= 110°C for 5 h, followed by heating at T= 200°C/ 300°C/ 400°C/ 600°C/ 900°C.	[126]
Calcium nitrate tetrahydrate ($Ca(NO_3)_2 \cdot 4H_2O$)	$(NH_4)_2HPO_4$	Distilled water	Citric acid ($C_6H_8O_7 \cdot H_2O$)	pH= 2-3 (adjusted with HNO_3) Mixing: T = 70°C- 80°C for 4- 6h Gelation: T = 110°C- 120°C for 1- 2 days Calcination: T = 200°C Sintering: T = 750°C for 1 h	[125]
Calcium acetate monohydrate ($Ca(CH_3COO)_2 \cdot H_2O$)	$(NH_4)_2HPO_4$	Acetic acid (CH_3COOH) and distilled water	EDTA or tartaric acid (TA)	Gelation: T = 65°C Calcination: T = 1000°C for 5 h	[129]

Recent study by Gopi et al. reported the synthesis and characterization of nanosize CHAp powders by a novel ultrasonic coupled sol–gel synthesis [132]. The resulting powders were sintered by conventional means at different temperatures. These results showed that nano-CHAp powders synthesized by ultrasonic coupled sol–gel synthesis a significant particle size reduction compared with the conventional sol–gel method, hence; these powders could be used as a coating material in biomedical applications [118].

2.4.2 Chemical precipitation

As indicated in Fig. 6 chemical precipitation process is applied predominantly to produce CHAp in comparison to other methods. One of the most obvious reasons for that is that among the various wet processing methods, conventional chemical precipitation is the simplest route for the synthesis of nanosized CHAp [98]. The chemical precipitation is based on the fact that, at room temperature and at pH 4.2, CHAp is the least soluble and usually the most stable CaP phase in an aqueous solution [98]. The precipitation reaction is, however, usually conducted at pH values higher than 4.2 (dominating pH values are 8-11) and temperatures ranging from room temperature to temperatures close to the boiling point of water (80-95 °C) [98, 133, 134]. Figure 8 demonstrates a schematic process diagram of the steps taking place in the production of CHAp by chemical precipitation method.

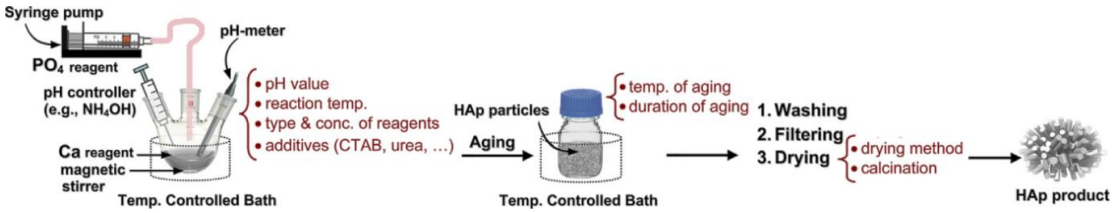

Figure 8. Schematic step by step preparation process of CHAp particles using chemical precipitation method [98].

To synthesize CHAp nanoparticles, chemical precipitation can be accomplished using different calcium- and phosphate containing reagents, e.g.

calcium hydroxide or calcium nitrate as the source of Ca^{2+} and orthophosphoric acid or diammonium hydrogen phosphate as the PO_4^{3-} source [127, 133, 134]. Typical procedure involves the dropwise addition of one reagent to another (at a speed varying from 2ml/min to 22 ml/min) under continuous and gentle stirring, while the molar ratio of elements (Ca/P) is kept at stoichiometry according to its ratio in CHAp (1.67) [98, 127, 133]. Then the mixture is aged at room temperature for several days. As the final step, the obtained precipitate is filtered, washed, dried and crushed into a powder [133]. Often calcination step is also present [127, 133, 134].

A powder prepared by simple precipitation is, however, usually non stoichiometric and poorly crystallized without any regular shape. This might be influenced by the fact that the shape, size and specific surface area of the CHAp nanoparticles obtained by this method are very sensitive to the reactant addition rate, and to the reaction temperature. The reactant addition rate determines the purity of the synthesized CHAp and is linked strongly to the pH obtained at the end of the synthesis and to the suspension stabilization. The reaction temperature determines whether the crystals are monocrystalline or polycrystalline. CHAp nanoparticles synthesized at low temperature ($T < 60$ °C) are monocrystalline. A transition temperature ($T=60$ °C) can be defined as a limit for the monocrystalline CHAp nanocrystal synthesis. Above this critical temperature nanocrystals become polycrystalline [134].

More recent studies suggest alternative routes based on various additives and/or modification of the basic procedure. Among the most reported precipitation processes, chemical agents such as citric acid, amino acids and ethylenediaminetetraacetic acid (EDTA) have been widely used to mediate CHAp nucleation and crystal growth [118]. Wang *et al.* used ethanolamine, citric acid and polyethylene glycol as dispersants to prevent products from aggregating during the synthesis process [133]. The results indicated that dispersant species had small effect on the shape of the CHAp particles; however they demonstrated a significant effect on their dispersibility. Ethanolamine was the best dispersant among the other tested [133].

Many researchers have employed urea instead of NH_4OH or NaOH to adjust the pH value, which led to more homogenous precipitation [98, 134].

2.4.3 Solid-state synthesis

The solid state synthesis at high temperatures has been generally used for processing ceramic powders and to study the stability of the phases. Solid-state reaction, as a relatively simple and inexpensive procedure, can be employed in the mass production of CHAp powder as it can also yield large amounts of material. Solid-state synthesis relies on the solid diffusion of ions amongst powder raw materials and thus requires relatively inefficient high temperature processing (<1250°C) to initiate the reaction. In a typical procedure, precursors are firstly blended and ground, then calcined at high temperature (e.g. 1000 °C) [98]. The precursors can be various calcium- and phosphate-containing salts and oxides. The high temperature of calcination leads to the formation of a well-crystallized structure. The general process is shown in Figure 9. As a disadvantage, the powder synthesized by a solid-state reaction often exhibits heterogeneity in its phase composition, owing to the small diffusion coefficients of ions within the solid phase [98]. In order to ensure homogeneity and sufficiently small particle sizes, it is advised to firstly ball mill starting materials for approximately 16 hours. There are studies suggesting that some particular additives might be favorable in this case as well (e.g. silicon dioxide, alumina, and hydrofluoric acid), a binder (e.g. PVA) and an organic vehicle (e.g. acetone), they are used to form a slurry before milling [135, 136].

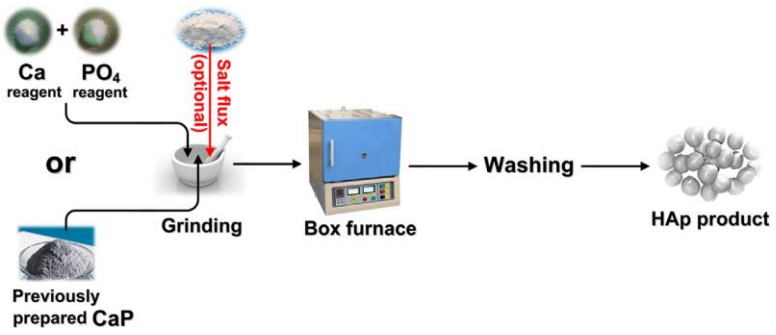

Figure 9. Schematic step by step preparation process of CHAp particles via solid-state synthesis [98].

Recently, Tseng et al. synthesized CHAp nanoparticles through a polyethylene glycol (PEG)-assisted reaction, using calcination of calcium dihydrogenphosphate and calcium hydroxide at 900°C in an oxygen atmosphere. Results of their study demonstrate that the process yields a well crystallized and non-aggregated powder with a nanometer particle size [98]. Pramanik et. al. employed cold-pressing in solid-state synthesis to obtain high mechanical strength CHAp [136]. Firstly, they mixed ingredients in a crucible using a mortar for 1 h. Subsequent mixing was carried out in a ball mill for 16 h in a mixed organic vehicle containing 30% (v/v) acetone and 0.2% (w/w) polyvinyl alcohol (PVA). The final mixed slurry was dried at 80 °C for 3 h, resulting into powder, that was pelletized using a cylindrical stainless steel and pressures varying from 46 to 135 MPa with dwell time of 15–400 s at ambient temperature [136]. The cold pressed CHAp pellets were sintered in air in a glow bar furnace at different temperatures from 500 to 1250°C. The results of this study indicated, that the surface hardness of the samples was 15–16 times larger than natural femoral bone and no appreciable change in the sample weight (dry state) was found after immersing the sample in simulated body fluid for 60 days [136].

Recently CHAp powders were synthesized by solid-state reaction at room temperature followed by calcination using diammonium phosphate, calcium nitrate and sodium carbonate as raw materials [135]. Results of this study indicated that calcination temperature was critical factor in controlling the size and shape of resulting CHAp particles. It was concluded that increase of calcination temperature was in favor of the crystallization of CHAp.

Regardless of these efforts, and as mentioned before, a solid state method usually suffers from the small diffusion of ions during the reaction; this is an inherent characteristic, and is why very little work is available on solid-state processing of CHAp. Moreover, despite reports of the production of single phase CHAp via this method it is highly likely that α-tricalcium phosphate may be present in the final product due to the high temperatures required to initiate the reaction.

2.4.4 Hydrothermal method

The hydrothermal method, a typical solution-based approach, was proven to be an effective and convenient process to prepare different inorganic materials with diverse, controllable morphologies and architectures [118]. The most notable advantages of this method include easily controllable reaction conditions, relatively large scale and high yield in terms of quantity of the desired products, and frequent use of water as the reaction medium [118]. Hydrothermal synthesis can also simply be considered as a chemical precipitation in which the aging step is conducted at a high temperature – typically above the boiling point of water – inside an autoclave or pressure vessel [98].

It has been demonstrated that CHAp nanoparticles obtained from the hydrothermal conditions is relatively stoichiometric and highly crystalline [248–253]. Moreover, phase purity and Ca/P ratio of CHAp precipitate significantly improved with increasing the hydrothermal temperature [254–258]. However, elevated temperature and pressure need expensive equipment, making the hydrothermal process more expensive than some of the other wet methods.

Zhang et al. developed a general strategy for the synthesis of nano- and microstructured CHAp using water as a reaction medium through a simple hydrothermal process [137]. Several dominant morphologies were achieved (nanorods, nanowires, microsheets, burr-like microspheres and microflowers) [118]. The pH value was demonstrated to play a vital role in obtaining CHAp samples with various morphologies [137]. The use of trisodium citrate also has an important influence on product shape [118]. Possible formation mechanisms for CHAp nano- and microcrystals with diverse morphology are presented in Figure 10.

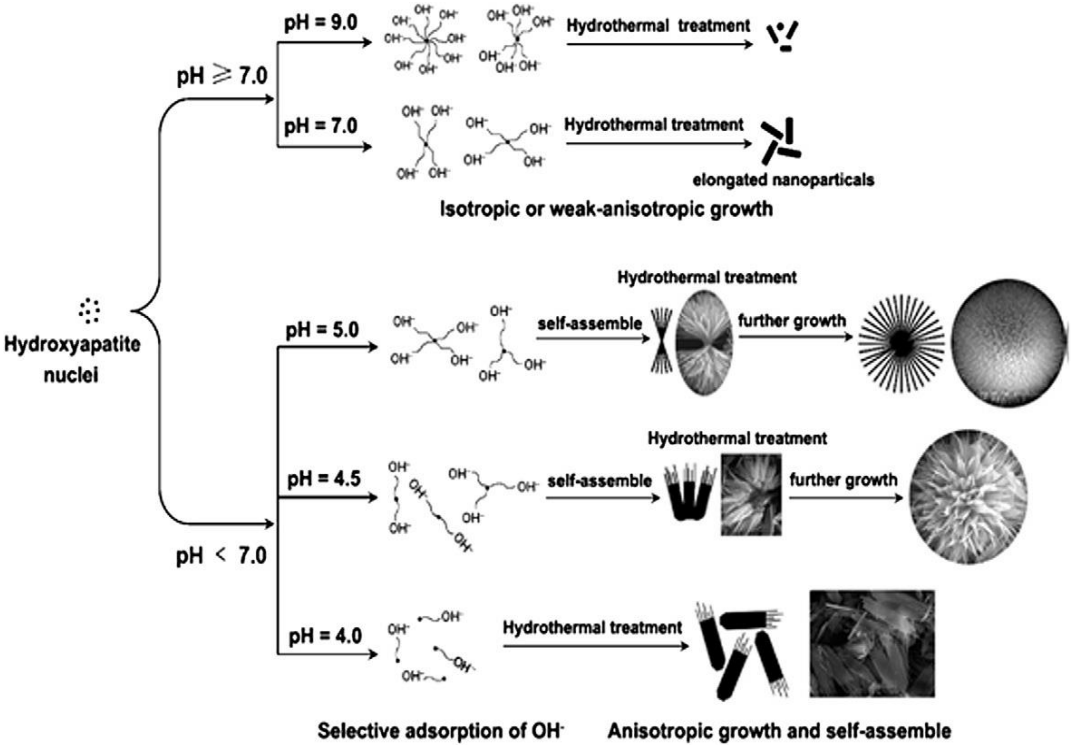

Figure 10. Schematic mechanism for the formation and morphology evolution of CHAp samples based upon different pH values [118].

The most notable disadvantage of hydrothermal method is the poor capability of the process to control the morphology and size distribution of nanoparticles [98]. As a matter of fact, the morphology of particles obtained by a conventional hydrothermal method is usually irregular, spherical, or at most rod-like, with a very broad size distribution, e.g. 0.7–3.0 μm, 10–80 nm, or 9–152 nm [98]. To improve the procedure and obtain CHAp powders of desired morphological characteristics organic modifiers, such as trisodium citrate, polyethylene glycol, cetyltrimethylamonium bromide (CTAB), EDTA, PVA and poly(amido-amine) (PAMAM) dendrimers are employed in hydrothermal synthesis [138]. Consequently, CHAp with nanofiber structue, rod-like, and ellipsoid-like morphologies were obtained, respectively [138]. Nathanael *et. al* reported the polyacrylamide (PAM)-assisted hydrothermal synthesis, which resulted in hierarchically arranged flower-like CHAp nanostructures [139]. Wang et. al. concluded, that the effect of the organic modifier on the particle size of the resultant CHAp nanorods depends on the interaction between the functional

groups present in the modifiers and the CHAp surface as well as the steric structure of the modifiers [140].

Recently, a novel hydrothermal synthesis route based on the liquid–solid–solution strategy has been developed by Wang et al. to synthesize surface-modified CHAp nanorods of various aspect ratios [98, 141]. According to this method, controlled growth of CHAp nanorods with tunable morphology can be acquired by properly tuning the interfaces between surfactants and the central atoms of CHAp. For this, linoleic acid and its corresponding sodium salts were chosen as anionic surfactants to complex with Ca^{2+} on the surface of CHAp [98].

Finally, nucleation and subsequent crystal growth can occur upon adding the calcium precursor and hydrothermal treatment, respectively. There are studies suggesting that the size and morphology of nanoparticles can be tailored by varying the synthesis conditions, including pH, hydrothermal temperature, and ratio of phosphate ions to the quaternary ammonium in the template [98].

2.4.5 Microwave irradiation

For oxide ceramics, microwave heating has been used for the last two decades but microwave sintering of phosphate ceramics is a relatively new proposition [142, 143]. Microwave sintering of calcium hydroxyapatite was first reported by Fang et al., demonstrating that microwave sintering ensures high density, better microstructure, and higher strength for CHAp with relatively shorter processing time compared to conventionally processed samples [144]. Microwave processing of CHAp can be conducted under either refluxing or hydrothermal conditions or even at atmospheric conditions with short time or long time irradiation (Fig. 11).

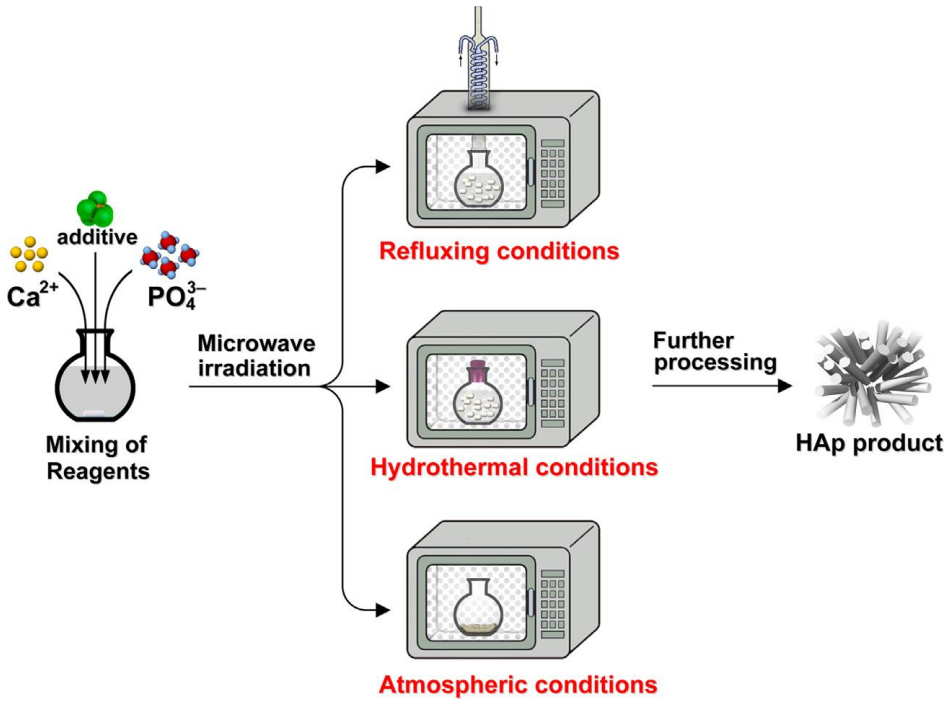

Figure 11. Schematic illustration of synthesis of CHAp through microwave irradiation [98].

Furthermore, several attempts have also been made to combine the microwave irradiation with solid-state, sonochemical, and solution combustion methods [98, 142, 143]. Notable advantages of microwave sintering are claimed to be shorter processing time and cost effectiveness in terms of energy savings [143]. Tarafder et al. achieved a significant increase in compressive strength of CHAp between 46% and 69% by microwave compared to conventional sintering as a result of efficient densification. Additionally, maximum compressive strengths of 10.95 ± 1.28 MPa and 6.62 ± 0.67 MPa were obtained for scaffolds with 500 μm designed pores (~ 400 μm after sintering) sintered in microwave and conventional furnaces, respectively [145].

2.5 CALCIUM HYDROXYAPATITE DERIVED FROM NATURAL SOURCES

With the ever-growing need to develop clean, non-toxic and environmentally friendly techniques, CHAp powders have been produced using biogenic raw sources like corals, seashells, fish and bovine bones, natural gypsum, eggshells,

etc. [146]. CHAp derived from natural products is proposed to be accepted better by the living organs, because of its physicochemical similarity to the human bone apatite [98]. The synthetic CHAp has a stoichiometric distribution of its components; therefore it does not have the same mineral traces of natural bone that play a significant role in the osteointegration process [147]. CHAp obtained from natural resources preserves some properties of the precursor material, such as pore structure (morphology), chemical composition as well as mechanical integrity [148].

Extraction of biominerals from biowastes is the most well-known method for the preparation of CHAp using biogenic sources. This is an interesting process, in particular, not only because of some superior characteristics of the extracted material, but also due to the economic and environmental benefits of waste recovery [98]. Detailed information on biological sources used in the production of CHAp as well as synthesis methods and characteristics of obtained CHAp product is provided in Table 6.

Table 6. Literature review on calcium hydroxyapatites derived from natural sources.

Biogenic Source	**Production method**	**Characteristics of CHAp product**	**References**
Eggshells			
Eggshells	Mechanochemical activation: ball milling and attrition milling	1. Crystalline CHAp. Impurities of CaO and Ca_3PO_4. 2. Ball milling: micrometer sized aggregated coarse grains with smooth surfaces. 3. Attrition milling: nanometer size grains.	[149], [150]
Hen's eggshells	Microwave irradiation	1. Nanocrystalline CHAp. 2. Platelets of length 33-50 nm and width 8-14 nm from TEM.	[151]
Chicken eggshells	Sol- gel precipitation method	1. Polycrystalline CHAp particles of high purity. 2. An average size of ~35 nm with a narrowly distributed particle size range from 5 to 90 nm.	[146]
Hen's eggshells	Chemical precipitation	1. Polycrystalline CHAp particles of high purity. 2. Thermally stable.	[152]
Marine organisms			

Seashells	Mechanochemical activation: ball milling and attrition milling	1. Crystalline CHAp. Impurities of CaO and Ca_3PO_4. 2. Ball milling: micrometer sized aggregated coarse grains with smooth surfaces. 3. Attrition milling: nanometer size grains.	[150]
Corals (*Porites* skeleton)	Hydrothermal conversion with and without the use of the mineralizer.	1. Direct conversion of aragonite into CHAp. 2. The presence of the mineralizer accelerated the conversion process.	[153]
Strombus gigas (conch) shells and Tridacna gigas (Giant clam) shells	Hydrothermal method	1. Dense CHAp structures were created at approximately 200°C. 2. In vivo tests of converted shell samples were performed in rat femoral defects for 6 weeks. 3. Histological study reveals that there is newly formed bone growing up to and around the implants. 4. Good biocompatibility and bioactivity of the converted shell implants.	[28]
Oyster shells	Solid state reactions through ball milling and subsequent heat treatment	1. CHAp with a small quantity of β-tricalcium phosphate (β-TCP). 2. By changing synthesis parameters pure CHAp could be obtained.	[154]
Red algae	Low-pressure hydrothermal process	1. CHAp was of high crystallinity and purity. $CaCO_3$ or β-TCP impurities depending on the processing temperature. 2. The micro-porous structure of the original algae.	[25]
Fish bones			
Cuttlefish bones	1. Drying. 2. Calcination (900°C). 3. Chemical precipitation.	1. Low crystallinity CHAp. 2. Needle like CHAp crystals.	[155]
Sword fish and tuna bones	Heat treatment	1. B type carbonated hydroxyapatite with higher Ca/P ratio. 2. Amount of carbonates is similar to carbonate content in human bones. 3. The presence of minor elements (Na, K, Mg and Sr) was found. 4. The in vitro cytotoxicity test assessed that all materials are non-cytotoxic.	[156]
Tilapia (*Oreochromis* sp.) scales	Enzymatic hydrolysis	1. High purity CHAp. 2. Nano- sized particles. 3. *In vitro* test confirmed that the resulting CHAp promote cell proliferation and differentiation.	[157]

Bones of birds and mammalians			
Bovine bone	1. Mechanical cleaning of the impurities and deprotonization by boiling. 2. Calcination (900°C). 3. Ball milling.	1. Highly crystalline CHAp. 2. Irregular shape particles; microporous structure with interconnecting pores.	[155]
Chicken femur bone	Chemical treatment followed by calcination	1. The nano CHAp particles with needle-shaped morphology. 2. CHAp sample was Ca-deficient with Na, Mg and carbonate substitutions. 3. Good solubility and resorbability, which are important for bone remodeling.	[158]
Bovine bone	Heat treatment (annealing)	1. High crystallinity and high purity of CHAp phase. 2. The organic compounds upon annealing at temperatures above 600 °C were completely removed from the matrices. 3. The interconnecting pore network being retained in the structure.	[159]
Bovine bone	Thermal decomposition	1. Pure CHAp of good crystallinity. 2. Nanorod shape hydroxyapatite with an average length of 300 nm.	[70]
Bovine bone	1. Subcritical water hydrothermal process 2. Alkaline hydrothermal process	1. Pure CHAp nanoparticles.	[70]
Vegetal Sources			
Catha edulis (Khat), basil, mint, green tea, trifolium	Washed and dried samples were annealed at at 600, 700 and 800°C	1. The existence of CHAp in C. edulis plants.	[160]
Biomolecular Templates			
1. Eggshells + grape peel 2. Eggshells + sweet potato peel 3. Eggshells + pomelo peel	Hydrothermal synthesis	1. Pure CHAp. Low crystallinity. 2. Aggregated particles with tiny needle-like or rod-like nanostructure were observed. 3. Needle-like nanostructures transformed into rod-like nanostructures and the aspect ratio decreased after hydrothermal reactions for 72 h.	[148]
1. Eggshells	Biomimetic synthesis	1. High purity nano-size CHAp.	[161]

+ orange peel 2. Eggshells + potato peel 3. Eggshells + papaya leaf 4. Eggshells + calendula flower extract			

The natural-biological origin CHAp have several important advantages, namely, worldwide availability in almost unlimited supply, low cost of raw materials, utilization of simple and inexpensive apparatuses, rapid and relatively efficient transformation from raw materials to CHAp.

2.6 PHYSICOCHEMICAL AND BIOLOGICAL PROPERTIES OF CALCIUM HYDROXYAPATITE

The present section will review the physical properties of synthetic CHAp as well as present general requirements for bone graft materials and suitability of CHAp for those applications.

2.6.1 Requirements for calcium hydroxyapatite as a bone graft material

The breakthrough in the nowadays development of bone substitute materials (BSM) was initially achieved by Barth and Ollier back in 19th century who carried out animal experiments in order to study different bone replacement materials for the first time [162]. Historically, autogenous bone grafts, allografts, and a variety of biomaterials have been used for the repair of osseous defects and the augmentation of compromised bone. Approximately 2.2 million bone graft procedures are performed worldwide annually to repair bone defects in orthopaedics, neurosurgery as well as in oral and maxillofacial surgery [163].

BSMs are required to repair segmental defects caused by the removal of infected tissue or bone tumors. In the context of large osseous augmentations, autogenous bone is still used as the preferred material, known as a “gold standart” [118, 163, 164]. However, the supply of autografts is limited and may lead to complications and morbidity at the donor site, because allogeneic tissue

bears the risk of infections and immune response (i.e. human immunodeficiency virus (HIV) or hepatitis B transmission is detrimental to the recipient) [74, 118]. Recent developments lead to innovative BSMs with new chemical, structural and subsequent biological properties that embrace a number of requirements to imitate the characteristics of the bone defect; therefore in certain clinical settings and appropriate indications a combination of BSM with living tissue/cells or BSM alone may be suitable. The current functions of BSM are as follows: (1) space maintenance for bone regeneration; (2) pre-setting of the desired anatomical shape; (3) supporting functions of the fibrous membrane of connective tissue covering bones as well as associated membranes; (4) stimulation of bone remodeling; (5) osteoconductive structural guidance for the regeneration of osseous tissue; (6) carrier substance for antibiotics, growth factors or approaches by gene therapy [163-170].

An ideal scaffold for bone tissue engineering is a matrix that acts as a temporary substrate supporting cell ingrowth and tissue development [118]. This occurs initially in vitro and eventually in vivo. The scaffold should be able to mimic the structure and biological function of the native extracellular matrix in terms of both chemical composition and physical structure [118, 163]. There is a number of rigorous requirements for an ideal BSM, as listed below [118, 163]: (1) biocompatibility: ensures the absence of toxicity, teratogenity or carcinogenicity; (2) osteoinduction and osteopromotion/osteoconduction: promotes growth, adhesion, proliferation and differentiation of bone cells; (3) mechanical support: provides stability under stress; (4) porosity: ensures the interactions of BSMs with the adjacent tissue structures promoting cell infiltration, bone growth and vascularization; (5) resorbability/degradability: assures bioactivity.

Since CHAp is chemically similar to the inorganic component of bone matrix, synthetic CHAp exhibits strong affinity to host hard tissues [118]. Chemical bonding with the host tissue offers CHAp a greater advantage in clinical applications compared to most other bone substitutes such as allografts or metallic implants [118, 171]. The main advantages of synthetic CHAp are its

biocompatibility, slow biodegradability in situ, and good osteoconductive and osteoinductive capabilities [118, 172]. A favorable atomic ratio of calcium phosphate-ceramics (Ca/P = 1.67) leads to an osteotropic interface mechanism, which means CHAp is a bioactive material that releases free calcium and phosphate ions in the organism, resulting in a micro-morphological anchorage of endosseous implants [163].

Nanosized CHAp particles are linked with a good cell attachments and cell growth of human osteoblasts [163, 173]. If the crystallite size of the CHAp ceramics is of nano-size (like in bone) and/or if there is carbonate incorporated, the biodegradation is strongly enhanced due to a higher solubility. Studies demonstrated that nanocrystalline CHAp powders exhibit improved sinterability and enhanced densification due to greater surface area, which may improve fracture toughness, as well as other mechanical properties [174]. Moreover, nano-CHAp, compared to coarser crystals, is expected to have better bioactivity [118, 175]. Thus, nano-CHAp particles can be utilized for engineered tissue implants with improved biocompatibility over other implants. It is worth mentioning, that nanotechnology has the potential to significantly benefit development of CHAp for biomedical applications [118].

2.6.2 Physical and mechanical properties of calcium hydroxyapatite

The biological behavior of CHAp ceramics depends on many factors, in particular, on their chemical and phase composition, microstructure, pore size, and pore volume. In surgery, use is made of both dense and porous ceramics, depending on the requirements for the bearing strength of implants. The key characteristics of dense ceramics are bending strength, tensile strength, and fracture toughness; detailed information on mechanical properties of dense CHAp are listed in Table 7 [176, 177].

Table 7. Mechanical properties of synthetic CHAp.

Mechanical properties of CHAp	Units	Comments
Bending strength	38–250 MPa	The large scatter is due to the random strength distribution and the effects of residual microporosity, grain size, impurities, etc. With increasing Ca:P ratio, the strength increases, reaches a peak at Ca:P ~1.67, and sharply decreases for Ca: P > 1.67
Compressive strength	120–150 MPa	
Tensile strength	38–300 MPa	
Weibull's Modulus	5-18	Characteristic of brittle materials
Decelerated crack propagation coefficient	26- 80 (in a dry atmosphere) 12 -49 (in a humid atmosphere)	Numbers indicate high sensitivity to decelerated crack propagation
Young's modulus (*E*)	35-120 GPa 44–88 GPa (in bending)	Significantly depends on the residual porosity and impurities
Vickers hardness (HV)	3-7 GPa	-
Superplasticity temperature	1000-1100°C	-
Fracture toughness (*KIc*)	0.8–1.2 MPa·$m^{1/2}$	It decreases almost linearly with increasing porosity (see Fig. 12)
Fracture energy	2.3–20 J/m^2	-

The low K_{Ic} and Weibull's modulus, coupled with the high sensitivity to decelerated crack propagation, reveal a relatively low reliability of articles made of dense CHAp ceramics (Fig. 12). Despite that fact, roots of teeth fabricated of dense CHAp ceramics were studied both in vivo and clinically [177-180]. The bonding between the gum and CHAp implant was comparable with the fixation of natural root cement [177, 178, 180]. Moreover, positive bonding was achieved between the implant and bone [177, 181]. These results are of significant importance because inadequate bonding leads to an increased mobility and, eventually, loss of teeth [177, 180]. Unfortunately, most of the loaded dental implants were destroyed within a year after implantation because of the low strength of the ceramic [177, 178]

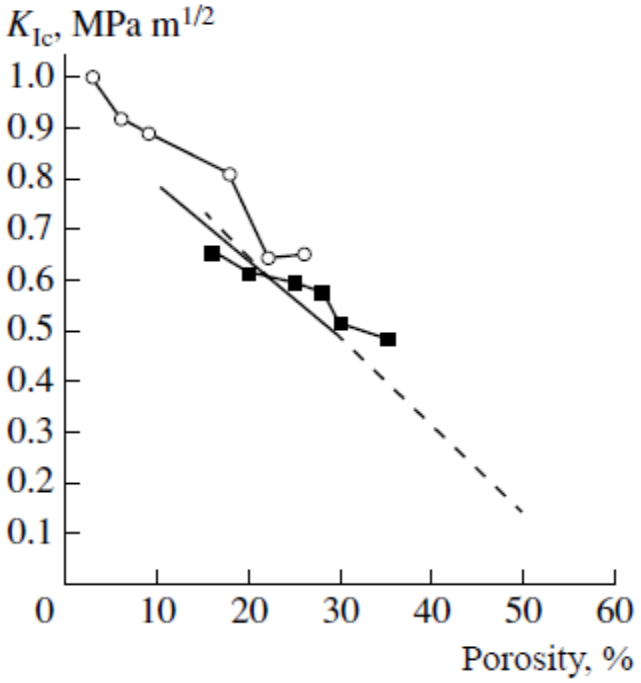

Fig. 12. Fracture toughness as a function of porosity for dense CHAp ceramics [176, 177].

Among the most important applications of dense CHAp ceramics are hypodermic devices for long-termambulant intestinal dialysis, monitoring of blood pressure and sugar, or optical examination of internal tissues [176]. Dense CHAp ceramics exhibit excellent biocompatibility with skin, significantly exceeding that of silicone rubber, which is widely used for these purposes [177].

For a number of applications, porous ceramics containing interconnected channel pores are more attractive. Porous ceramics have low strength and are, therefore, suitable for implantation into tissues which experience no substantial stresses (operations for the middle ear and some maxillofacial applications) and for local drug delivery [176]. Minimum pore size, required to enable ingrowth of the surrounding bone together with blood supply, is about 100 μm [177]. Pores of smaller size favor protein adsorption and adhesion of osteogenic cells [176]. Therefore, the pore-size distribution in porous ceramics should be bimodal. Pore morphology is of significant importance to the osteointegration process. Bending strength, compressive strength, and tensile strength of available porous CHAp implants are in the ranges of 2–11 MPa, 2–100 MPa, and 3 MPa, respectively

[177]. With increasing porosity, both strength and fracture toughness decrease dramatically (see Fig. 13 [177]). Studies report, that by changing pore geometry, it is possible to control the strength of the porous CHAp [176, 177]. More to add, porous CHAp ceramics is considerably less fatigue resistant than dense CHAp. However, the strength increases gradually when the bone grows into the porous network of the CHAp implant [176].

One more important property of CaP is its solubility in water, since the *in vivo* behaviour of CaPs can be predicted to a large extent by their solubility [182]. If the solubility of a CaP is less than the mineral part of bone, it degrades extremely slowly if at all. In case solubility of a CaP is greater than that of the mineral part of bone, it is degraded.

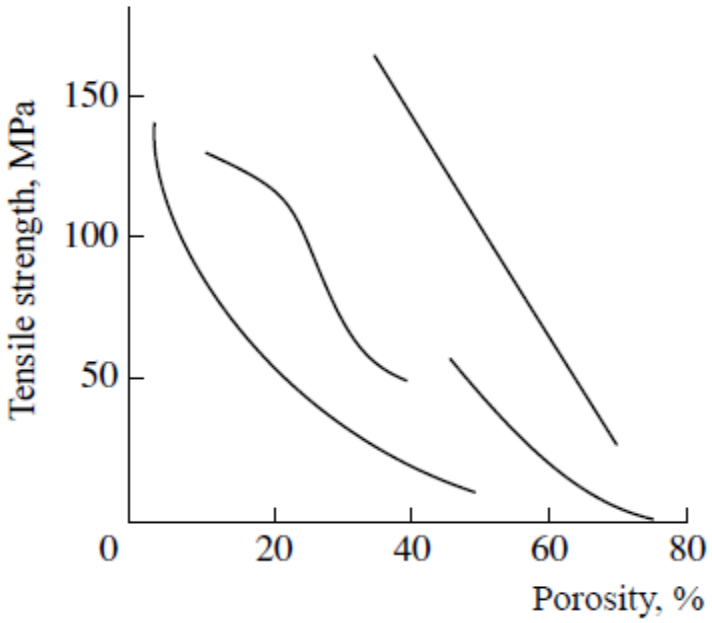

Fig. 13. Tensile strength as a function of porosity for CHAp ceramics [177]

The solubility of CHAp was studied already in 1978 [183]. It was calculated, that solubility product of a well-characterized sample of hydroxyapatite (Ca:P ratio of 1.664 ± 0.002) was constant over the pH range 4.56 to 9.67, ionic strength range 0.0003 to 1.03 and solid solution range 0.0625 to 5.55 g/250 ml in spite of non-stoichiometric dissolution of the solid [183].

The surface of a highly-soluble CaP can be reactive and may become covered with a poorly soluble CaP, hence reducing its degradation rate. In aqueous solutions and at ambient temperature (21ºC), the most important calcium phosphate salts may be identified. Factors affecting the solubility of CHAp include the method of preparation, the resultant crystallinity, density and the extent of ionic substitutions into the apatite lattice [184]. While the forming method and exact stoichiometry will have an effect on solubility, the generally accepted order of solubility of widely used CaPs at different pH is as shown in Fig 14, retrieved from [185].

Under normal physiological conditions (pH 7.2), CHAp is the stable calcium phosphate compound [186]. This can drop to as low as a pH of 5.5 in the region of tissue damage, although this eventually returns back to a pH of 7.2 over a period of time. Even under these conditions CHAp still remains a stable phase [186].

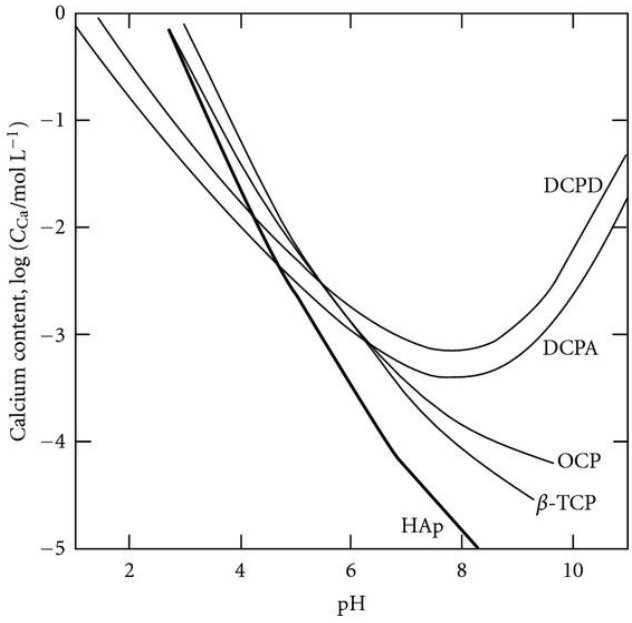

Figure 14. Solubility curves of calcium orthophosphate compounds at 37°C, depending on pH in aqueous solution. HAp: hydroxyapatite ($Ca_{10}(PO_4)_6(OH)_2$), TCP: tricalcium phosphate ($Ca_3(PO_4)_2$), OCP: octacalcium phosphate ($Ca_8H_2(PO_4)_6 \cdot 5H_2O$), DCPA: dicalcium phosphate anhydrous ($CaHPO_4$), DCPD: dicalcium phosphate dihydrate ($CaHPO_4 \cdot 2H_2O$).

3 EXPERIMENTAL

3.1 MATERIALS AND REAGENTS

The compounds for characterization, namely coral calcium, dairy calcium as well as beef bone derived calcium were received directly from manufacturers and they are listed in Table 8 below along with the characteristics provided by suppliers.

Table 8. Naturally derived calcium compounds.

Name of an ingredient	Company	Characteristics (provided by manufacturers)
Coral/sea-shells derived calcium		
Coral calcium powder	Coral LLC	Coral LLC only harvests pristine white fossilized coral heads which are protected beneath a layer of soil. After the pristine coral rocks are collected; they are taken to a cGMP certified grinding facility where it undergoes a three stage grinding process before purification. Eco Safe above sea coral minerals, do not contain pollutants such as high amounts of heavy metals, chemicals, fertilizers, etc. found in the contaminated oceans. The ingredient meets or exceeds the following standards: • US Pharmacopeia • Food Chemical Codex • European Pharmacopeia • California Proposition 65
Natural calcium carbonate	Coral LLC	High purity.
White oyster shell powder	Coral LLC	Oyster Shell Powder (OSP) is harvested from ancient oyster shell beds located in the Caribbean islands; hence it is white in color. The ingredient meets or exceeds the following standards: • US Pharmacopeia • Food Chemical Codex • European Pharmacopeia • California Proposition 65
Coral water	Coral LLC	When added to water, the mineral sachets are claimed to raise the pH of drinking water or beverage, to buffer chlorine antioxidant properties, to add ionic minerals.
Beef bone derived calcium		
MCH-Cal™ (Microcrystalline	Waitaki	MCH-Cal™ may also be known as

hydroxyapatite calcium)	Biosciences	MCHA, ossein hydroxyapatite, MCHC, or calcium hydroxyapatite. MCH-Cal™ features: • MCH-Cal™ is a natural, bone derived nutraceutical ingredient • MCH-Cal™ delivers the elements present in healthy bone tissue, in their physiological ratios • Minimum 24% Calcium and 10% Phosphorous in a microcrystalline structure • Minimum 22% bone protein, including Type I Collagen and bioactive growth factors to enhance absorption and promote bone formation • Contains a broad range of trace minerals as well as glycosaminoglycans found naturally in the bone matrix • Independent testing verifies very low levels of lead, making Waitaki's MCH-Cal™ compliant with Californian Proposition 65 requirements • MCH-Cal™ is manufactured from 100% New Zealand sourced bone from prime, export grade, free range, pasture fed beef • MCH-Cal™ is manufactured using proprietary low temperature processes to ensure maximum retention of the bioactive components.
Dairy derived calcium		
Capolac ®	Arla Foods Ingredients Group P/S	Capolac® MM-0525 BG is a natural milk mineral concentrate for calcium fortification of infant formula, child nutritional products and functional food and beverages. Calcium phosphate in Capolac® MM-0525 BG is similar to the calcium composition of teeth and bone.
Lactoval® HiCal	DMV International	Lactoval® HiCal is a natural milk mineral complex rich in calcium, phosphorus, and magnesium. It is made from milk via a state-of- art isolation process. Lactoval® HiCal contains high levels of minerals from milk, mainly in the form of calcium phosphate and citrate complexes. It has the following benefits: • Containing bio-available milk

		minerals, proven to be effective for healthy bones • Ca:P ratio of 2.20 : 1 contributes to efficient calcium absorption • Derived from a natural dairy source
CALCIANE ®	Lactalis Ingredients	CALCIANE is obtained from selected cheese whey through physical process. The micronised quality of CALCIANE is obtained due to the use of a micronisor that guarantees a very small and homogeneous particle size (<7μm). Features: • Bioavailable milk calcium, that plays a major role in bone growth , osteoporosis and fracture prevention • Provides an optimum Ca/P ratio, for a greater retention of calcium • The contribution of the milk minerals (Ca, Mg, et P)
Dairy powder	Fabelco	_
TruCal® milk calcium	Glanbia Nutritionals, Inc.	TruCal is a source of natural milk minerals. Bone is a dynamic system consisting of living cells embedded in a mineralized matrix including calcium, phosphorus, magnesium, potassium, zinc and copper. Minerals, such as those found in TruCal, are critical for the production of this matrix. Research has shown that TruCal is both readily absorbed and highly bioavailable. A human clinical study measured TruCal's impact in women (versus calcium carbonate) on two sensitive bone biomarkers – Urine Helical Peptide (bone resorption) and Bone Alkaline Phosphatase (bone turnover). Consumption of TruCal resulted in significantly lower UHP and BAP values, indicating a decreased loss of bone mass, and thus stronger bones.

The reagents used to produce CHAp from seashells as well as iron substituted CHAp are listed in Table 9. For these experiments *Macoma balthica* (*L.*) seashells collected from the seashore by the town of Palanga, Lithuania, were

used as a source of calcium. The seashells were mechanically cleaned and washed with boiling water until waters ran clear, then dried at room temperature for 24 h. In a following step, they were grinded in an agate mortar with subsequent milling to powders.

Table 9. List of reagents used for the synthesis of CHAp.

Reagent name	Chemical formula	Purity	Concentration	Producer
Ethylenediaminetetraacetic acid (EDTA)	$C_{10}H_{16}N_2O_8$	≥ 99 %	-	Sigma - Aldrich
Urea (carbamide)	CH_4N_2O	An. gr.	-	Eurochemicals Ltd.
Diammonium hydrogenphosphate	$(NH_4)_2HPO_4$	An. gr.	-	Eurochemicals Ltd.
Ammonium hydroxide	NH_4OH	-	25 %	Eurochemicals Ltd.
Nitric acid	HNO_3	-	66 %	Eurochemicals Ltd.
Iron(III) nitrate nonahydrate	$Fe(NO_3)_3 \cdot 9H_2O$	98–100 %	-	Fluka

3.2 SYNTHESIS AND ANALYSIS METHODS

For sol-gel synthesis, a stoichiometric amount of ammonium–hydrogen phosphate, $(NH_4)_2HPO_4$, and corresponding amount of seashell powders were used as P and Ca precursors, respectively. Seashells were firstly dissolved in an adequate amount of 2M HNO_3, and then the undissolved residue was removed by filtration using a Buchner flask and Buchner funnel. In order to obtain water-soluble calcium complexes and thereby avoid undesirable crystallization of calcium phosphates, ethylene diamine tetra-acetic acid (EDTA) as complexing agent was added to the seashell solution. The resulting mixture was stirred for 1 h at 70 °C. The pH of the reaction mixture was regulated within the range of 10.00–11.00 using ammonium hydroxide and maintained above 10 throughout processing. In the following step, $(NH_4)_2HPO_4$ was added to the solution under continuous mixing at the same temperature. As the last reagent urea was poured as a gelling and ammonium donor agent. After concentrating the solution by slow evaporation at 90 °C under stirring the Ca–P–O sol turned into a transparent gel.

The oven dried (100 °C) gel powders were ground in an agate mortar, annealed for 5 h at 800°C in air (heating rate was 1 °C/min); as a final step calcination was performed for at 1000 °C for 10 h in air (heating rate was 2 °C/min).

For the preparation of iron-substituted calcium hydroxyapatite, adequate amount of $Fe(NO_3)_3 \cdot 9H_2O$ was added to the filtrated seashell solution. Subsequent steps of the synthesis were identical to the ones described above.

To evaluate the decomposition behaviour of the organic matter and calcium carbonate present in seashells, the thermal analysis was carried out. The thermal decomposition of selected samples was analyzed through thermogravimetric and differential scanning calorimetric analysis (TG/DSC) using Perkin Elmer STA 6000 Simultaneous Thermal Analyzer. Dried sample of about 10 mg was heated from 30 to 900 $^{\circ}$C at a heating rate of 10 $^{\circ}$C/min in a dry air flow (20 ml/min).

The simultaneous TG/DSC thermogram of seashells (Fig. 15) shows a continuous weight loss from 600 °C to 810 °C, which can be associated with decarbonation of the samples. This conclusion is supported by the DSC analysis, which showed a small exothermic peak at about 800 °C. There was no weight loss between 810 °C and 995 °C indicating that all carbonates were completely removed at about 800 °C. Total weight loss associated with heat treatment of *Macoma balthica (L.)* seashell powders was calculated to be approximately 44%. Thus, the thermal analysis results confirmed once again, that the major compound presented in the investigated samples is $CaCO_3$. Calculations were based on TG data and the following reaction: $CaCO_3 \rightarrow CaO + CO_2$. From this equation the amount of $CaCO_3$ present in seashell powders was calculated for the estimation of Ca/ P ratio necessary for the synthesis.

The amount of Ca^{2+} present in the seashell powders was also evaluated using atomic absorption spectrophotometer (HITACHI 170-50, Japan). According to the results of this measurement, 99.5% of all the metals present in the seashells are Ca^{2+}.

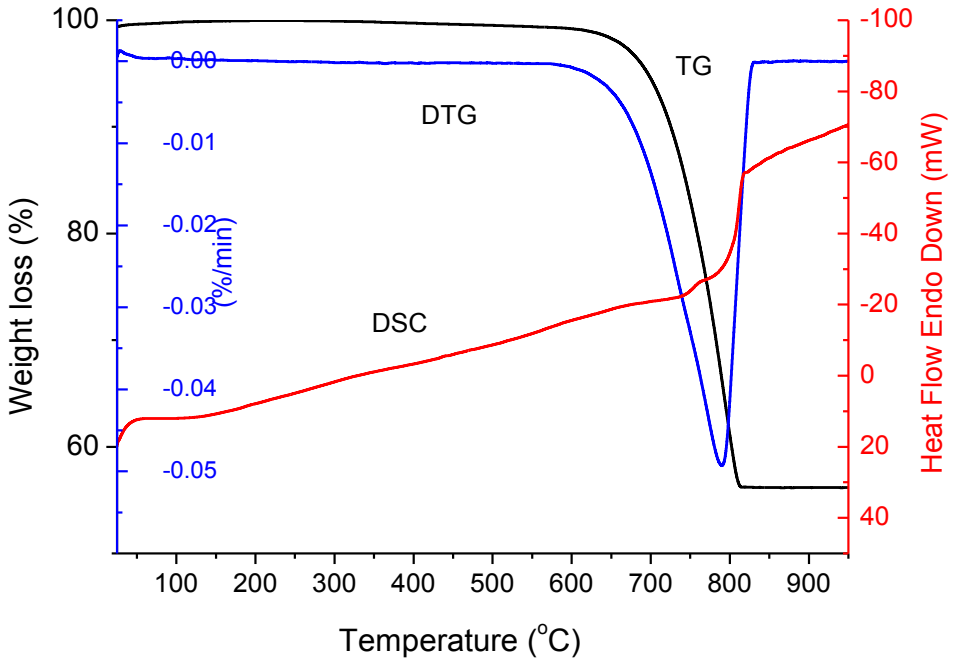

Figure 15. TG/DTG-DSC curves of seashell powders.

3.3 CHARACTERIZATION

The products of calcinations were investigated by infrared spectroscopy (FT-IR), X-ray powder diffraction (XRD) analysis and scanning electron microscopy (SEM). The IR spectra were recorded on FT-IR spectrometer (Frontier FT-IR, Perkin Elmer) with a resolution of 4.00 cm^{-1} at room temperature, which covers the wave number range of 4000-400 cm^{-1} to evaluate the functional groups of the samples. X-ray diffraction (XRD) pattern data were obtained at room temperature using powder samples in an Rigaku miniFlex II diffractometer operating with Cu $K_{\alpha 1}$ radiation (λ = 1.540562 Å). Intensity data were collected by the step-counting method (step size: 0.01, time per step: 0.06 s) between 10.000° to 70.000° (2 θ). The morphology of the prepared samples was examined using Hitachi SU-70 (Japan), with accelerating voltage 2 kV.

In order to evaluate the remineralization of enamel by using dairy derived CHAp, the samples were tested for 3 times and 10 minutes for each treatment. Fig. 16 shows the procedure of tooth remineralization.

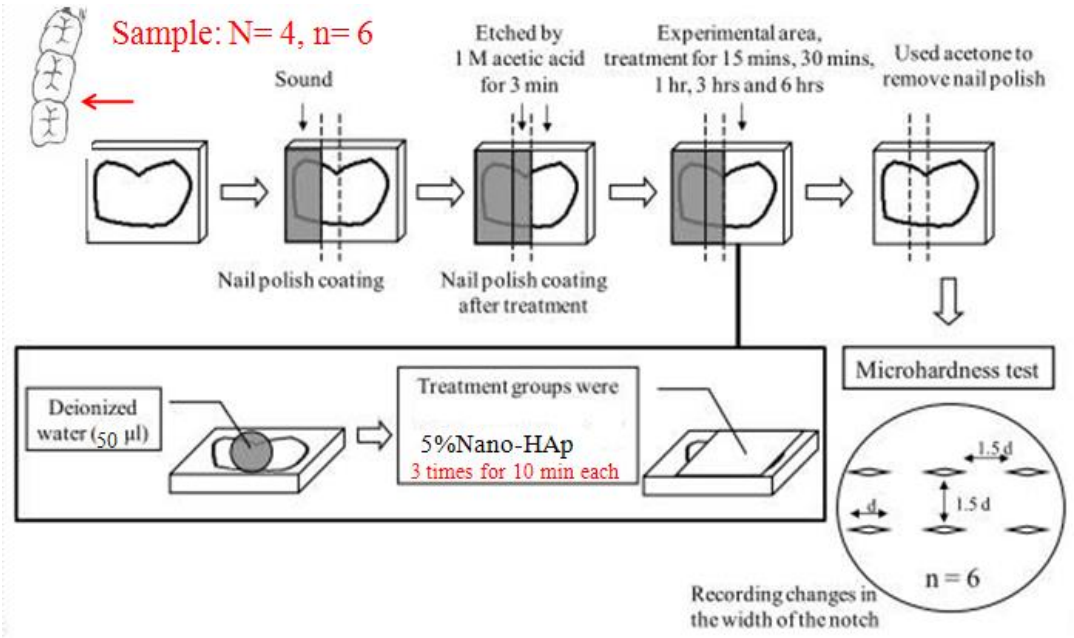

Figure 16. Tooth remineralization procedure.

Teeth remineralization was carried out from Eq (1).

$$\text{Remineralization (\%)} = \frac{KHN_{Treated} - KHN_{Etched}}{KHN_{Sound} - KHN_{Etched}} \times 100 \quad (1)$$

4. RESULTS AND DISCUSSIONS

4.1 CHARACTERIZATION OF NATURALLY DERIVED CALCIUM COMPOUNDS USED IN FOOD INDUSTRY

Calcium compounds for this study were selected from the ones that are already used in food and food supplements industry. All samples are derived from natural sources and their brand names as well as manufacturers are introduced in section 3.1. Samples were divided into three categories: coral/sea-shell calcium, beef bone calcium and dairy calcium.

The XRD patterns of coral and sea shell derived samples are shown in Fig. 17.

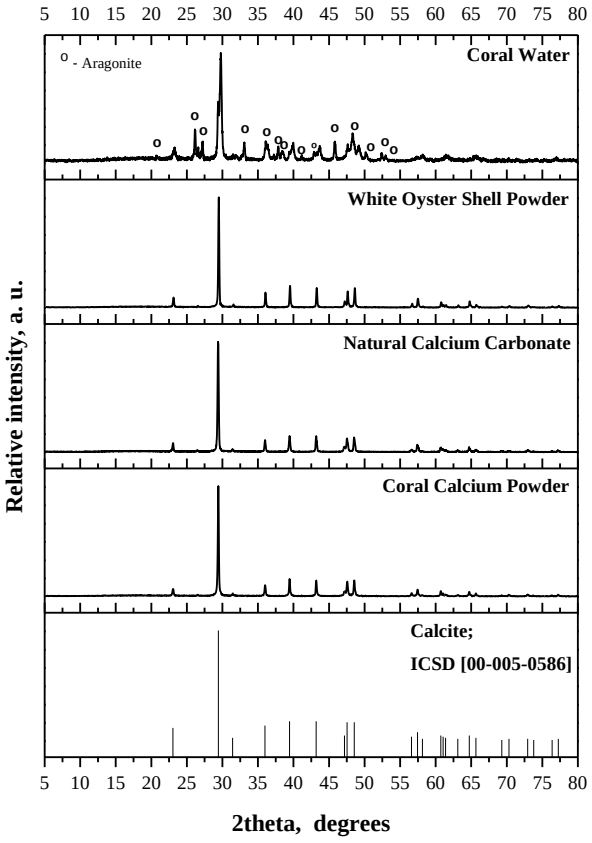

Figure 17. XRD patterns of coral and sea- shell derived samples.

The obtained *d* spacings were compared with the standard data (ICSD). It can be seen that only one component of *Coral calcium powder* sample is a calcium carbonate in the form of calcite with rhombohedral crystal system. The XRD pattern of *Coral water* implies that the major compound present in this sample is

calcite as well. However, aragonite phase was also determined. XRD pattern of *White oyster shell powders* indicates that dominating crystal phase in this sample is calcium carbonate as well. According to XRD results the predominant compound in coral and sea-shell derived sample is calcite, however, in the sample of *Coral water* aragonite phase is also present.

The FTIR spectra of the corresponding coral and sea-shell derived compounds are presented in Fig. 18.

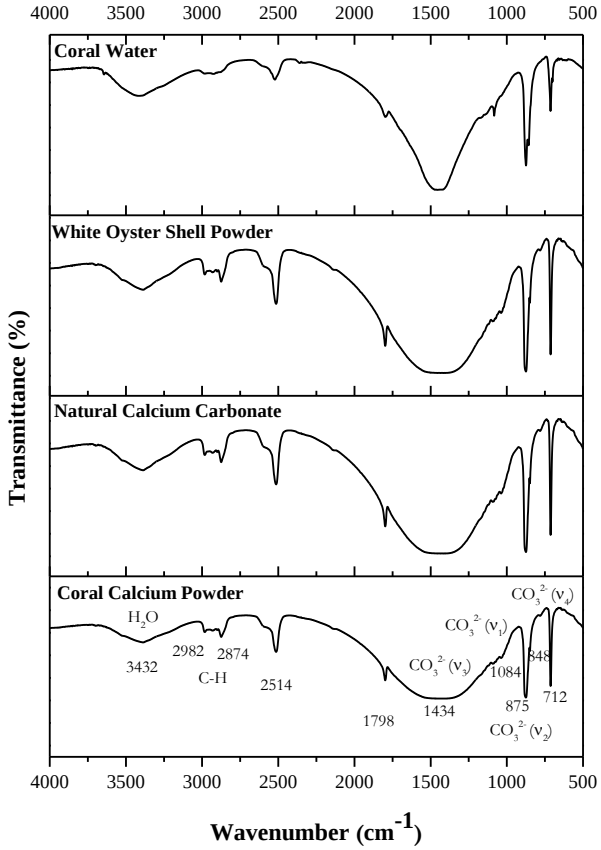

Figure 18. FTIR spectra of the corresponding coral and sea-shell derived compounds.

As seen all spectra are almost identical, confirming that the predominant compound is an ionic carbonate. The corresponding characteristic bands of stretching vibrations of CO_3^{2-} are at 1084 cm^{-1} (ν_1), 875 cm^{-1} (ν_2), 1434 cm^{-1} (ν_3) and 712 cm^{-1} (ν_4) [187-189]. The observed non-split peaks ν_2 and ν_4 in the FTIR spectra indicate the presence of calcite, if splitting occurs, the aragonite phase is present. Band assigned to the adsorbed water is also present at 3432 cm^{-}

[1]. The absorptions observed between 3000 and 2870 cm^{-1} are due to vibrations of aliphatic C-H. The splitting of the 712 cm^{-1} band is characteristic only to aragonite phase.

The SEM micrographs of the corresponding coral and sea-shell derived compounds are presented in Fig 19.

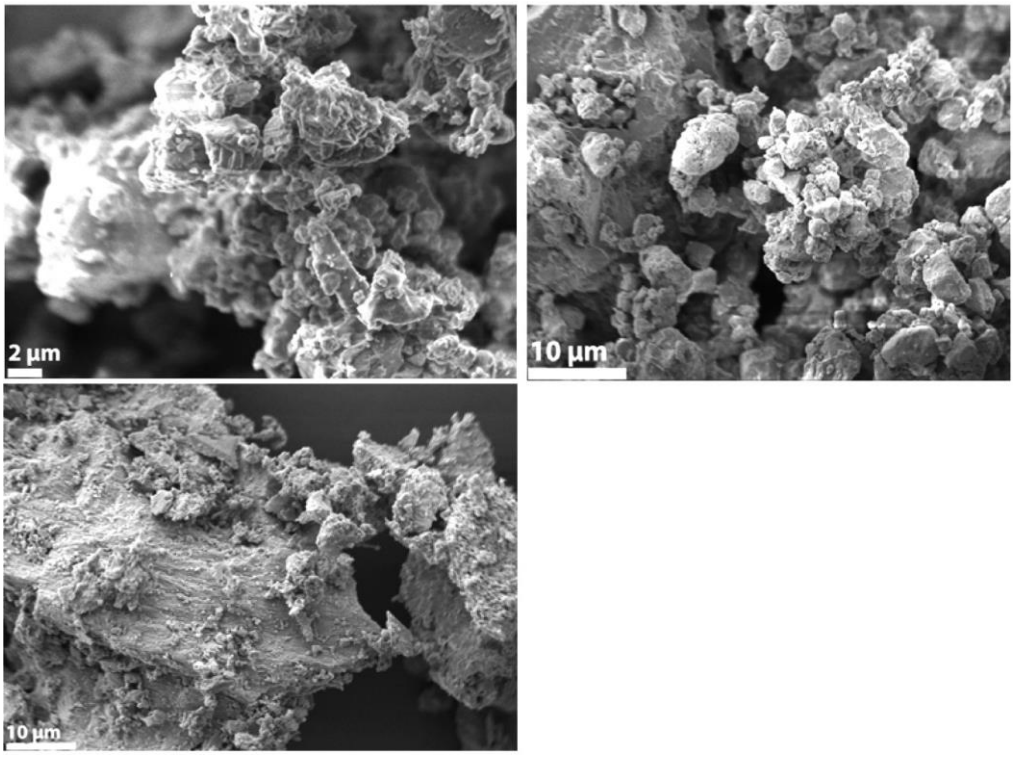

Figure 19. SEM micrographs of *Coral calcium powders* (top, left), *White oyster shell powders* (top, right) and *Coral water* (bottom).

As seen from Fig. 19 (top, left), the *Coral calcium powders* consist of the irregular shaped particles with a size of 5–10 µm forming porous agglomerates. The powders show essentially a mixture of particles of different sizes, whereas each particle is an assembly of numerous distinguishable angular grains with the size between approximately 5 and 10 µm. It is obvious that *White oyster shell powders* (Fig. 19; top, right) consist of grain shaped particles with size of 2–10 µm tend to form porous agglomerates. SEM image of *Coral water* (Fig. 19, bottom) indicates that this sample consists of plate shape particles with a size of approximately 1–10 µm. It can be also observed that the particles form rigid agglomerates. In principle, very similar surface morphology was determined for all three investigated samples.

TG/DTG and DSC curves of coral and sea shell specimens are almost identical. So, only TG/DTG and DSC curves for the representative coral calcium are shown in Fig. 20.

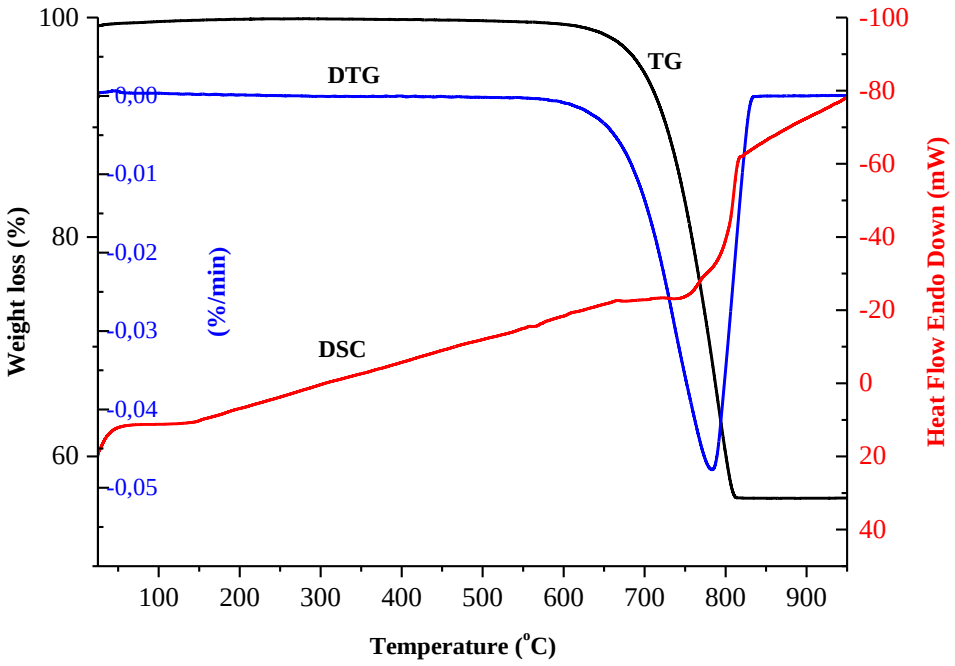

Figure 20. TG/DTG-DSC curves of *Coral calcium powders*.

From 600 °C to 810 °C a continuous weight loss was observed, which can be associated with decarbonation of the samples. This conclusion is supported by the DSC analysis, which showed a small exothermic peak at about 800 °C. There was no weight loss between 810 °C and 995 °C indicating that all carbonates were completely removed at about 800 °C. Total weight loss associated with heat treatment of coral calcium was calculated to be approximately 44%. Thus, the thermal analysis results confirmed once again, that the major compound presented in the investigated samples is $CaCO_3$. Calculations were based on TG data and the following reaction: $CaCO_3 \rightarrow CaO + CO_2$. Concluding from the obtained results there could be stated that limited usage of coral and sea-shell derived sample powders in food fortification due to their low solubility. Therefore these calcium compounds mainly could be used in food supplements.

It is well known, that the chemical composition of dairy derived calcium compounds highly depends on the isolation (extraction, filtration, precipitation, etc.) method used by the company. The XRD patterns of dairy derived powder samples are shown in Fig. 21.

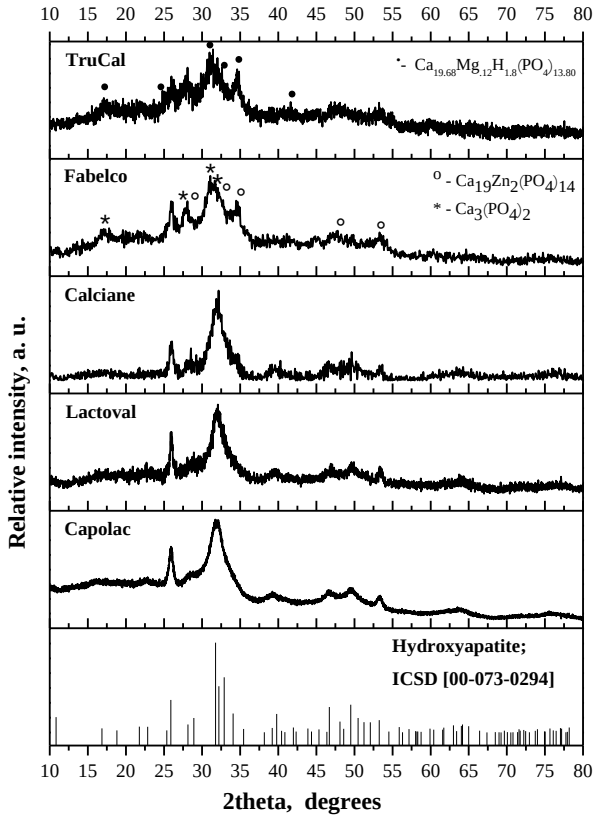

Figure 21. XRD patterns of dairy derived samples.

It is evident that the main crystalline component in all the samples is calcium hydroxyapatite (ICSD [00-073-0294]). However the obtained XRD patterns have well-pronounced backgrounds. This observation let us to conclude that samples consist an amorphous phase along with crystalline. In the sample which named *TruCal* the calcium magnesium hydrogen phosphate was identified, whereas in *Fabelco* calcium zinc phosphate along with tricalcium phosphate are present.

FTIR spectra of the corresponding dairy derived compounds are shown in Fig. 22.

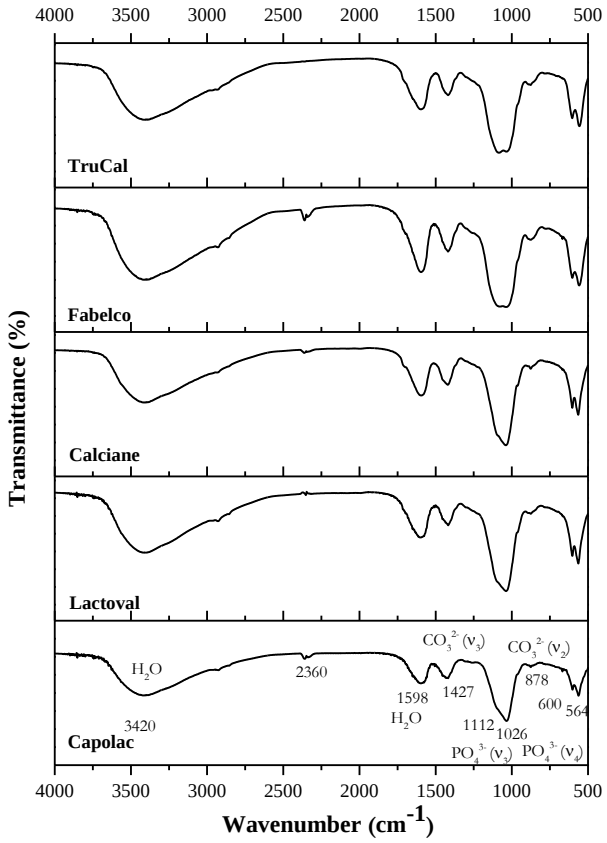

Figure 22. FTIR spectra of corresponding dairy derived compounds.

All FTIR spectra are almost identical as well. The absorption bands of significant intensity located at 1026 cm $^{-1}$ and 1112 cm $^{-1}$ could be attributable to the factor group splitting of the ν_3 fundamental vibration mode of the PO_4^{3-} tetrahedral. The bands observed at 956-960 cm^{-1} and doublet at 564-600 cm $^{-1}$ correspond to ν_1 and ν_4 symmetric P-O stretching vibration of the PO_4^{3-} ion, respectively [129, 190-193]. FTIR analysis also indicated that the apatites present in dairy samples were carbonated hydroxyapatites. Characteristic band from inorganic carbonate ion is present at 1427 cm $^{-1}$. The ν_3 carbonate bands at 1427 cm^{-1} and the ν_2 mode at 878 cm^{-1} correspond to carbonated calcium hydroxyapatite [187, 193], i.e., OH^- substituted by CO_3^{2-}. Broad band located at 3600-3350 cm $^{-1}$ as well as the band cantered at ~1600 cm $^{-1}$ correspond to O-H vibrations from adsorbed water on the surface [129].

The SEM micrographs of dairy samples are shown in Fig 23.

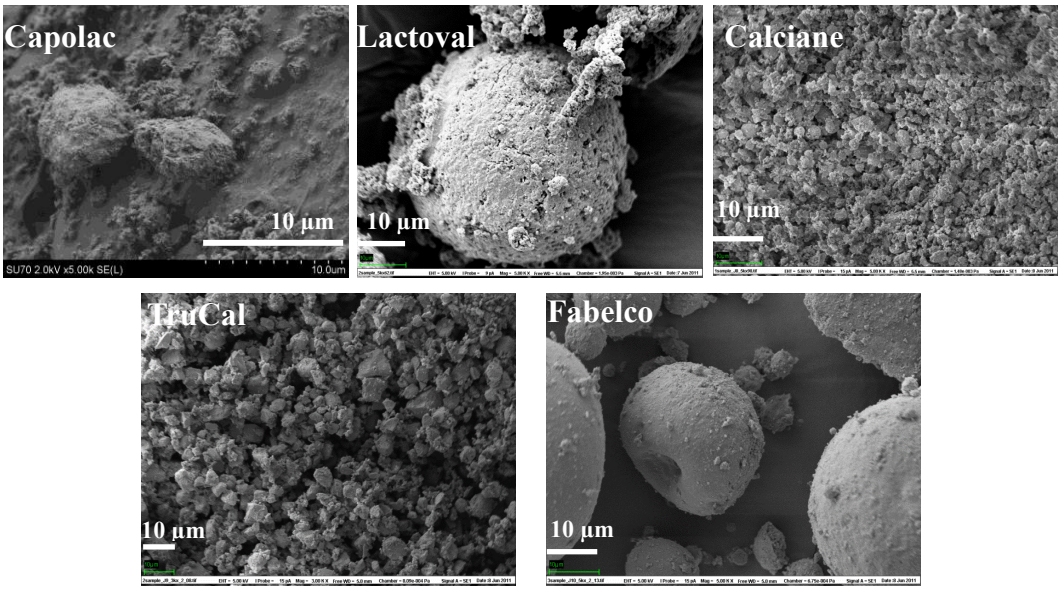

Figure 23. SEM micrographs of as-received dairy derived samples.

It could be observed that *Capolac* sample contains particles with size from 1 to 5 µm evenly distributed on the surface. From EDX measurement the Ca/P ratio was calculated to be 1.9 for this sample. EDX measurement also revealed that there are other elements present in the sample, e.g. magnesium (0.6 %). *Lactoval* consists of porous spherical particles with size of 10-15 µm. Ca/P ratio was calculated to be 1.92 for this sample. EDX measurement also indicated that this compound contains 0.45 % magnesium. Grain shape angular particles with the size of approximately 2-5 µm are observed in the SEM images of both *Calciane* and *TruCal*. Again, from EDX measurements the Ca/P ratio was calculated to be 1.7 (*Calciane*) and 1.51 (*TruCal*). These samples also contain minor amount of magnesium 0.98 % (*Calciane*) and 1.2 % (*TruCal*). *Fabelco* particles are spherical with the size of 10 µm. From EDX measurements the Ca/P ratio was calculated to be 1.5. This sample contains 0.6 % of magnesium as well. Thus, dairy derived calcium compounds have higher solubility and could be widely used for the enrichment of food (dairy products, beverages, biscuits, ice cream, etc.) as well as in food supplements.

Main advantage of dairy derived calcium compounds is the presence of CHAp which has been clinically tested for the prevention of osteoporosis [194].

Fig. 24 presents the XRD pattern of bovine bone derived sample.

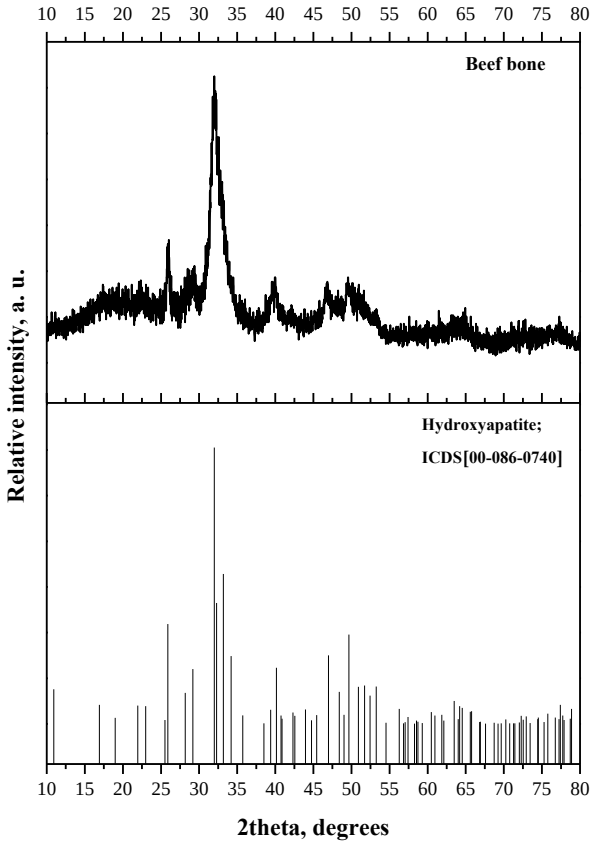

Figure 24. XRD pattern of beef bone derived sample.

It shows the presence of nanocrystalline calcium hydroxyapatite (ICSD [00-086-0740]) in the bone matrix.

The FTIR spectrum of beef bone sample is shown in Fig. 25. It indicates the presence of ionic phosphate (PO_4^{3-}), hydroxyl (OH^-) and carbonate (CO_3^{2-}) groups in the sample. Moreover N-H stretching band around 2927 cm^{-1} and amide bands at 1506 cm^{-1} were also observed [25, 74, 159]. These two bands are characteristic to macromolecules of protein in the bovine bone matrix, collagen in particular.

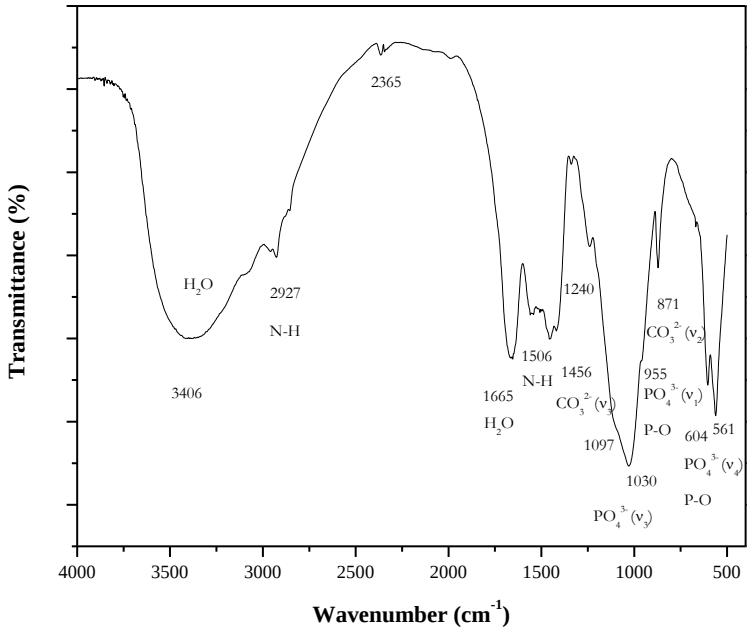

Figure 25. FTIR spectrum of beef bone derived sample.

Fig. 26 shows the representative SEM picture of as received bovine bone. The microstructure of this sample appears to be dense due to the presence of organic substances in beef bone matrix.

Since beef bone derived calcium material predominantly is composed of calcium hydroxyapatite with microcrystalline structure, it mainly could be suggested for usage in food supplements.

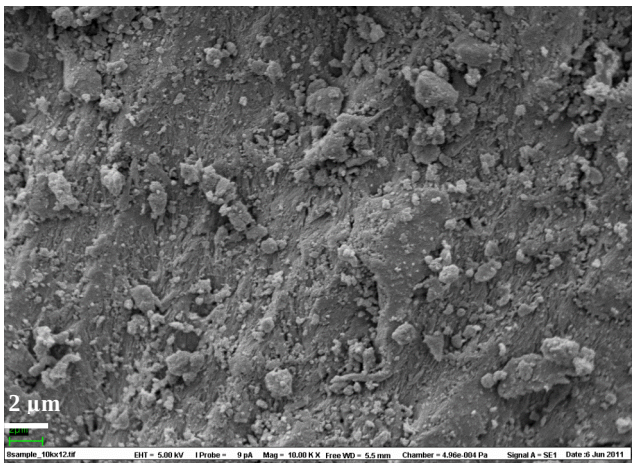

Figure 26. SEM micrograph of as-received bovine bone.

4.2. CALCIUM HYDROXYAPATITE/ WHITLOCKITE OBTAINED FROM DAIRY PRODUCTS

In this part of dissertation the results on the synthesis and characterization of calcium hydroxyapatite and whitlockite ($Ca_{18}Mg_2H_2(PO_4)_{14}$) composite obtained from dairy product are presented. Dairy calcium powder (DCP) under the trade mark *Capolac* was provided by industrial collaborator, Arla Foods Ingredients (Denmark), producing milk calcium on a large-scale and using state-of-the-art methodology and purification treatment. DCP consisted of calcium phosphopeptide/citrate mixture. In the laboratory calcium containing compound can be precipitated from whey permeate applying adequate pH and temperature. Previous studies suggested that the most efficient conditions are at pH = 8 and 50 °C temperature. The precipitate then is collected using membrane filtration and dried [195]. According to the information provided by the DCP manufacturer, the main constituents of as-received DCP samples were calcium (24 %), phosphorus (12.5 %) and magnesium (0.6 %).

4.2.1 X- ray diffraction analysis

The XRD patterns of the DCP powders sintered at the temperatures ranging from 700 to 1000 °C are presented in Fig. 27. As seen, the broad bumps observed in the XRD patterns of as-received DCP samples (Fig. 21, *Capolac*) completely disappeared during the heat treatment. Thus, all organic materials were removed and amorphous substances were transformed to the crystalline ones upon heating at elevated temperatures and only crystalline phases have formed. Surprisingly, two crystalline phases were identified in all samples, namely calcium hydroxyapatite and calcium magnesium hydrogen phosphate $Ca_{18}Mg_2H_2(PO_4)_{14}$, whitlockite (ICSD [00-070-2064]) having rhombohedral crystal system. The formation of whitlockite as secondary phase was rather unexpected despite the starting powders contained about 0.6 % of magnesium. On the other hand, the formed biphasic $Ca_{10}(PO_4)_6(OH)_2$ and $Ca_{18}Mg_2H_2(PO_4)_{14}$ composite could be even more useful for biomedical, structural and environmental applications [196-198].

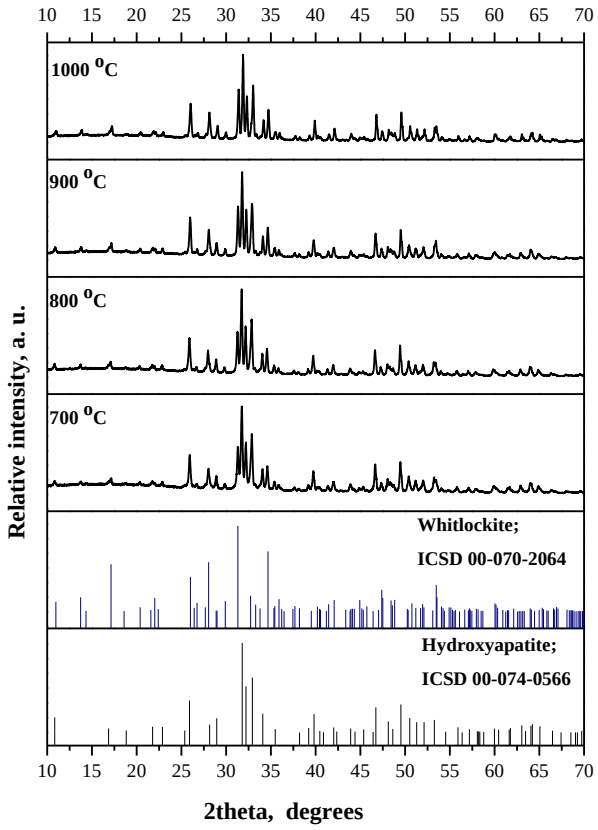

Figure 27. XRD patterns of DCP powders annealed at different temperatures.

Finally, the XRD analysis results show that phase composition and crystallinity of the end product are independent on the used synthesis temperature (700-1000 °C). No any phase transformations could be detected with increasing annealing temperature. Thus, the temperature of 700 °C is sufficient to obtain highly crystalline CHAp with impurity of whitlockite from dairy calcium powders.

4.2.2 EDX analysis

The Ca/P molar ratios of samples were calculated relying on EDX measurements and they are as follows: 1.57 (700 °C), 1.58 (800 °C), 1.54 (900 °C) and 1.51 (1000 °C). For stoichiometric calcium magnesium hydrogen phosphate (whitlockite) and CHAp, the Ca/P ratios are 1.29 and 1.67, respectively. As seen, for the obtained biphasic composite powders the Ca/P ratio is between 1.29 and 1.67. Therefore, the EDX analysis data confirmed that the

samples are composed of two phosphates, where the main crystalline phase is CHAp. These results correlate very well with XRD analysis data (53.3 % CHAp and 46.7 % whitlockite). Moreover, the EDX measurements confirmed the presence of magnesium in all of the samples. It was estimated that the amount of Mg is approximately of 0.56 %.

4.2.3 FTIR spectroscopy

The FTIR spectra of heat-treated samples are shown in Fig. 28.

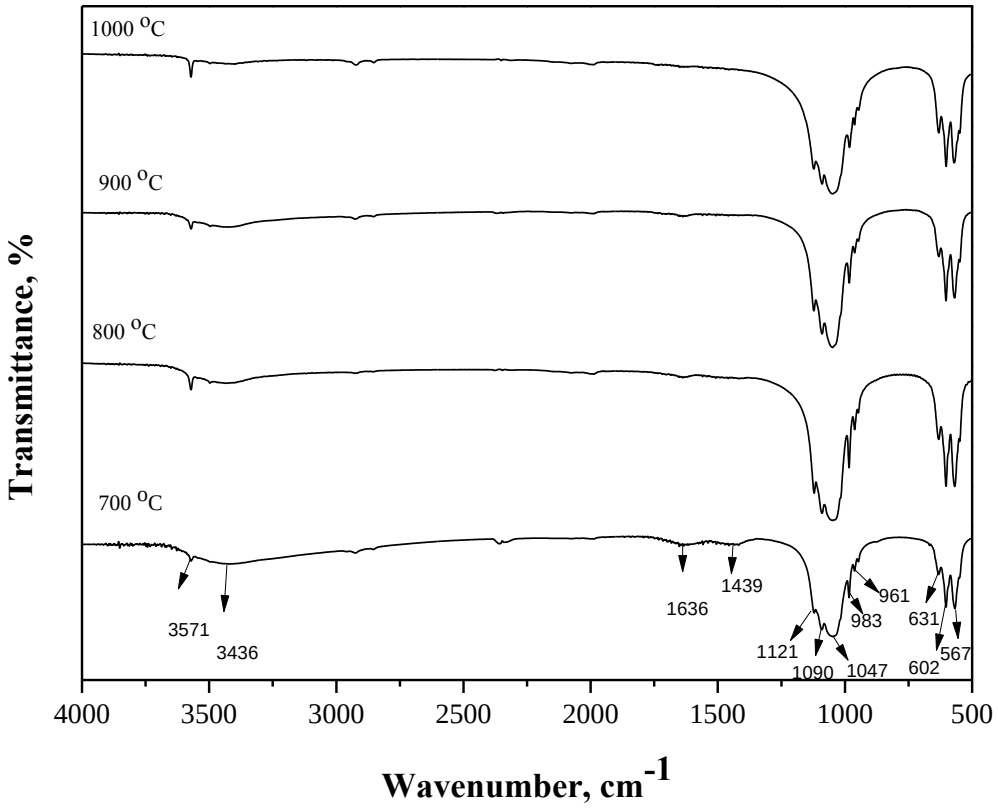

Figure 28. FTIR spectra of DCP powders annealed at different temperatures.

All samples exhibit characteristic stretching and vibration modes of OH^- groups at 3571 cm^{-1} (ν_S) and 631 cm^{-1} (ν_L), whereas the internal modes corresponding to the PO_4^{3-} groups occur at 1090 and 1047 cm^{-1} (ν_3), 961 cm^{-1} (ν_1), 602 and 567 cm^{-1} (ν_4) corresponding to that of CHAp [151]. The bands at 3436 and 1636 cm^{-1} correspond to adsorbed H_2O while band at 1439 cm^{-1} is that

of CO_3^{2-} ions which suggests incorporation of carbonate ion in synthesized CHAp [187, 193]. However, the later band is present only in the sample heated at 700 °C. In the samples heated from 800 to 1000 °C this band is absent. The band located at 1121 cm^{-1} has been confirmed to arise from protonated phosphate groups [152]. Origin of the band at 983 cm^{-1} probably is from PO_4^{3-} ions presented in non-apatitic/non-stoichiometric environment [199]. A band at ~631 cm^{-1} arising from OH^- vibration becomes more intense and greater-resolved with increasing the heating temperature. This evolution indicates higher crystallinity for the materials heated at higher temperatures [152].

4.2.4 SEM analysis

Fig. 29 shows the SEM micrographs of DCP powders annealed at different temperatures. Evidently, the particle size of synthesis products increases gradually with increasing annealing temperature. SEM analysis indicated that CHAp sample obtained at 700 ^oC consists of plate-like crystals with size of ~0.5 μm which are covered with prolonged tiny spherical particles less than 200 nm. However, with increasing temperature up to 800 ^oC the "necked" to each other spherical particles have formed. There were larger aggregates of tiny particles and the aggregates did not possess any definite shape. The larger aggregates (2-5 μm) with similar morphological features have formed at 900 and 1000 ^oC. In general, it can be observed that particle size of dairy derived CHAp is highly dependent on the heating temperature. Moreover, the SEM micrographs also demonstrate that formed biphasic $Ca_{10}(PO_4)_6(OH)_2$ and $Ca_{18}Mg_2H_2(PO_4)_{14}$ composite tends to form highly porous agglomerates. The powders show essentially a mixture of particles of different sizes, whereas each particle is an assembly of numerous distinguishable round particles with different size which is dependent on synthesis temperature.

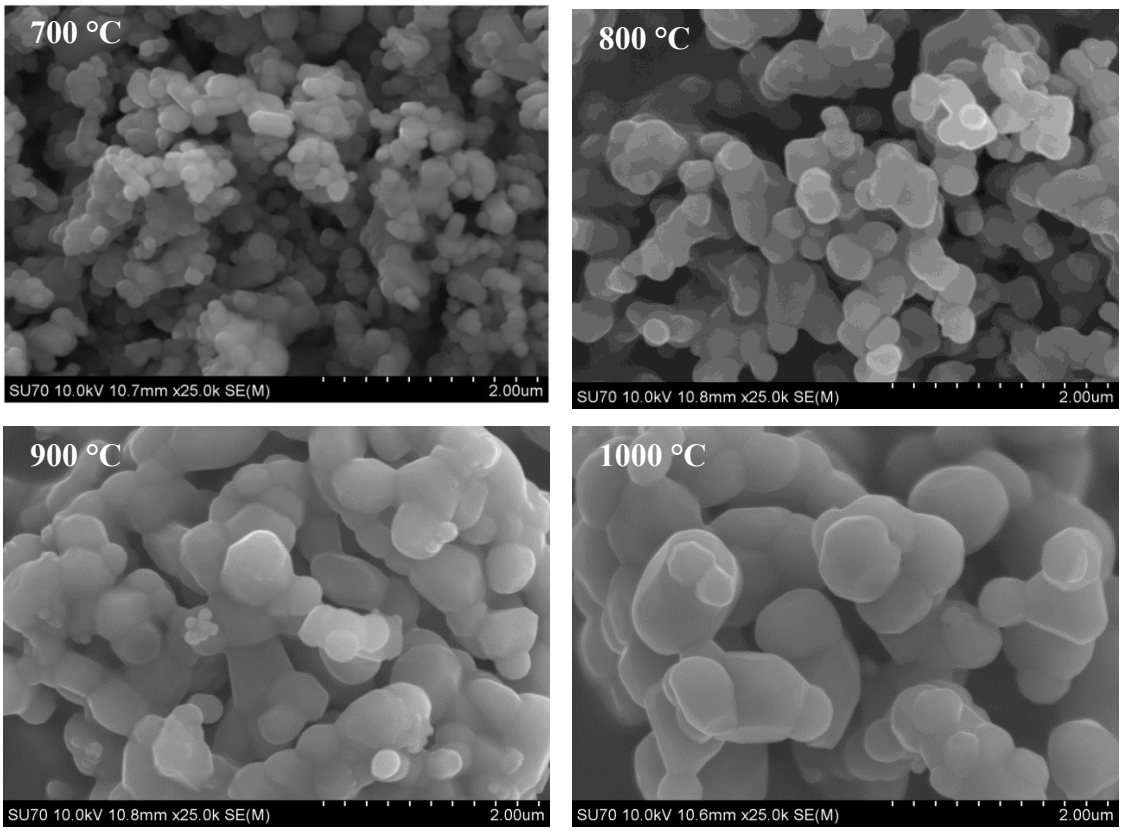

Figure 29. SEM micrographs of DCP powders annealed at different temperatures.

4.2.5 Remineralization studies

In order to evaluate the remineralization of enamel, ball-milled calcium hydroxyapatite and whitlockite composite was applied on the surface of teeth samples for 3 times and 10 minutes for each treatment (Fig. 30).

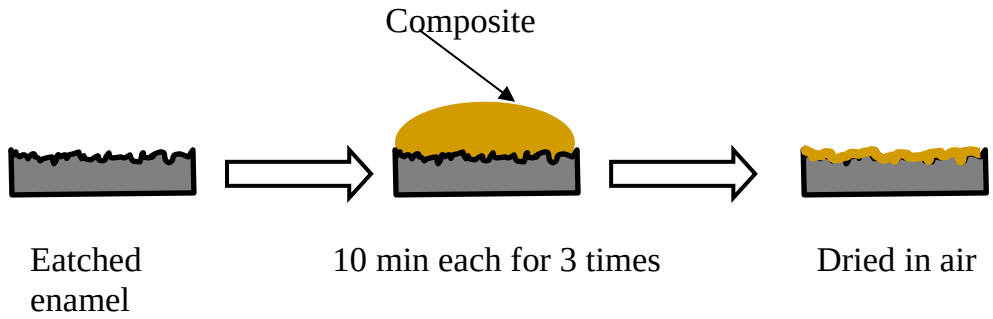

Figure 30. Scheme of preparation samples for remineralization test.

However, the remineralization of the teeth using calcium hydroxyapatite and whitlockite composite was rather pure. For example, the remineralisation after 10

min was achieved only 1.62±0.76%, after the second 10 min was 0. 92±0.61 and finally after third 10 min was 1.50 ±0.88. Thus, the successfully developed composite composed of calcium hydroxyapatite and whitlockite cannot be effectively used directly for teeth remineralization. However, further modification of this composite and possible application *for* teeth remineralisation is still under investigation.

4.2.6 Conclusions

Dairy calcium powders (DCP) provided by industrial collaborator and obtained by precipitation from whey permeate have been characterized. The results of XRD analysis and FTIR spectroscopy showed that the main crystalline component of the heated at different temperatures DCP is calcium hydroxyapatite $Ca_{10}(PO_4)_6(OH)_2$. However, as-received DCP sample mostly consisted of an amorphous phase along with the minor amount of crystalline phase. Highly crystalline biphasic calcium phosphate mixture (CHAp/whitlockite) was obtained from the initial DCP powders by heat treatment in the temperature range of 700-1000 °C. The SEM micrographs of DCP powders annealed at different temperatures confirmed evidently that the particle size of synthesis products increases with increasing annealing temperature. Moreover, the SEM micrographs also demonstrated that formed biphasic $Ca_{10}(PO_4)_6(OH)_2/Ca_{18}Mg_2H_2(PO_4)_{14}$ composite tends to form highly porous agglomerates. In conclusion, a novel simple, environmentally benign and green preparation technology for calcium phosphates (CHAp/whitlockite) was proposed.

4.3. SUSTAINABLE CHEMICAL PROCESS FOR THE SYNTHESIS OF CALCIUM HYDROXYAPATITE FROM SEASHELLS

In this part, high purity crystalline CHAp was produced from seashells collected along the Palanga coastline using environmentally friendly sol-gel synthesis route. Based on the results of TG analyses performed with the seashells (described in the section 3.2, Fig. 15), there was decided to conduct an experiment using four different amounts of seashells. For that the following assumptions were made:

a) 1. 05 g of seashells equals to 1 g of $CaCO_3$ (sample A);

b) 1. 1 g of seashells equals to 1 g of $CaCO_3$ (sample B);

c) 1. 15 g of seashells equals to 1 g of $CaCO_3$ (sample C);

d) 1.2 g of seashells equals to 1 g of $CaCO_3$ (sample D).

4.3.1 X- ray diffraction analysis

XRD patterns of the powders sintered at temperatures using different amount of seashells are presented in Fig. 31. The d spacings were compared with the standard data (ICSD). X-ray diffraction pattern of the sample A indicates clearly that pure crystalline phase of calcium hydroxyapatite ($Ca_{10}(PO_4)_6(OH)_2$, ICSD [00-009-0432]) with hexagonal crystal system was obtained.

The CHAp is the main crystalline phase in the sample B as well. However, the minor amount of side CaO (lime; ICSD [00-037-1497]) phase has also formed. As seen from X-ray diffraction patterns, with increasing the amount of sea shells (they act as a precursor of calcium ions) in the precursor used for the synthesis (samples C and D), the amount of secondary phase of calcium oxide increases (the characteristic diffraction peak of CaO becomes more and more pronounced). From these data, we can conclude that when increasing the amount of seashells in the starting precursors, the stoichiometry of main elements in the final product was lost. Therefore, for further investigations different CHAp specimens were prepared using sample A.

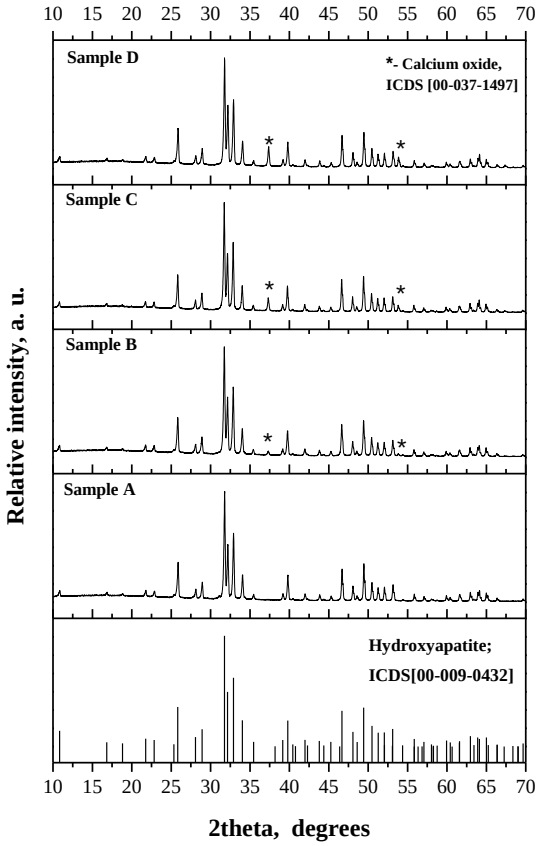

Figure 31. The XRD patterns of corresponding CHAp samples using seashells as calcium source for the preparation of CHAp.

4.3.2 FTIR spectroscopy

The FTIR spectra of corresponding CHAp samples are shown in Fig. 32. The same applies to the doublet at 571-602 cm^{-1}; it corresponds to ν_4 symmetric P-O stretching vibration of the PO_4^{3-} ion [129, 190-193]. Band in the area of 1988 cm^{-1} is assigned to asymmetric (ν_3) stretching mode of P-O in PO_4^{3-}. There are two shoulder peaks at 632 cm^{-1} and 3572 cm^{-1} present in all four spectra. They are typical stretching vibration and bending modes of CHAp's structural OH^- group. As the amount of seashells used for the synthesis increases, the band of OH^- at 3572 cm^{-1} gradually increases in its intensity. This can be attributed to the increase of CHAp's crystallinity. Broad band located at 3452 cm^{-1} as well as the band cantered at 1643 cm^{-1} reflecting H_2O adsorbed on the surface are also observed [129].

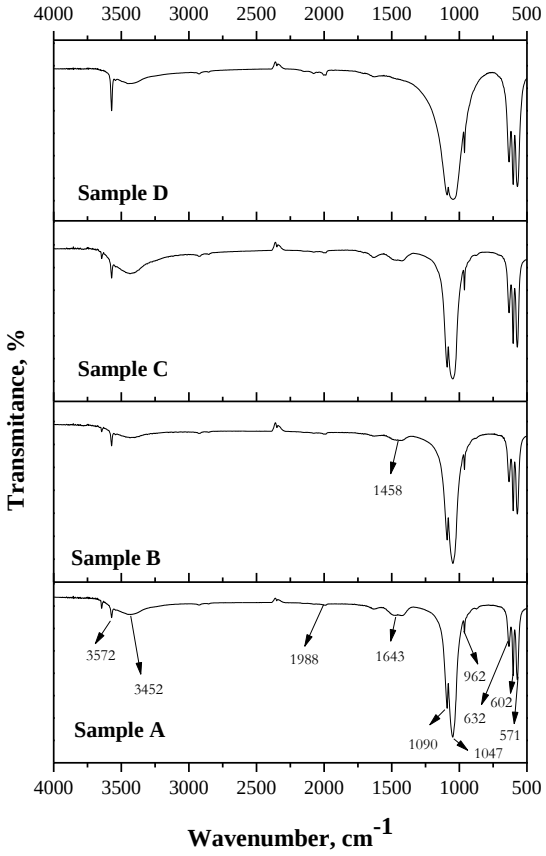

Figure 32. FTIR spectra of corresponding CHAp samples.

No traces for acid phosphate (HPO_4^{2-} peak around 540–530 cm^{-1}), characteristic for immature bone mineral or incomplete apatite phase is present [149]. However, when increasing the amount of seashells used for the syntheses the band in the area of 1458 cm^{-1} becomes more pronounced. This band is attributed to the bending mode of the CO_3^{2-} group [200]. It might be due to the absorption of atmospheric carbon dioxide during the sample preparation. However XRD data demonstrate that the CO_3 groups did not influence the purity of CHAp. Finally, for samples B, C and D the band for PO_4^{3-} vibrational modes becomes better defined and the OH^- bands are better resolved, as a consequence of the increase in particle size [201].

4.3.3 SEM analysis

Fig. 33 shows the SEM morphology of the CHAp powders produced from seashells collected along the Palanga coastline using sol-gel synthesis route. SEM

analyses indicate that all samples A, B, C and D consist of spherical particles with size of 250 nm- 1.5 μm. From the SEM pictures, it is clearly observed that the crystallites of the samples of spherulite morphology tend to form highly porous alveolate agglomerates. The powders show essentially a channel like assembly of spherical agglomerates. No substantial correlation between seashell mass used for the syntheses and particle size and morphology is observed.

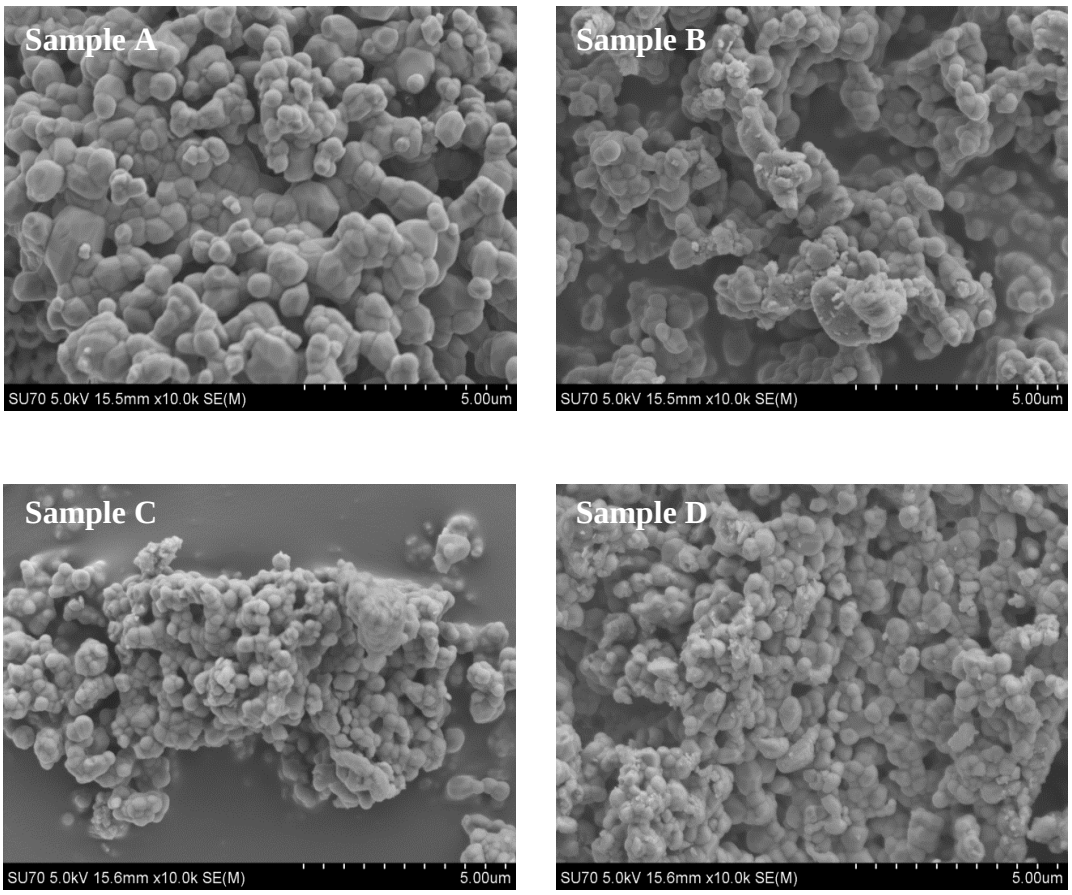

Figure 33. SEM micrographs of the CHAp samples produced from seashells.

4.3.4 Conclusions

Pure crystalline calcium hydroxyapatite has been successfully synthesized from seashells using environmetally friendly sol-gel synthesis route. The seashells appear to be a promising source of calcium for preparing nanocrystalline calcium hydroxyapatite with adequate properties essential for hard tissue replacement.

4.4 CALCIUM HYDROXYAPATITE DERIVED FROM SEASHELLS COLLECTED FROM VARIOUS BALTIC COUNTRIES: A COMPARATIVE STUDY

Since CHAp was successfully obtained using as calcium precursor the Baltic Sea seashells collected at the Lithuanian coast, it was decided to synthesize and compare CHAp from the seashells from coastlines of different Baltic Sea countries (Fig. 34) listed in Table 10.

Figure 34. Baltic Sea countries [202].

Table 10. List of countries and locations from which seashells were collected.

Country	Location	Sample name
Lithuania	Palanga	LT
Latvia	Nida	LV
Estonia	Pirita	EE
Finland	Helsinki	FIN
Sweden	Torekov	SE
Norway	Drøbak	NO
Denmark	Hou	DK
Germany	Zingst	DE
Poland	Sopot	PL

The access of the Baltic Sea to the world's oceans is via the North Sea and the Skagerrak (Denmark). The Baltic Sea constitutes a (nearly) closed system which is connected to the North Sea through narrow Belts and the Sound, leading to a complex system behaviour [203]. Baltic Sea coasts of different countries vary in their oceanographic and hydrographic characteristics, geological built up, sedimentological conditions and geomorphological features (Fig. 35) [204].

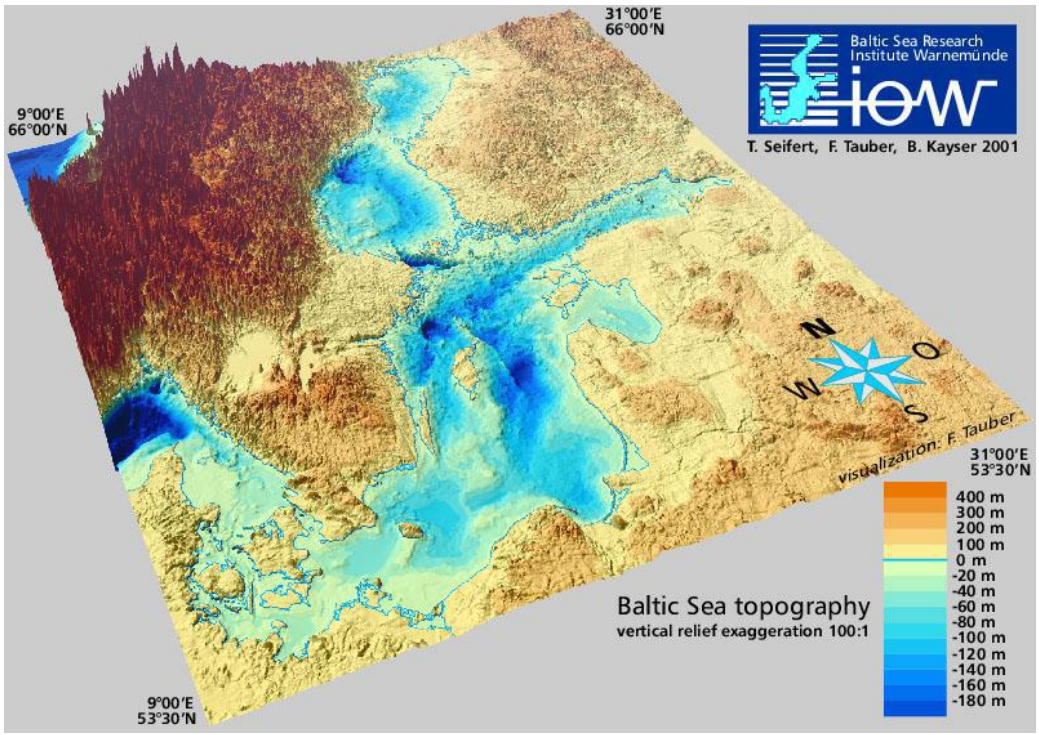

Figure 35. The bathymetry of the Baltic Sea [205].

In the non-tidal Baltic Sea storms from north-easterly directions induce the highest water levels and have the strongest influence on coastal changes. Recent study revealed that differences between the areas, one open to the sea and one semi-enclosed (particular investigation was focused on Swedish coasts), were reflected both in the residence times and in the settling patterns of the sediment particles [206]. Moreover, salinity of water in different regions of the Baltic Sea varies as well. Due to the mentioned reasons elemental constitution, pre dominant crystal phase as well as morphology of seashells from different regions of the Baltic Sea might slightly or significantly vary. That could possibly influence the

characteristics of the final CHAp product even after the chemical treatment employed during the synthesis process.

In this study, firstly, with the kind help of relatives, friends and colleagues seashells were collected from the different Baltic countries, and then they were treated and prepared for the synthesis as described in Section 3.1.

Figs. 36 and 37 represent the XRD spectra of corresponding seashells.

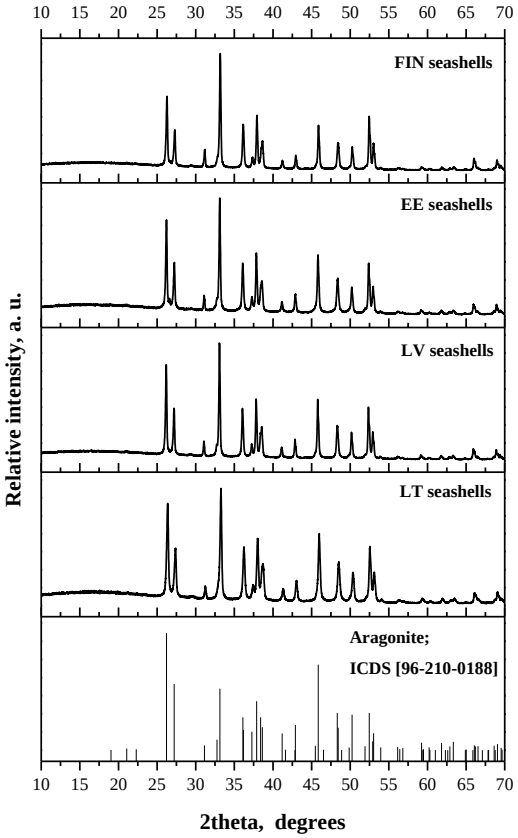

Figure 36. The XRD patterns of corresponding seashells.

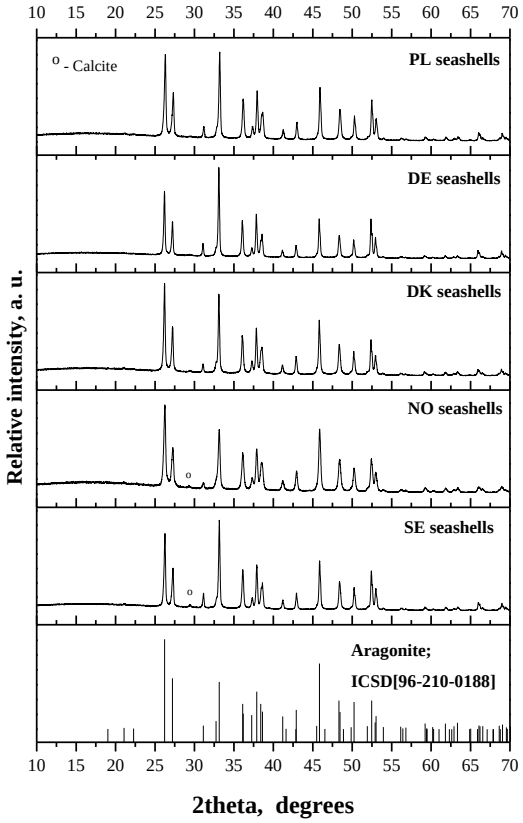

Figure 37. The XRD patterns of corresponding seashells.

As XRD data indicates, the dominant crystalline phase in all the seashell powders was calcium carbonate, $CaCO_3$, aragonite in particular (ICSD [96-210-0188]). However, a trace amount of calcite is present in Nordic as well as Swedish seashells ([96-101-0229]) as shown in Fig. 37.

FTIR spectra of the corresponding seashell powders are presented in Figs. 38 and 39. FTIR spectroscopy is an important tool used to identify different phases of organic and inorganic compounds and, especially, calcium carbonate phases due to the differences in their carbonate ions, CO_3^{2-}. Carbonate ions and similar molecules have four normal modes of vibration peaks: ν_1, symmetric stretching; ν_2, out of-plane bending; ν_3, doubly degenerate planar asymmetric stretching; and ν_4, doubly degenerate planar bending [207, 208].

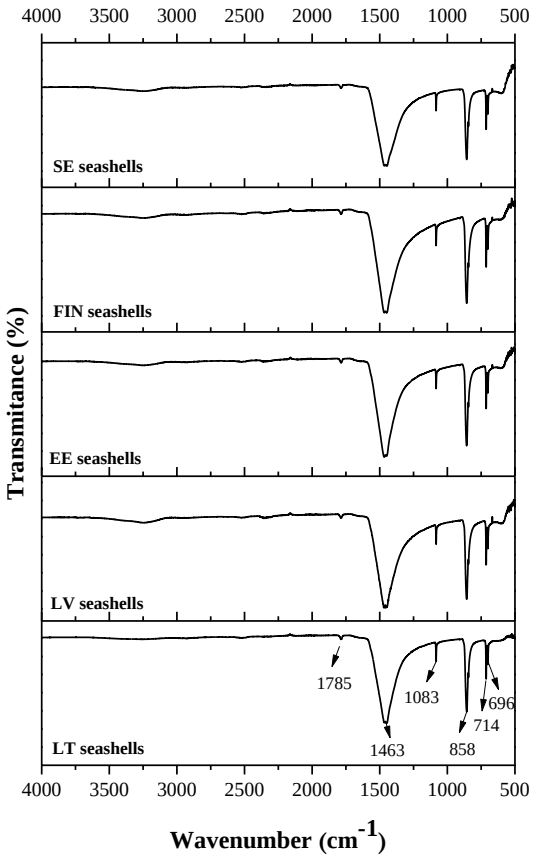

Figure 38. FTIR spectra of corresponding seashells.

The spectral data obtained for the samples reveal an absorption peak of CO_3^{2-} at ~1463 cm^{-1}, ~1083 cm^{-1}, ~ 1785 cm^{-1}, ~858 cm^{-1}, and ~714 cm^{-1}, which have been reported to be the characteristic features of the carbonate ions in calcium carbonate and are the fundamental modes of vibration for this particular compound [207, 209].

However, the observed bands at ~1083 cm^{-1} and ~858 cm^{-1} were assigned as ν_1 symmetric stretching and ν_2 out-of plane bending modes of CO_3^{2-}, respectively. The peak at ~ 1083 cm^{-1} is only observed for the aragonite phase calcium carbonate, whose CO_3^{2-} ions are inactive in the infrared region. The doubly degenerate peak that appears at ~709 cm^{-1} can be attributed to the ν_4 in-plane bending mode of CO_3^{2-} ions, which indicates a structural change in the calcium ions from the symmetry of the calcite phase [207].

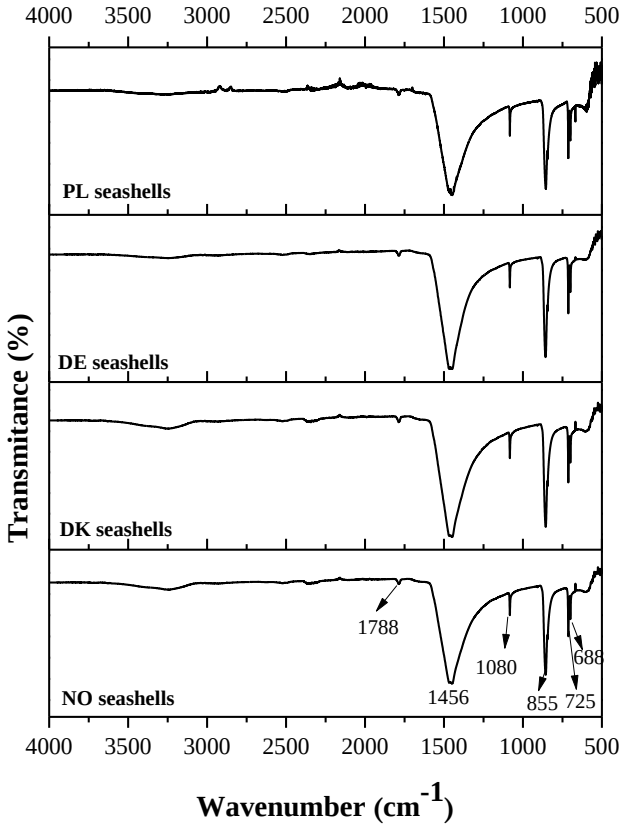

Figure 39. FTIR spectra of corresponding seashells.

This degeneracy can only be removed by splitting the band into two; thus, the band is attributed to the aragonite phase only, which has been confirmed in the literature [207, 209]. This observation was also supported by a broad doubly degenerate band ν_3 at ~1463 cm^{-1}, which confirms the structural changes in the symmetry of the CO_3^{2-} molecular ions that correspond to the asymmetric stretching mode of CO_3^{2-}. The fundamental changes in the positions of the vibration mode of a molecule as explained in the literature are caused by a modification of the electrostatic valence of the Ca–O bond due to changes in the coordination, while the Ca–O bond alteration occurs because the displacement of the carbonate vibration mode changes in the environment of oxygen atoms [207, 210, 211]. The observed FTIR frequency at ~1785 cm−1 is due to the combination of the fundamental vibration frequencies of the carbonate molecular ions assigned between (ν_1 and ν_4) and (ν_1 and ν_3), respectively, as reported in the literature [140, 207, 209, 210].

Sea shells display a crossed lamellar microstructure which can be observed in SEM images provided in Fig. 40. Micrographs reveal rigid and dense morphology of grounded seashells. This property is due to the organic phase present in the shells.

Data retrieved from the ICP-OES analysis measurement are summarized in Table 11 as well as graphically represented in Figs. 41 and Fig. 42. The major constituent present in seashells is calcium as expected, however trace elements are also present as demonstrated in Fig. 42.

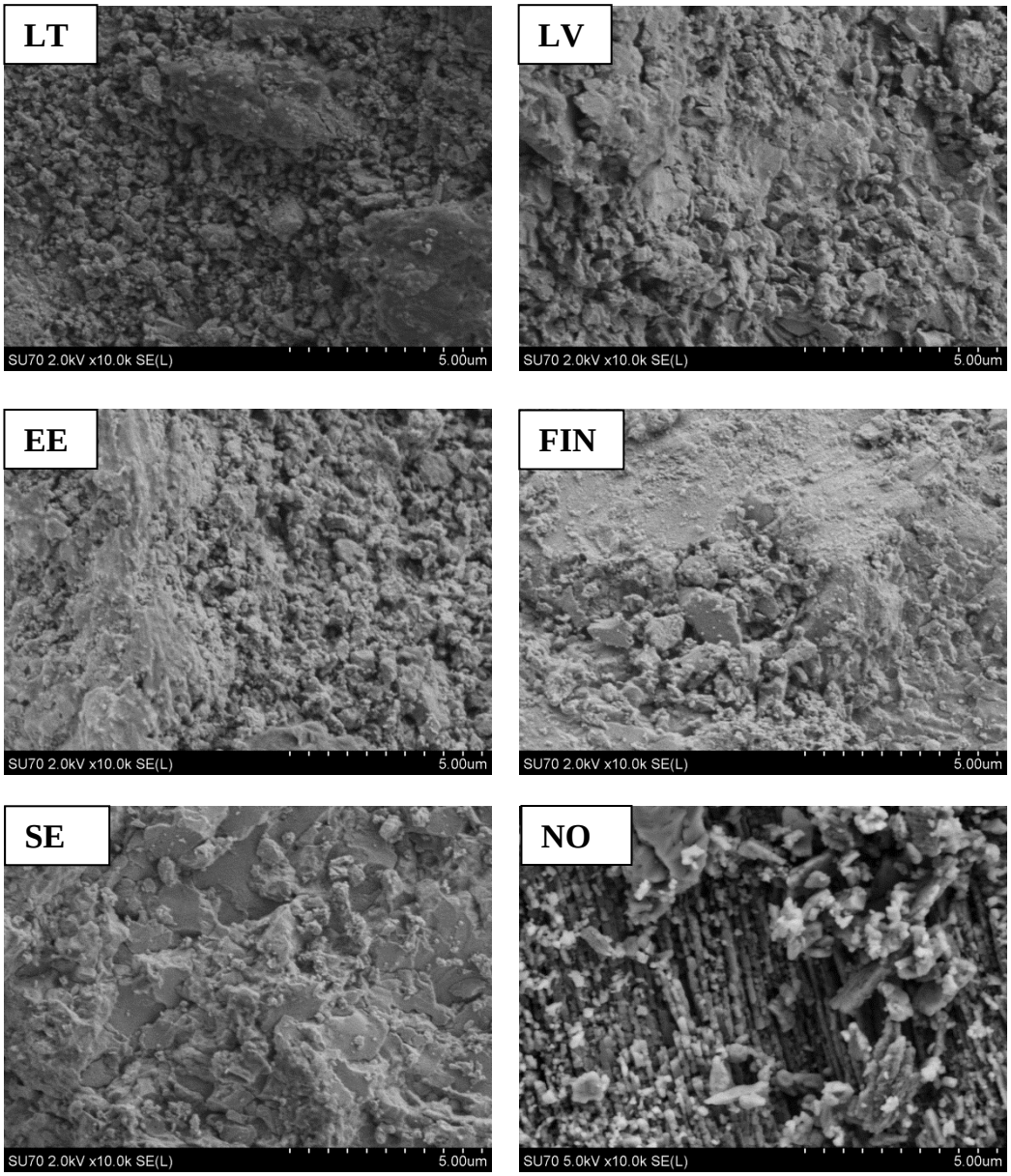

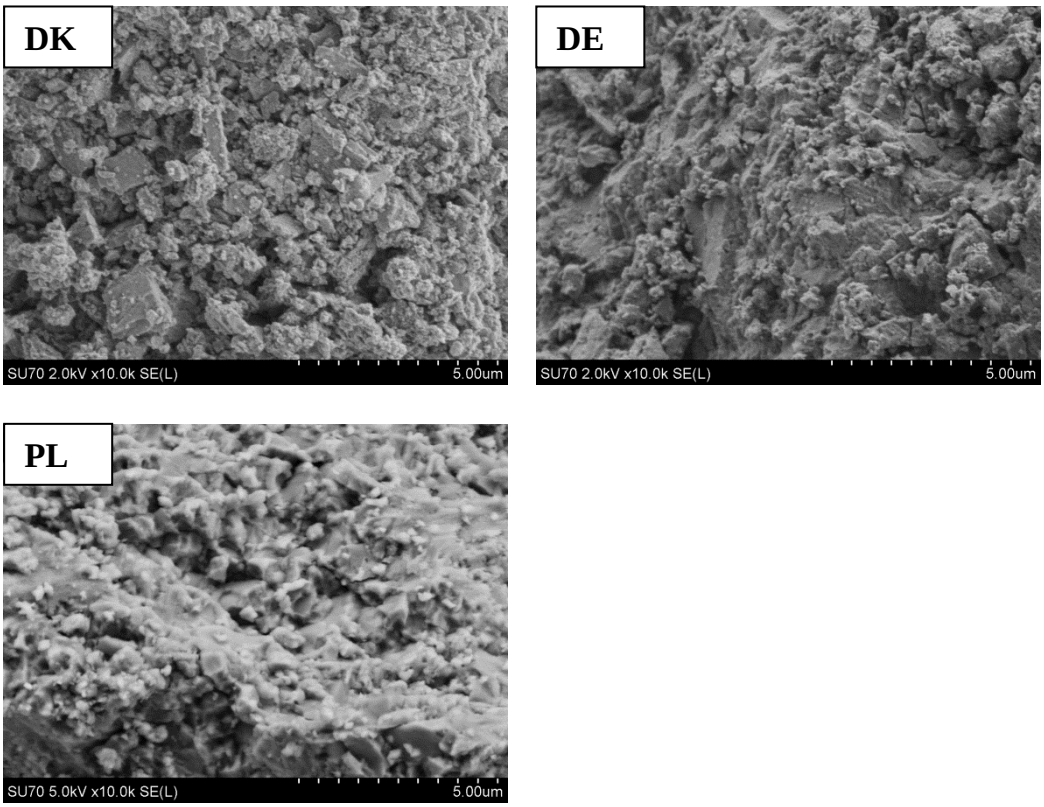

Figure 40. SEM micrographs of the corresponding seashells.

Table 11. Amount of corresponding elements present in the seashells.

Sample	**Analyte (mean, μg/g)**											
	Ca*	**Na**	**Ba**	**Cr**	**Cu**	**Fe**	**K**	**Mg**	**Mn**	**Ni**	**Sr**	**Zn**
LT	378	352	45	19	4	186	42	110	27	555	1818	4
LV	389	633	65	68	3	409	68	163	37	1897	2328	4
EE	372	734	29	24	8	266	63	139	20	687	2008	5
FIN	373	713	45	52	3	369	73	179	29	1488	2231	3
NO	377	820	13	26	3	239	134	208	14	711	1806	4
SE	382	737	47	55	2	288	149	149	24	1538	1975	11
DK	390	1051	7	36	2	296	148	249	33	1016	1768	4
DE	388	790	23	39	1	241	89	211	25	1079	2038	3
PL	387	556	39	2	6	243	99	166	47	2	2329	11

*- mg/g

Cobalt, cadmium and lead were not detected. These elements were of interest due to their toxic properties.

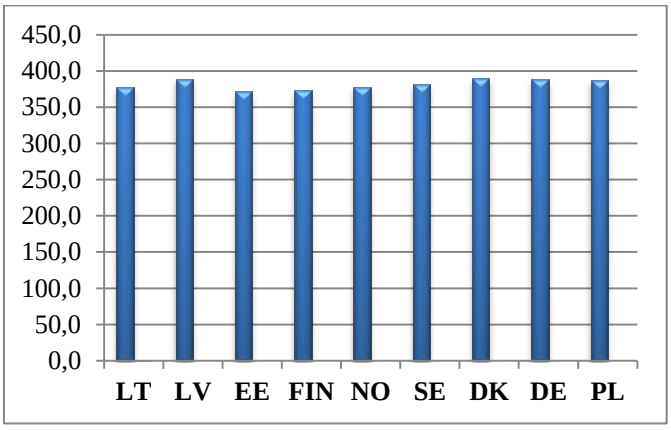

Figure 41. Amount of calcium present in the seashells from different Baltic Sea countries (mg/g).

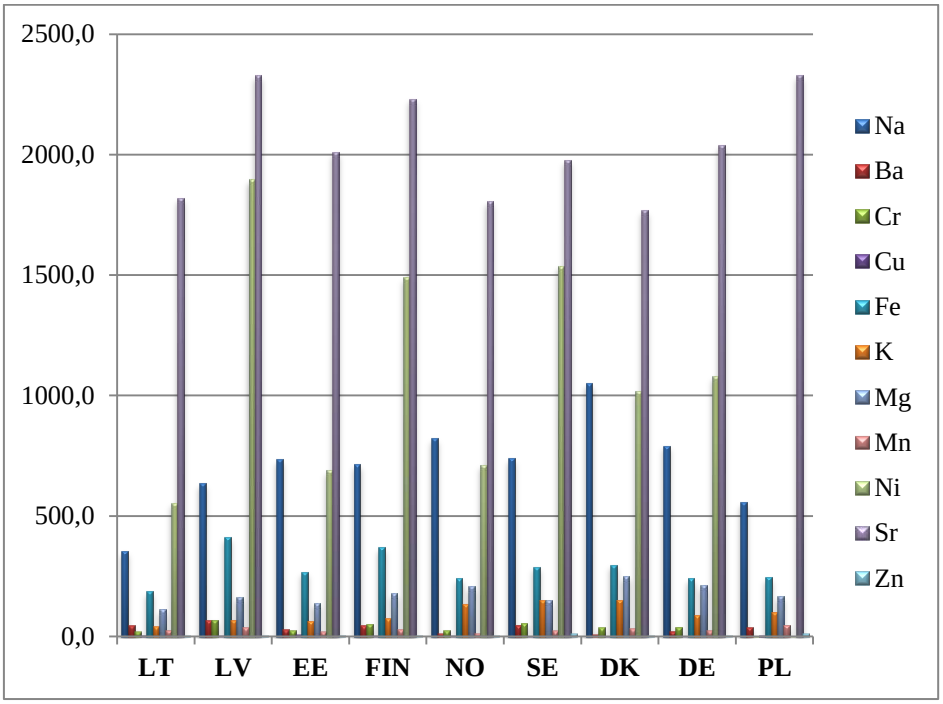

Figure 42. Amount of corresponding elements present in the seashells from different Baltic Sea countries (µg/g).

To conclude the analyzed characteristics of seashells, it could be said that shell is comprised almost entirely of inorganic material and a small amount of organic matter. This was demonstrated with the use TG/DSC. The inorganic component of the shells is calcium carbonate ($CaCO_3$), occurring as the aragonite polymorph, established via XRD. FTIR spectra are in agreement with known aragonite materials.

4.4.1 X- ray diffraction analysis

XRD patterns of the seashells derived CHAp powders are presented in Figs. 43, 44 and 45. The d spacings were compared with the standard data (ICSD). The XRD patterns indicate that main crystalline phase of calcium hydroxyapatite ($Ca_{10}(PO_4)_6(OH)_2$, ICSD [00-009-0432]) with hexagonal crystal system was obtained in all of the cases. In some cases as designated in Fig. 43, a minor amount of secondary phase of calcium oxide, lime (CaO, ICSD [00-037-1497]) was present as well.

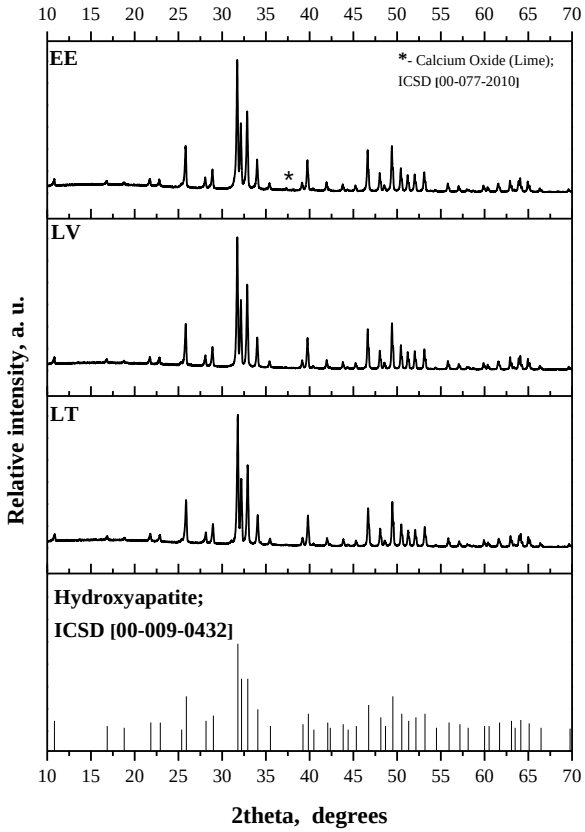

Figure 43. XRD patterns of CHAp derived from seashells from EE, LV and LT.

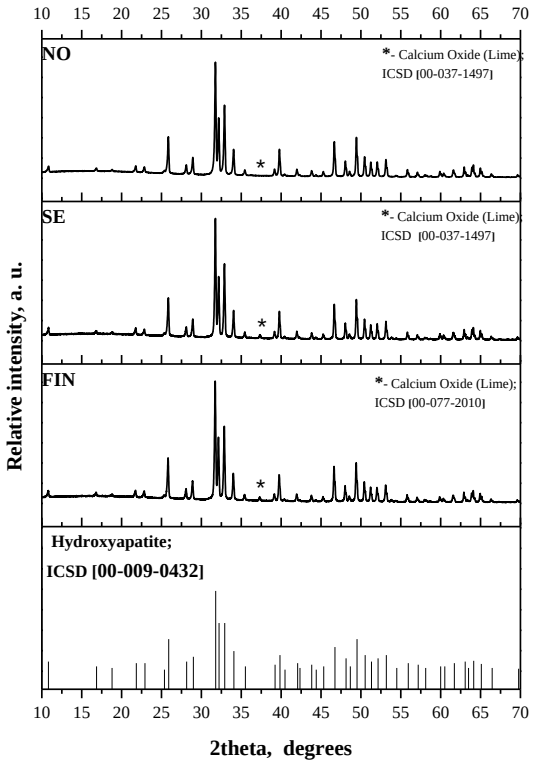

Figure 44. XRD patterns of CHAp derived from seashells from NO, SE and FIN.

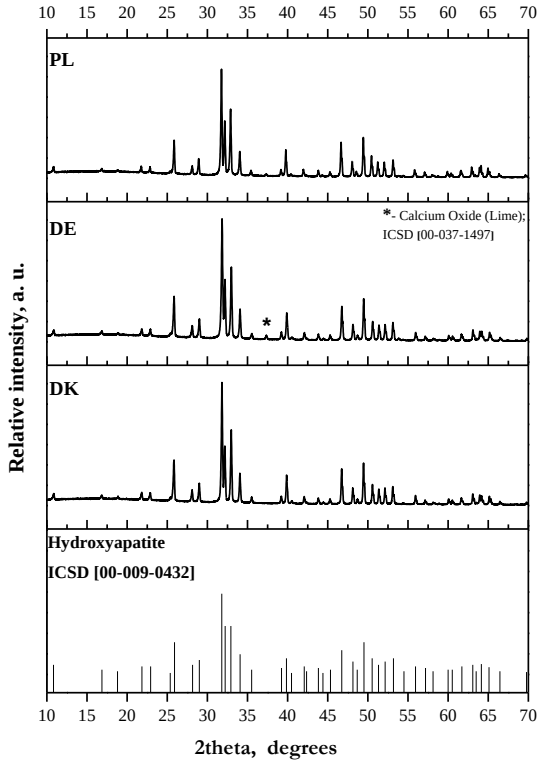

Figure 45. XRD patterns of CHAp derived from seashells from PL, DE and DK.

4.4.2 EDX analysis

The data collected from this measurement are in a good agreement with XRD, confirming that samples are consisted of calcium, phosphorus as well as oxygen in relevant ratios.

4.4.3 FTIR spectroscopy

FTIR spectra (Figs. 46 and 47) of the corresponding CHAp samples show characteristic bands due to PO_4^{3-} ions (ν_1 — 963 cm^{-1}, ν_3 — 1036 and 1095 cm^{-1}, ν_4 — 568 and 600 cm^{-1}), OH^- groups (stretching vibration at 3570 cm^{-1} and liberation mode at 630 cm^{-1}) [212].

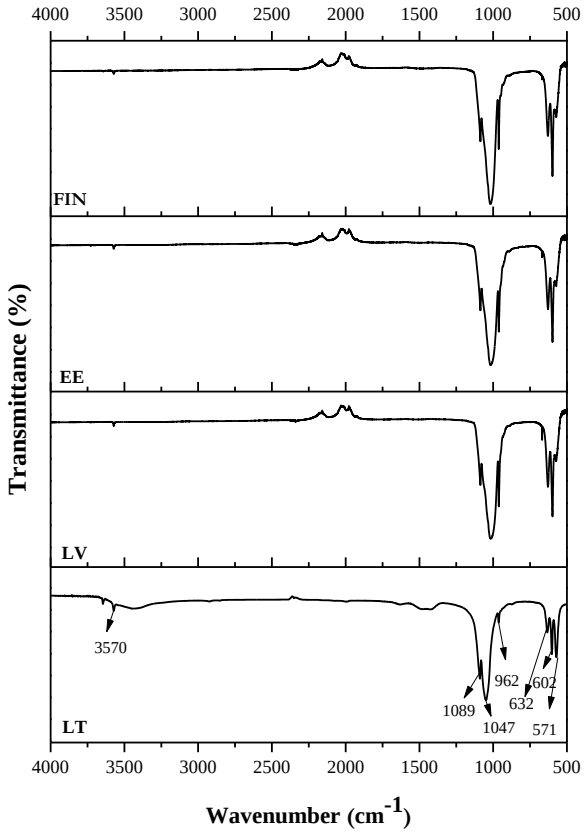

Figure 46. FTIR spectra of CHAp derived from seashells from corresponding countries.

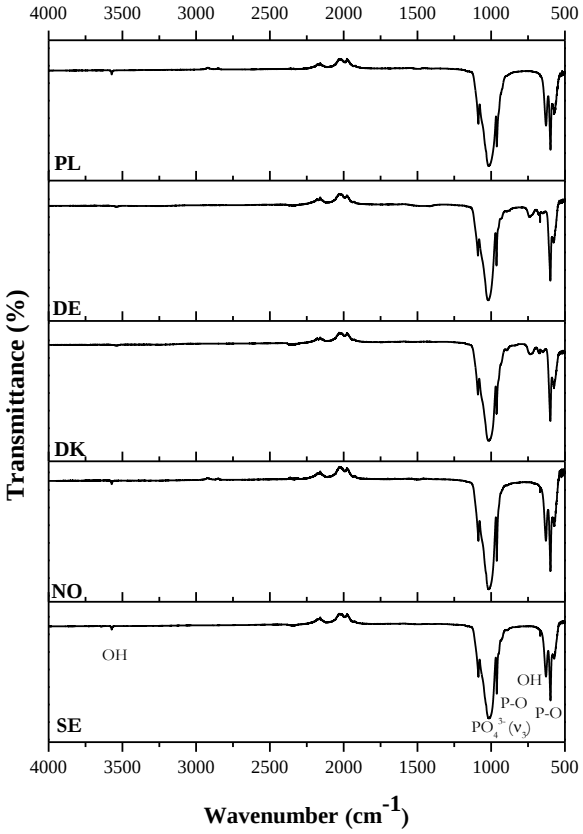

Figure 47. FTIR spectra of CHAp derived from seashells from corresponding countries.

4.4.4 SEM analysis

Even though all samples were identified to be CHAp and all of them were prepared using seashells as a source of calcium, all of them underwent the same chemical treatment, the morphology of final CHAp products vary greatly as demonstrated in SEM images (Fig. 48).

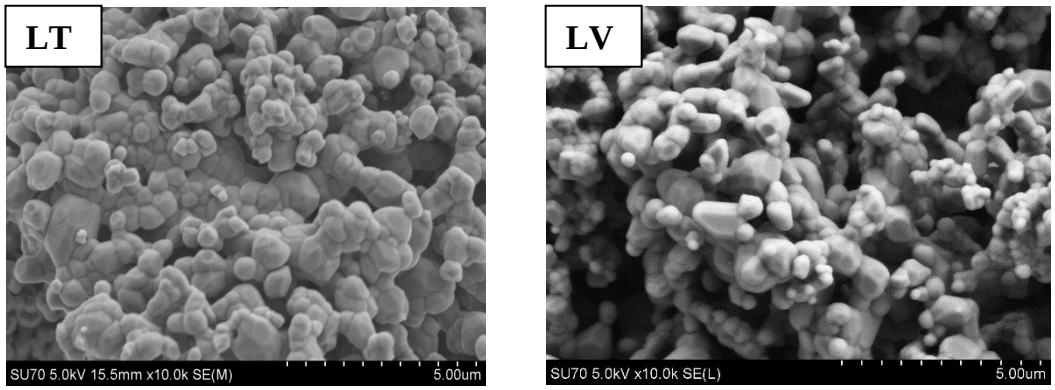

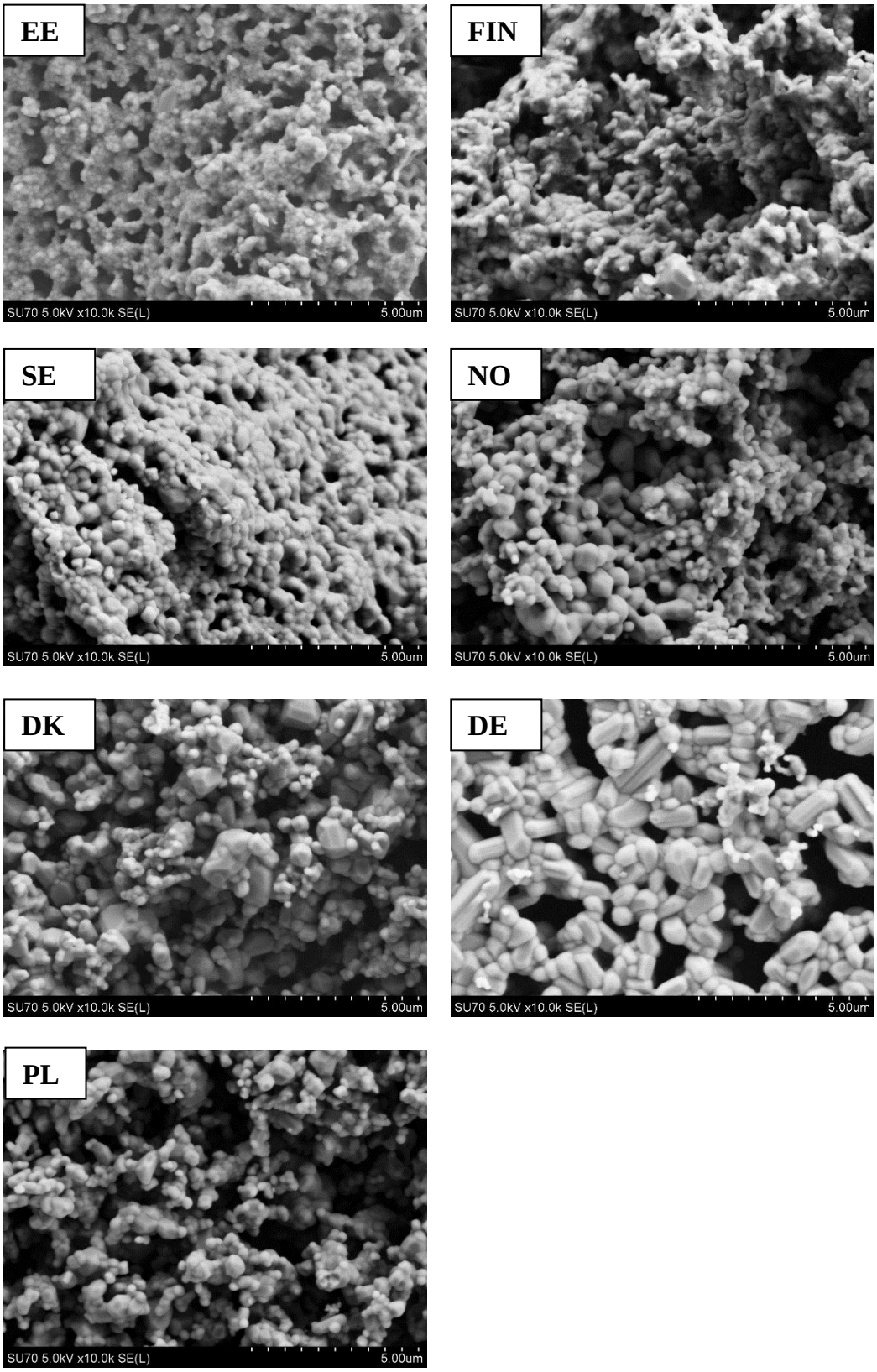

Figure 48. SEM micrographs of CHAp derived from seashells from corresponding countries.

The main surface morphological features and particle size characteristics of corresponding CHAp samples are summarized in Table 12.

Table 12. Morphological data of CHAp derived from seashells from different Baltic Sea regions.

CHAp Sample	Morphology	Size
LT	Irregular formless spheres	250 nm- 1 μm
LV	Irregular formless spheres and hexagonal prisms	250 nm-1 μm
EE	Highly agglomerated spherical particles; interconnected granular microporosity	100- 250 nm
FIN	The same	100- 250 nm
SE	Highly agglomerated spherical particles; dense agglomerates	100- 300 nm
NO	Spherical particles; porous agglomerates	150- 300 nm
DK	Spheres, prisms; interconnected granular microporosity	150 nm -1.5 μm
DE	Hexagonal prisms; interconnected granular microporosity	150 nm- 1.5 μm
PL	Particle shape: spherical and hexagonal prisms; porous agglomerates	250 nm- 400 nm

4.4.5 Conclusions

In this study highly crystalline and pure CHAp powders were successfully synthesized through the sol-gel synthesis route using seashells from different seashores of the Baltic Sea as calcium source. The identity of obtained CHAp samples was determined using XRD, FTIR and SEM characterization methods. The surprising discovery was significant morphological differences of final CHAp product.

4.5 SYNTHESIS AND CHARACTERIZATION OF IRON SUBSTITUTED CALCIUM HYDROXYAPATITE

In this study, seashells were used as a calcium precursor for the synthesis of Fe(x)/CHAp using an environmentally friendly sol-gel synthesis route. While synthetic materials have been widely used in the biomedical field with great success, natural structural materials are providing an abundant source of novel biomedical applications [30, 213]. The advantage of using natural sources of $CaCO_3$ for bone repair is primarily for its unique morphology. These materials have high surface areas which help improve the solubility of the implant and facilitates cellular activity. Recently, the usage of magnetic nanoparticles (MNPs) for biological and medical purposes has been increasing as well [214-216]. MNPs have been used in the last decade for in vitro and in vivo applications, as support materials for enzyme immobilization, drug-delivery agents, contrast agents for magnetic resonance imaging (MRI) as well as heat mediators for hyperthermia-based anti-cancer treatments and many other significant biotechnological procedures [217-220]. However, only a small number of studies suggested the use of MNPs in orthopedic applications and/or for bone tissue engineering [221-223]. The favorable relation between iron and bone density was shown in clinic by the association of dietary iron and a healthy bone mineral density [224, 225]. Previous studies also indicate that iron restriction can have an inhibitory effect on the mineralization of osteoblasts in vitro; in addition, scientific evidence implies that there may be some positive association between iron metabolism and the in vitro proliferation of bone or non-bone cell lines [213, 226, 227].

Considering the importance of having non-toxic MNPs for the above-mentioned applications, and the important role of iron in bone regeneration and remodelling, this study aimed to produce and analyze bioactive and bioresorbable nanoparticles obtained by doping sea shell derived hydroxyapatite (CHAp) with Fe ions in ideal condition aimed at limiting the formation of poorly tolerated magnetic secondary phase (i.e. Fe_3O_4).

In this study, eleven samples of iron doped hydroxyapatite (Fe(x)/CHAp) with different iron concentrations (x= 0, 0.01, 0.05, 0.1, 0.5, 1, 2, 3, 4, 5 and 10 mol %) were synthesized.

4.5.1 X- ray diffraction analysis

XRD analysis revealed that the Fe/CHAp crystallizes in the hexagonal structure with space group P63/m (ICSD [00-073-0294]). The XRD patterns are shown in Figs. 49 and 50.

As it is indicated in the XRD patterns, Fe(0.01%)/CHAp-Fe(0.5%)/CHAp samples have a minor impurity phase of calcium oxide (CaO, lime; ICSD [00-077-2010]), which transforms into calcium phosphate ($Ca_3(PO_4)_2$; ICSD [00-086-1585]) in Fe(1%)/CHAp sample (characteristic peaks for β-TCP located at 2θ angles of 27.7°, 31.1°, 44.5°). Impurity phases disappear in the subsequent samples (Fe(2%)/CHAp-Fe(4%)/CHAp) where pure and high crystalline CHAp is observed. For the CHAp samples with 5 and 10 mol % of iron, mixtures of different compounds were obtained, including CHAp, β- TCP, Fe_2O_3 as well as CaO, that are difficult to interpret correctly due to the fact that peaks overlap significantly.

Average crystallites size of the products was calculated by using Scherrer's equation $D= K \lambda/\beta \cos \theta$ (where K is the shape factor (0.9), β is the full-width at half- maximum (fwhm) of diffraction peaks (h k l) measured in radians, λ is the wavelength of the X-rays (λ = 1.540562 Å) and θ is Bragg's diffraction angle). The average crystallite sizes of undoped CHAp and Fe(x)/CHAp were found to be 490 nm and 400-450 nm, respectively. So, the doped CHAp possess smaller values of crystallite size in comparison to non-doped. The reduced crystallite size and a small upward shift in peak positions suggest that the dopant Fe^{3+} (ionic radius 0.645 Å) substitutes at the Ca^{2+} (ionic radius 0.99 Å) site in the CHAp [228].

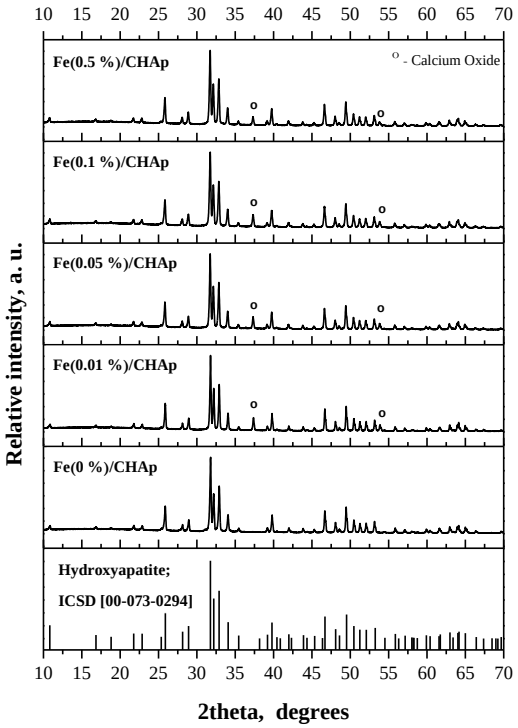

Figure 49. The XRD patterns of corresponding (Fe(0%)/CHAp-Fe(0.5%)/CHAp) samples.

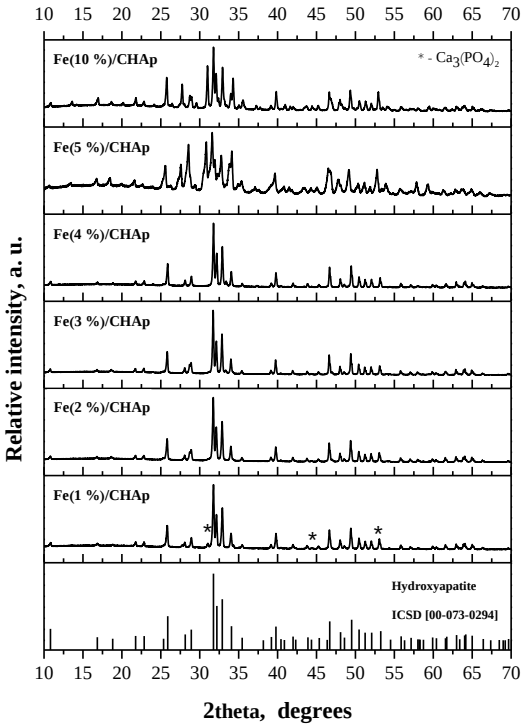

Figure 50. The XRD patterns of corresponding ((Fe(1%)/CHAp-Fe(10%)/CHAp)) samples.

4.5.2 FTIR spectroscopy

The FTIR spectra of all the samples are shown in Figs. 51 and 52.

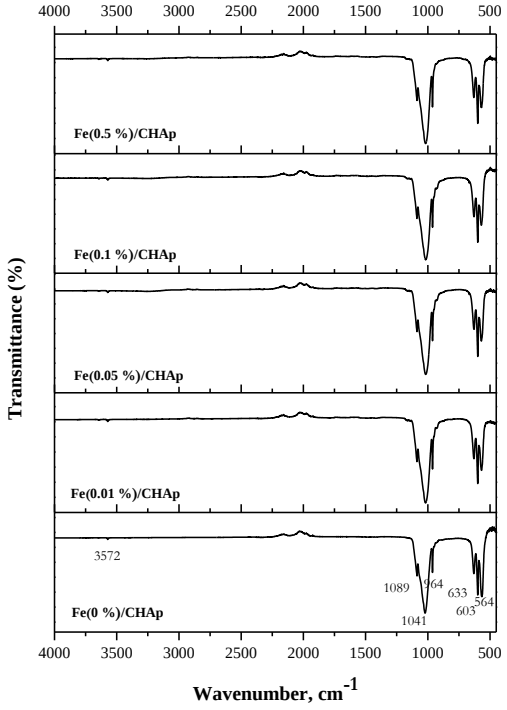

Figure 51. FTIR spectra of corresponding (Fe(0%)/CHAp-Fe(0.5%)/CHAp) samples.

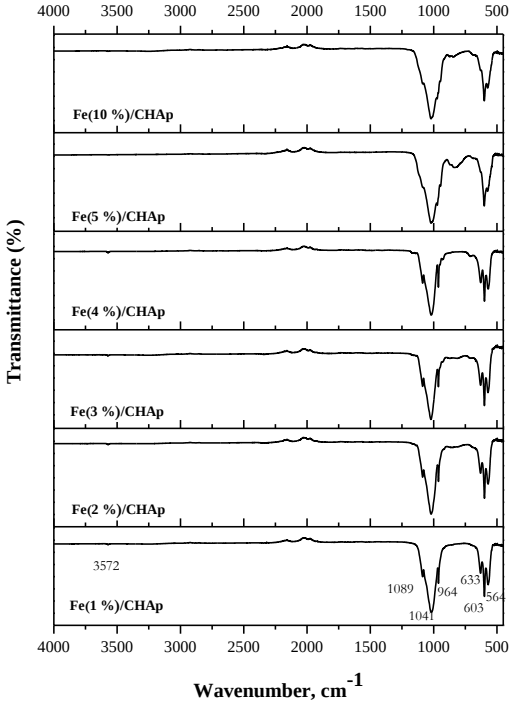

Figure 52. FTIR spectra of corresponding ((Fe(1%)/CHAp-Fe(10%)/CHAp)) samples.

The formation of apatite layer appears clearly in Fe(0%)/CHAp-Fe(4%)/CHAp samples as they possess the fundamental functional groups of CHAp. To account for them, the ν_1 phosphate mode is observed at 952 cm^{-1}, whereas the peak pairs found at 1089 and 1041 cm^{-1} and 603 and 564 cm^{-1} are attributed to the ν_3 and ν_4 modes of phosphate respectively [190, 192]. Besides, the hydroxyl stretching vibrational mode is observed at 3572 cm^{-1} represented by a very low intensity peak, which is considered to be confirmative peak for CHAp [132]. The FTIR spectra of Fe(0.01%-4%)/CHAp samples are similar to that of CHAp, except for a decrease of the intensity of the OH band at 633^{-1} cm and the P-O stretching band around 564 cm^{-1}. The decrease is often observed when cation exchange is performed in the apatite. Literature suggests that this behaviour can be attributed to the substitution of Ca^{2+} by Fe^{3+}, which provokes the elimination of the protons of the hydroxyls located in the apatite tunnels in order to counterbalance the electric excess due to the incorporation of Fe^{3+} ions [229].

It is worth mentioning that for the 0.01% - 4% iron doped samples the band due to the OH group is present, whilst it is not observed for the 5% and 10% iron doped ones. This behaviour suggests that there are no OH groups in the more iron-concentrated samples. The same applies to characteristic CHAp PO_4^{3-} bands- they are absent in Fe(5%)/CHAp and Fe(10%)/CHAp samples. Thus, it was found that with increasing iron concentration the percentage of the apatite phase decreases. This observation is also consistent with the results obtained from X-ray analysis.

4.5.3 SEM analysis

Fig. 53 shows SEM images of the synthesized Fe(x)/CHAp samples. SEM analyses indicated that Fe(0.01%)/CHAp and Fe(0.1%)/CHAp samples consist of spherical particles with size of 150 nm- 1 μm; on the other hand, the average particle size for non-doped CHAp is observed to be in the range of 250 nm -1.5 μm. From SEM pictures, it is clearly observed that the crystallites of these samples of spherulite morphology tend to form highly porous alveolate

agglomerates (porosity also increases when increasing iron concentration in the sample). The powders show essentially a channel like assembly of spherical agglomerates.

In Fe(0.5%)/CHAp-Fe(4%)/CHAp samples the presence of large and dense agglomerates of particles showing well-defined grain boundaries is observed. In these samples, the grain has an average size between 50 nm and 400 nm. There is also observed particle size reduction upon Fe doping, which is in accordance with the XRD results. The samples Fe(5%)/CHAp and Fe(10%)/CHAp were not taken into consideration when measuring SEM data, due to the reason that these samples do not contain desirable phase.

4.5.4 Conclusions

The results obtained indicate successful synthesis of the Fe-doped/substituted calcium hydroxyapatite. It was determined that 4% is the highest iron molar concentration to be used.

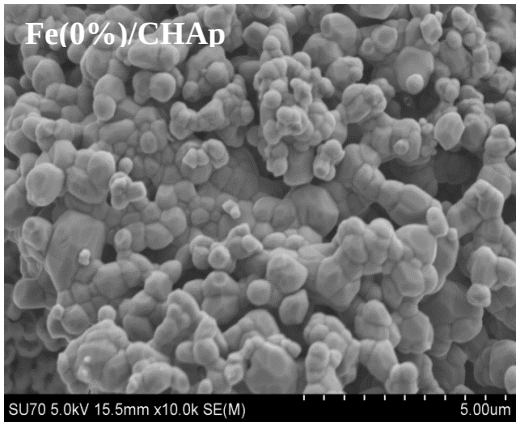

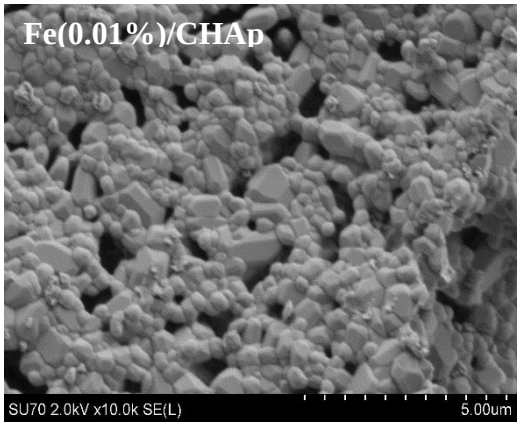

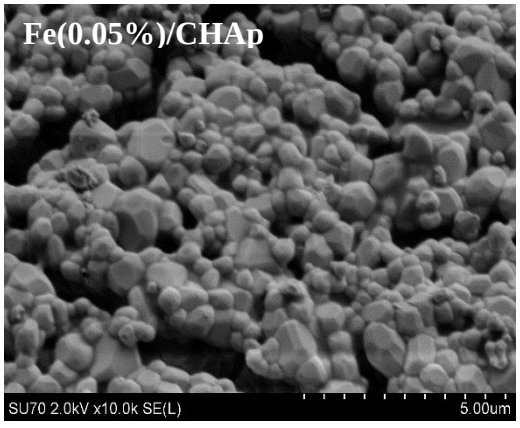

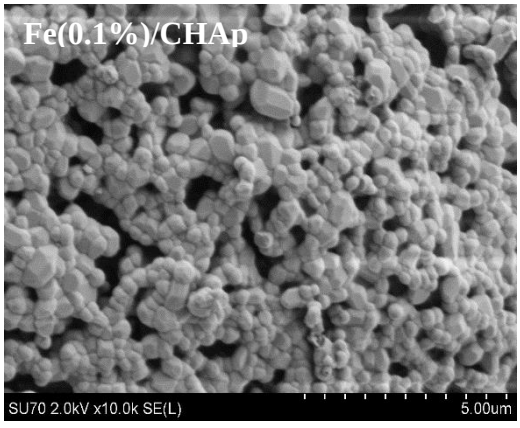

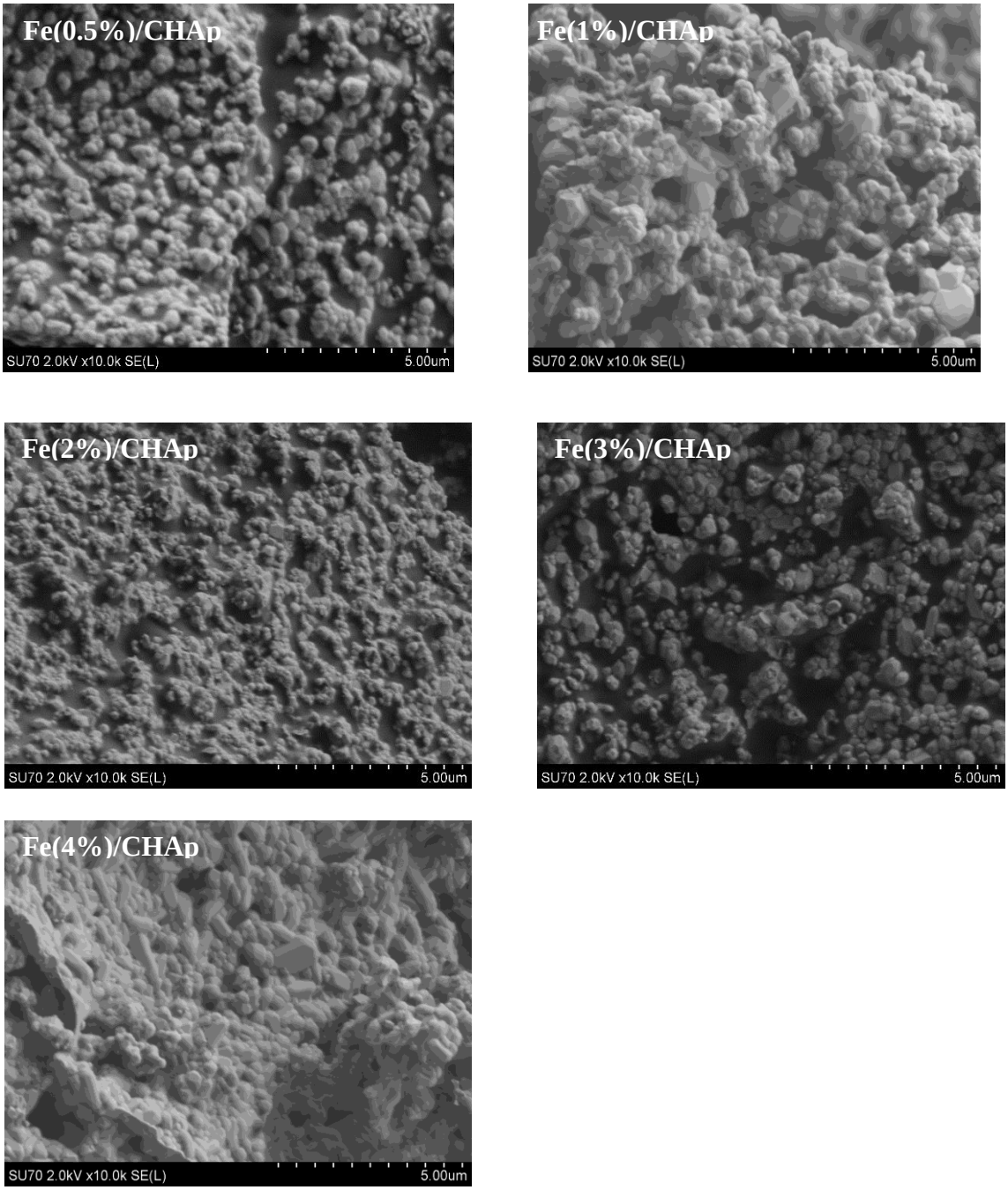

Figure 53. SEM micrographs of the corresponding Fe(x)/CHAp samples.

5. CONCLUSIONS AND FUTURE PLANS

1. Dairy derived calcium phosphates are the optimal compounds to be used for functional food/ food supplement applications due to their solubility, Ca/P ratio as well as pureness from toxic elements.

2. According to XRD results the predominant compound in coral and sea-shell derived sample was calcite ($CaCO_3$), however, in the sample of coral water aragonite phase was also identified. The XRD patterns of dairy derived powders showed that the main crystalline component in all the samples was calcium hydroxyapatite ($Ca_{10}(PO_4)_6(OH)_2$, CHAp). Finally, the presence of nanocrystalline CHAp in the bovine bone matrix was determined.

3. Calcium hydroxyapatite and whitlockite ($Ca_{18}Mg_2H_2(PO_4)_{14}$) composite for biomedical applications were produced when heating dairy powder at rather low temperature (700 °C). The SEM micrographs demonstrated that formed $Ca_{10}(PO_4)_6(OH)_2/Ca_{18}Mg_2H_2(PO_4)_{14}$ composite using environmentally benign and green preparation technology had porous and agglomerated microstructure.

4. High purity crystalline CHAp was produced from seashells collected along the Palanga coastline using environmentally friendly sol-gel synthesis route. The SEM analyses of the CHAp powders produced from seashells indicated that samples consist of spherical particles with size of 1- 6 μm. The remineralization tests on seashell derived CHAp will be conducted in near future.

5. The CHAp samples were synthesized using the seashells from coastlines of different Baltic Sea countries (Denmark, Estonia, Finland, Germany, Latvia, Lithuania, Norway and Sweden). It was demonstrated that the geographical origin of sea-shells collected at the coast of the Baltic Sea did

not significantly influenced chemical composition and phase purity of resulting CHAp powders.

6. However, the particle size, shape as well as surface morphology of final CHAp product depends greatly the geographical origin of sea-shells. It was obtained that irregular formless spheres or hexagonal prisms, or highly agglomerated spherical particles with interconnected granular microporosity, or only porous and agglomerated spherical particles can form depending on the sea-shells origin.

7. Sea-shell derived Fe-substituted calcium hydroxyapatite ($Ca_{10-x}Fe_x)(PO_4)_6(OH)_2$ was successfully produced via the same sol-gel chemistry approach and characterized. In this study, eleven samples of iron doped hydroxyapatite (Fe(x)/CHAp) with different iron concentrations (x= 0, 0.01, 0.05, 0.1, 0.5, 1, 2, 3, 4, 5 and 10 mol %) were synthesized.

8. It was determined that 4% is the highest iron molar concentration to be used for the preparation of Fe(x)/CHAp without destroying apatite crystal structure. To evaluate magnetic behaviour and to determine the exact position of Fe^{3+} ions in the CHAp crystal lattice the Mössbauer spectroscopy will be performed.

6. LIST OF PUBLICATIONS

Articles in journals

1. J. Trinkūnaitė-Felsen, A. Žalga, A. Kareiva. Characterization of naturally derived calcium compounds used in food industry. *Chemija,* **23** (2012) 76-85.
2. J. Trinkunaite-Felsen, Z. Stankeviciute, J.C. Yang, Thomas C.K. Yang, A. Beganskiene, A. Kareiva. Calcium hydroxyapatite/whitlockite obtained from dairy products: Simple, environmentally benign and green preparation technology. *Ceramics International,* **40** (2014), 12717–12722

Published contributions to academic conferences

1. J. Trinkūnaitė-Felsen, A. Kareiva. Characterization and suggested usage in food industry of naturally derived calcium compounds. Conference "Химия в современном мире: пятая всероссийская конференция студентов и аспирантов". *Saint Petersburg, Russia, (2010)* 213-214.
2. J. Trinkūnaitė-Felsen, A. Žalga, A. Kareiva. Characterization and suggested usage in food industry of naturally derived calcium compounds. 10th international conference of Lithuanian chemists "Chemistry 2011". Vilnius, Lithuania, 14-15 October (2011) 111.
3. J. Trinkūnaitė-Felsen, M. Semaško. Chemical analyses and characterization of dairy derived hydroxyapatite. International conference of young chemists "Nanochemistry and nanomaterials". Palanga, Lithuania, 7-9 December (2012) 50.
4. V. Vičkačkaitė, J. Trinkūnaitė-Felsen, A. Beganskienė, A. Padarauskas, A. Kareiva. Nanostructured innovative materials designed for medical applications. 3rd international conference "Multifunctional, Hybrid and Nanomaterials". Sorrento, Italy, 3-7 March (2013) [B.1.8.2].
5. J. Trinkūnaitė Felsen, A. Beganskienė, A. Kareiva. Novel approach to dairy powder: source of calcium hydroxyapatite. 11th international

conference of Lithuanian chemists “Chemistry 2013”. Vilnius, Lithuania, 27 September (2013) 54.

6. J. Trinkūnaitė Felsen, K. Gross, J.C. Yang, Thomas C.K. Yang, A. Kareiva. Seashells derived calcium hydroxyapatite: synthesis and characterization. International Conference “ACIN 2013: Evolution and Revolution”. Namur, Belgium, 15-19 July (2013) P-042.
7. J. Trinkūnaitė Felsen, A. Beganskienė, A. Kareiva. Iron-doped/substituted calcium hydroxyapatite from seashells: synthesis and characterization. 18th international scientific conference “EcoBalt 2013”. Vilnius, Lithuania, October 25-27 (2013) 81.
8. M. Semaško, J. Trinkūnaitė-Felsen, A. Kareiva. Calcium hydroxyapatite with biological-natural origin: synthesis and spectroscopic characterization. XIIth International Conference on Molecular Spectroscopy “From molecules to nano- and biomaterials”. Poland, 8-12 September (2013) 261.
9. M. Semaško, J. Trinkūnaitė-Felsen, A. Beganskienė, A. Kareiva. Synthesis and characterization of chromium substituted calcium hydroxyapatite. International conference “Chemistry and chemical technology”. Kaunas, Lithuania, 25 April (2014) 141-143.

Patent Application

1. J. Trinkūnaitė Felsen, A. Prichodko, A. Kareiva. Sustainable chemical process for the synthesis of calcium hydroxyapatite. Appl. No. LT2014 502. (06 March 2014; submission number 100006).

7. ACKNOWLEDGMENTS

The achievement of this PhD thesis has been a real challenge and would not have been possible without the help of some people.

Foremost, I would like to express my sincere gratitude to my supervisor, Prof. habil. Dr. Aivaras Kareiva, for his constructive guidance and words of motivation as well as relentless encouragement throughout the duration of this research study and moreover for the inspiration he provided to ensure the completion of this work. His expertise, availability to discuss ideas and willingness to give of his knowledge were of significant importance.

I would also like to thank my colleagues, especially the ones from sol- gel research group for their advices, support and continuous help. There is a great number of people (relatives, friends as well as colleagues from other academic institutions) who deserve an exceptional gratitude for their kind will and help to make this project happen by providing seashells from different Baltic regions.

Finally, special thanks to my family for all their love, understanding, patience and dedication.

8. LITERATURE REFERENCES

[1] Rao LG, Khan T, Gluck G. Calcium from LactoCalcium milk mineral after digestion with pepsin stimulates mineralized bone nodule formation in human osteoblast-like SaOS-2 cells in vitro and may be rendered bioavailable in vivo. Biosci Biotechnol Biochem. 2007;71:336-42.
[2] Muehrcke DD, Shimp WM, Aponte-Lopez R. Calcium Phosphate Cements Improve Bone Density When Used in Osteoporotic Sternums. The Annals of Thoracic Surgery. 2009;88:1658-61.
[3] Bonjour JP, Carrie AL, Ferrari S, Clavien H, Slosman D, Theintz G, et al. Calcium-enriched foods and bone mass growth in prepubertal girls: a randomized, double-blind, placebo-controlled trial. J Clin Invest. 1997;99:1287-94.
[4] Sharma SV, Hoelscher DM, Kelder SH, Diamond P, Day RS, Hergenroeder A. Psychosocial factors influencing calcium intake and bone quality in middle school girls. J Am Diet Assoc. 2010;110:932-6.
[5] Chan GM, McElligott K, McNaught T, Gill G. Effects of dietary calcium intervention on adolescent mothers and newborns: A randomized controlled trial. Obstet Gynecol. 2006;108:565-71.
[6] Lau EM, Woo J, Leung PC, Swaminathan R, Leung D. The effects of calcium supplementation and exercise on bone density in elderly Chinese women. Osteoporos Int. 1992;2:168-73.
[7] Meng X, Kerr DA, Zhu K, Devine A, Solah V, Binns CW, et al. Calcium intake in elderly Australian women is inadequate. Nutrients. 2010;2:1036-43.
[8] Lee YH, Lim YW, Ling PS, Tan YY, Cheong M, Lam KS. Inadequate dietary calcium intake in elderly patients with hip fractures. Singapore Med J. 2007;48:1117-21.
[9] Vargas-Zárate M, Becerra-Bulla F, Prieto-Suárez E. [Evaluating university students' dietary intake in Bogotá, Colombia]. Rev Salud Publica (Bogota). 2010;12:116-25.
[10] Ervin RB, Wang CY, Wright JD, Kennedy-Stephenson J. Dietary intake of selected minerals for the United States population: 1999-2000. Adv Data. 2004:1-5.
[11] Plawecki KL, Evans EM, Mojtahedi MC, McAuley E, Chapman-Novakofski K. Assessing calcium intake in postmenopausal women. Prev Chronic Dis. 2009;6:A124.
[12] Heaney RP. Calcium, dairy products and osteoporosis. J Am Coll Nutr. 2000;19:83S-99S.
[13] Committee to Review Dietary Reference Intakes for Vitamin D and Calcium FaNB, Institute of Medicine. Dietary Reference Intakes for Calcium and Vitamin D. Washington, DC: National Academy Press; 2010.
[14] Food and Nutrition Board IoM. Calcium. Dietary Reference Intakes: Calcium, Phosphorus, Magnesium, Vitamin D, and Fluoride. Washington, D.C.: National Academy Press; 1997.
[15] Weaver C, Heaney R. Calcium. In: Modern Nutrition in Health and Disease. 9th ed. Baltimore: Lippincott Williams & Wilkins; 1999. p. 141-55.
[16] Guéguen L, Pointillart A. The bioavailability of dietary calcium. J Am Coll Nutr. 2000;19:119S-36S.
[17] Wang Y, Li S. Worldwide trends in dairy production and consumption and calcium intake: is promoting consumption of dairy products a sustainable solution for inadequate calcium intake? Food Nutr Bull. 2008;29:172-85.
[18] Weaver CM, Heaney RP. Isotopic exchange of ingested calcium between labeled sources. Evidence that ingested calcium does not form a common absorptive pool. Calcif Tissue Int. 1991;49:244-7.

[19] Deladino L, S. Navarro A, N. Martino M. Microstructure of minerals and yerba mate extract co-crystallized with sucrose. Journal of Food Engineering. 2010;96:410-5.
[20] Ismaya WT, Rozeboom HJ, Weijn A, Mes JJ, Fusetti F, Wichers HJ, et al. Crystal structure of Agaricus bisporus mushroom tyrosinase: identity of the tetramer subunits and interaction with tropolone. Biochemistry. 2011;50:5477-86.
[21] Toda Y, Okada S, Misaka T. Establishment of a new cell-based assay to measure the activity of sweeteners in fluorescent food extracts. J Agric Food Chem. 2011;59:12131-8.
[22] Ukrainczyk M, Gredičak M, Jerić I, Kralj D. Interactions of salicylic acid derivatives with calcite crystals. J Colloid Interface Sci. 2012;365:296-307.
[23] Shea JE, Miller SC. Skeletal function and structure: implications for tissue-targeted therapeutics. Adv Drug Deliv Rev. 2005;57:945-57.
[24] Giannoudis PV, Dinopoulos H, Tsiridis E. Bone substitutes: an update. Injury. 2005;36 Suppl 3:S20-7.
[25] Walsh PJ, Buchanan FJ, Dring M, Maggs C, Bell S, Walker GM. Low-pressure synthesis and characterisation of hydroxyapatite derived from mineralise red algae. Chemical Engineering Journal. 2008;137:173-9.
[26] Hench LL, Polak JM. Third-generation biomedical materials. Science. 2002;295:1014-7.
[27] Tank KP, Sharma, P., Kanchan, D. K. and Joshi, M. J. FTIR, powder XRD, TEM and dielectric studies of pure and zinc doped nano-hydroxyapatite. Cryst Res Technol. 2011;46:1309–16.
[28] Vecchio KS, Zhang X, Massie JB, Wang M, Kim CW. Conversion of bulk seashells to biocompatible hydroxyapatite for bone implants. Acta Biomater. 2007;3:910-8.
[29] Hu J, Russell J, Ben-Nissan B, Vago R. Production and analysis of hydroxyapatite from Australian corals via hydrothermal process. Mater Sci Letters. 2001;20:85-7.
[30] Green D, Walsh D, Mann S, Oreffo ROC. The potential of biomimesis in bone tissue engineering: lessons from the design and synthesis of invertebrate skeletons. Bone. 2002;30:810-5.
[31] Kaplan DL. Mollusc shell structures: novel design strategies for synthetic materials. Current Opinion in Solid State and Materials Science. 1998;3:232-6.
[32] Behradmanesh S, Nasri H. Association of serum calcium with level of blood pressure in type 2 diabetic patients. J Nephropathol. 2013;2:254-7.
[33] Gopinath B, Flood VM, Wang JJ, Burlutsky G, Mitchell P. Lower dairy products and calcium intake is associated with adverse retinal vascular changes in older adults. Nutr Metab Cardiovasc Dis. 2014.
[34] Report of a WHO Study Group. Geneva WHO. Assessment of fracture risk and its application to screening for postmenopausal osteoporosis. WHO Technical Report Series, No. 843.
[35] Organization WH. The world health report 2004: changing history. Geneva2004.
[36] Moyer VA, Force* USPST. Vitamin D and calcium supplementation to prevent fractures in adults: U.S. Preventive Services Task Force recommendation statement. Ann Intern Med. 2013;158:691-6.
[37] Agency FS. The Composition of Foods, Sixth Summary Edition.: Cambridge: Royal Society of Chemistry; 2002.
[38] Albertson AM, Tobelmann RC, Marquart L. Estimated dietary calcium intake and food sources for adolescent females: 1980-92. J Adolesc Health. 1997;20:20-6.
[39] Straub DA. Calcium supplementation in clinical practice: a review of forms, doses, and indications. Nutr Clin Pract. 2007;22:286-96.

[40] Andon MB, Peacock M, Kanerva RL, De Castro JA. Calcium absorption from apple and orange juice fortified with calcium citrate malate (CCM). J Am Coll Nutr. 1996;15:313-6.
[41] Meneghini C, Dalconi MC, Nuzzo S, Mobilio S, Wenk RH. Rietveld refinement on x-ray diffraction patterns of bioapatite in human fetal bones. Biophysical journal. 2003;84:2021-9.
[42] WF dJ. La substance minerale dans les os.: Recl Trav Chim Pays – Bas Belg; 1926. p. 445–8.
[43] Rey C, Combes C, Drouet C, Glimcher MJ. Bone mineral: update on chemical composition and structure. Osteoporos Int. 2009;20:1013-21.
[44] Smith EL, Hill RL, Lehman IR, Lefkowitz RJ, Handler P, White A. Principles of Biochemistry: Mammalian Biochemistry, 7th ed. New York: McGraw-Hill Book Company; 1983.
[45] Liu Q, Huang S, Matinlinna JP, Chen Z, Pan H. Insight into biological apatite: physiochemical properties and preparation approaches. Biomed Res Int. 2013;2013:929748.
[46] Skinner H. Mineral and human health. In Environmental Mineralogy. EMU Notes in Mineralogy. Budapest: University Press; 2000. p. 383–412.
[47] Cannizzaro G, Felice P, Minciarelli AF, Leone M, Viola P, Esposito M. Early implant loading in the atrophic posterior maxilla: 1-stage lateral versus crestal sinus lift and 8 mm hydroxyapatite-coated implants. A 5-year randomised controlled trial. Eur J Oral Implantol. 2013;6:13-25.
[48] Stavropoulos A, Karring T. Guided tissue regeneration combined with a deproteinized bovine bone mineral (Bio-Oss) in the treatment of intrabony periodontal defects: 6-year results from a randomized-controlled clinical trial. J Clin Periodontol. 2010;37:200-10.
[49] Driessens FCM, Verbeeck RMH. Biominerals. CRC Press, Boca Raton; 1990. p. 179-209.
[50] Palmer LC, Newcomb CJ, Kaltz SR, Spoerke ED, Stupp SI. Biomimetic systems for hydroxyapatite mineralization inspired by bone and enamel. Chem Rev. 2008;108:4754-83.
[51] Vallet-Regí M. Biomimetic Nanoceramics in Clinical Use from Materials to Applications. UK: Royal Society of Chemistry, Cambridge, 1st edition; 2008.
[52] Weiner S, Wagner H. THE MATERIAL BONE: Structure-Mechanical Function Relations. 1998;28:271-98.
[53] Luz GM, Mano JF. Mineralized structures in nature: Examples and inspirations for the design of new composite materials and biomaterials. Composites Science and Technology. 2010;70:1777-88.
[54] Ritchie RO. The conflicts between strength and toughness. Nat Mater. 2011;10:817-22.
[55] Fernandez-Moran H, Engstrom A. Electron microscopy and X-ray diffraction of bone. Biochem Biophys Acta. 1957;23:260–3.
[56] Traub W, Arad T, Weiner S. Three-dimensional ordered distribution of crystals in turkey tendon collagen fibers. Proc Natl Acad Sci U S A. 1989;86:9822-6.
[57] Feng JQ, Ward LM, Liu S, Lu Y, Xie Y, Yuan B, et al. Loss of DMP1 causes rickets and osteomalacia and identifies a role for osteocytes in mineral metabolism. Nature Genetics. 2006;38:1310-5.
[58] Olszta MJ CX, Jee SS, Kumar R, Kim YY, Kaufman MJ, Douglas EP, Gower LB. Bone structure and formation: A new perspective. 2007;58:77–116.

[59] Burger C, Zhou HW, Wang H, Sics I, Hsiao BS, Chu B, et al. Lateral packing of mineral crystals in bone collagen fibrils. Biophys J. 2008;95:1985-92.
[60] Fonseca J. Bone biology: from macrostructure to gene expression. Medicographia. 2012;34:142-8.
[61] Weiner S, Addadi L. Design strategies in mineralized biological materials. Journal of Materials Chemistry. 1997;7:689-702.
[62] Mayya A, Banerjee A, Rajesh R. Mammalian cortical bone in tension is non-Haversian. Sci Rep2013.
[63] Posner AS. The mineral of bone. Clin Orthop Relat Res. 1985:87-99.
[64] Currey JD. The design of mineralised hard tissues for their mechanical functions. J Exp Biol. 1999;202:3285-94.
[65] Fratzl P, Gupta HS, Paschalis EP, Roschger P. Structure and mechanical quality of the collagen-mineral nano-composite in bone. Journal of Materials Chemistry. 2004;14:2115-23.
[66] LeGeros RZ. Calcium Phosphate-Based Osteoinductive Materials. Chem Rev. 2008;108:4742-53.
[67] Kolmas J, Szwaja M, Kolodziejski W. Solid-state NMR and IR characterization of commercial xenogeneic biomaterials used as bone substitutes. 2012;61:136–41.
[68] Kuhn L, Grynpas M, Rey C, Wu Y, Ackerman J, Glimcher M. A Comparison of the Physical and Chemical Differences Between Cancellous and Cortical Bovine Bone Mineral at Two Ages. Calcified Tissue International. 2008;83:146-54.
[69] Elliott JC. Structure and Chemistry of the Apatites and Other Calcium Orthophosphates Amsterdam, The Netherlands: Elsevier, 1st edition; 1994.
[70] Nasser A.M. Barakat KAK, Faheem A. Sheikh, A.M. Omran, Babita Gaihre, Soeb M. Khil, Hak Yong Kim. Physiochemical characterizations of hydroxyapatite extracted from bovine bones by three different methods: Extraction of biologically desirable HAp. 2008;28:1381–7.
[71] Janus AM, Faryna M, Haberko K, Rakowska A, Panz T. Chemical and microstructural characterization of natural hydroxyapatite derived from pig bones. Microchimica Acta. 2008;161:349-53.
[72] Joscheka S, B N, R K, A G. Chemical and physicochemical characterization of porous hydroxyapatite ceramics made of natural bone. 2000;21:1645–58.
[73] Kim SH, Shin JW, Park SA, Kim YK, Park MS, Mok JM, et al. Chemical, structural properties, and osteoconductive effectiveness of bone block derived from porcine cancellous bone. J Biomed Mater Res B Appl Biomater. 2004;68:69-74.
[74] Joschek S, Nies B, Krotz R, Göpferich A. Chemical and physicochemical characterization of porous hydroxyapatite ceramics made of natural bone. Biomaterials. 2000;21:1645-58.
[75] Boanini E, M G, A B. Ionic substitutions in calcium phosphates synthesized at low temperature. 2010;6:1882–94.
[76] García F, Ortega A, Domingo JL, Corbella J. ACCUMULATION OF METALS IN AUTOPSY TISSUES OF SUBJECTS LIVING IN TARRAGONA COUNTY, SPAIN. J ENVIRON SCI HEALTH. 2001;A(36):1767–86.
[77] Carlisle EM. Silicon: a possible factor in bone calcification. Science. 1970;167:279-80.
[78] Roschger P MB, Klaushofer K. The complexity and heterogeneity of bone material. Medicographia. 2012;34:155-62.
[79] Hulmes DJ. Building collagen molecules, fibrils, and suprafibrillar structures. J Struct Biol. 2002;137:2-10.

[80] Maria Fátima Vaz HCoaJoEF. Advances in Composite Materials - Analysis of Natural and Man-Made Materials. Bone: a composite natural material Composite Materials: InTech; 2011. p. 195-228.
[81] Feron J. An architect's dream: a self-repairing structure. Medicographia. 2012;34:185-90.
[82] Rho JY, Tsui TY, Pharr GM. Elastic properties of human cortical and trabecular lamellar bone measured by nanoindentation. Biomaterials. 1997;18:1325-30.
[83] Caetano-Lopes J, Nery AM, Canhao H, Duarte J, Cascao R, Rodrigues A, et al. Chronic arthritis leads to disturbances in the bone collagen network. Arthritis Res Ther. 2010;12:R9.
[84] Marie P, Debiais F, Cohen-Solal M, de Vernejoul MC. New factors controlling bone remodeling. Joint Bone Spine. 2000;67:150-6.
[85] Marie J. Bone remodeling: a social network of cells. Medicographia. 2012;34:149-54.
[86] Lajeunes se D, Pelletier J, Martel -Pelletier J. Osteoporosis and osteoarthritis: bone is the common battleground. Medicographia. 2010;32:391-8.
[87] Karsenty G, Oury F. The central regulation of bone mass, the first link between bone remodeling and energy metabolism. J Clin Endocrinol Metab. 2010;95:4795-801.
[88] Giustina A, Mazziotti G, Canalis E. Growth hormone, insulin-like growth factors, and the skeleton. Endocr Rev. 2008;29:535-59.
[89] PJ M. Bone cell-matrix protein interactions. Osteoporos Int. 2009;20:1037-42.
[90] Rodan GA, Martin TJ. Role of osteoblasts in hormonal control of bone resorption--a hypothesis. Calcif Tissue Int. 1981;33:349-51.
[91] Sims NA, Gooi JH. Bone remodeling: Multiple cellular interactions required for coupling of bone formation and resorption. Semin Cell Dev Biol. 2008;19:444-51.
[92] Malmberg P, Nygren H. Methods for the analysis of the composition of bone tissue, with a focus on imaging mass spectrometry (TOF-SIMS). Proteomics. 2008;8:3755-62.
[93] Batchelar DL, Davidson MT, Dabrowski W, Cunningham IA. Bone-composition imaging using coherent-scatter computed tomography: assessing bone health beyond bone mineral density. Med Phys. 2006;33:904-15.
[94] Chen D, Tang C, Chan K, etc. Dynamic mechanical properties and in vitro bioactivity of PHBHV/HA nanocomposite. 2007;67:1617–26.
[95] Chen L, McCrate JM, Lee JC, Li H. The role of surface charge on the uptake and biocompatibility of hydroxyapatite nanoparticles with osteoblast cells. Nanotechnology. 2011;22:105708.
[96] Pelin I, Maier S, Chitanu G, Bulacovschi V. Preparation and characterization of a hydroxyapatite–collagen composite as component for injectable bone substitute. 2009;29:2188–94.
[97] O'Hare P, Meenan BJ, Burke GA, Byrne G, Dowling D, Hunt JA. Biological responses to hydroxyapatite surfaces deposited via a co-incident microblasting technique. Biomaterials. 2010;31:515-22.
[98] Sadat-Shojai M, Khorasani MT, Dinpanah-Khoshdargi E, Jamshidi A. Synthesis methods for nanosized hydroxyapatite with diverse structures. Acta Biomater. 2013;9:7591-621.
[99] Elliott JC, Mackie PE, Young RA. Monoclinic hydroxyapatite. Science. 1973;180:1055-7.
[100] Ma G, Liu X. Hydroxyapatite: hexagonal or monoclinic? Crystal Growth and Design. 2009;9:2991–4.
[101] Misra A, Ching WY. Theoretical nonlinear response of complex single crystal under multi-axial tensile loading. Sci Rep. 2013;3.

[102] Kannan S, Goetz-Neunhoeffer F, Neubauer J, Ferreira JMF. Ionic Substitutions in Biphasic Hydroxyapatite and β-Tricalcium Phosphate Mixtures: Structural Analysis by Rietveld Refinement. Journal of the American Ceramic Society. 2008;91:1-12.
[103] Rivera-Muñoz EM. Hydroxyapatite-Based Materials: Synthesis and Characterization. Biomedical Engineering - Frontiers and Challenges: InTech; 2011.
[104] de Lima IR, Alves GG, Soriano CA, Campaneli AP, Gasparoto TH, Ramos ES, et al. Understanding the impact of divalent cation substitution on hydroxyapatite: an in vitro multiparametric study on biocompatibility. J Biomed Mater Res A. 2011;98:351-8.
[105] LeGeros RZ. Properties of osteoconductive biomaterials: calcium phosphates. Clin Orthop Relat Res. 2002:81-98.
[106] Hench L, J. An Introduction to Bioceramics. Adv Ser Ceram 1 World Scientific Publishing Co.Pte.Ltd; 1998. p. 139-80.
[107] Habibovic P, Kruyt MC, Juhl MV, Clyens S, Martinetti R, Dolcini L, et al. Comparative in vivo study of six hydroxyapatite-based bone graft substitutes. Journal of Orthopaedic Research. 2008;26:1363-70.
[108] Rabiee S, Moztarzadeh F, Solati-Hashjin M. Synthesis and characterization of hydroxyapatite cement. 2010;969:172–5.
[109] Dorozhkin SV, Epple M. Biological and Medical Significance of Calcium Phosphates. Angewandte Chemie International Edition. 2002;41:3130-46.
[110] Stefini R, Esposito G, Zanotti B, Iaccarino C, Fontanella MM, Servadei F. Use of "custom made" porous hydroxyapatite implants for cranioplasty: postoperative analysis of complications in 1549 patients. Surg Neurol Int. 2013;4:12.
[111] Hou CH, Hou SM, Hsueh YS, Lin J, Wu HC, Lin FH. The in vivo performance of biomagnetic hydroxyapatite nanoparticles in cancer hyperthermia therapy. Biomaterials. 2009;30:3956-60.
[112] Li J, Yin Y, Yao F, Zhang L, Yao K. Effect of nano- and micro-hydroxyapatite/chitosan-gelatin network film on human gastric cancer cells. 2008;62:3220–3.
[113] Venugopal A, Scurrell M. Hydroxyapatite as a novel support for gold and ruthenium catalysts: Behaviour in the water gas shift reaction. 2003;245:137–47.
[114] Boucetta C, Kacimi M. Oxidative dehydrogenation of propane over chromium-loaded calcium-hydroxyapatite. 2009;356:201–10.
[115] Gomez del Rio JA, Morando PJ, Cicerone DS. Natural materials for treatment of industrial effluents: comparative study of the retention of Cd, Zn and Co by calcite and hydroxyapatite. Part I: batch experiments. J Environ Manage. 2004;71:169-77.
[116] Lemlikchi W, Sharrock P, Mecherri MO, Fiallo M, Nzihou A. Treatment of Textile Waste Waters by Hydroxyapatite Co-Precipitation with Adsorbent Regeneration and Reuse. Waste and Biomass Valorization. 2012;3:75-9.
[117] Smiciklas I, Onjia A, Raicevic S, Janackovic D, Mitric M. Factors influencing the removal of divalent cations by hydroxyapatite. J Hazard Mater. 2008;152:876-84.
[118] Zhou H, Lee J. Nanoscale hydroxyapatite particles for bone tissue engineering. Acta Biomater. 2011;7:2769-81.
[119] Ivanchenko L, Pinchuk N. Making Calcium Phosphate Biomaterials. Powder Metallurgy and Metal Ceramics. 2003;42:357-71.
[120] Russell SW, Luptak KA, Suchicital CTA, Alford TL, Pizziconi VB. Chemical and Structural Evolution of Sol-Gel-Derived Hydroxyapatite Thin Films under Rapid Thermal Processing. Journal of the American Ceramic Society. 1996;79:837-42.
[121] Chai S, Gross K, Ben-Nissan B. Critical ageing of hydroxyapatite sol–gel solutions. 1998;19:2291–6.

[122] Liu DM, Troczynski T, Tseng WJ. Water-based sol-gel synthesis of hydroxyapatite: process development. Biomaterials. 2001;22:1721-30.
[123] Beganskiene A, Dudko O, Sirukaitis R, Giraitis R. Water-based sol–gel synthesis of hydroxyapatite. Materials Science. 2003;9:383-6.
[124] Anee Kuriakose T, NK, S, Palanichamy M, Arivuoli D, Dierks K, Bocelli G, et al. Synthesis of stoichiometric nano crystalline hydroxyapatite by ethanol-based sol–gel technique at low temperature. 2004;263:517–23.
[125] Han Y, Li S, Wang X, Chen X. Synthesis and sintering of nanocrystalline hydroxyapatite powders by citric acid sol-gel combustion method. Materials Research Bulletin. 2004;39:25-32.
[126] Velu G, Gopal B. Preparation of Nanohydroxyapatite by a Sol–Gel Method Using Alginic Acid as a Complexing Agent. Journal of the American Ceramic Society. 2009;92:2207-11.
[127] Guzman Vazquez C, Munguia N, PB, C. Stoichiometric hydroxyapatite obtained by precipitation and sol gel processes. Revista Mexicana de Fisica. 2005;51:284-93.
[128] Fathi M, Hanifi A, Mortazavi V. Preparation and bioactivity evaluation of bone-like hydroxyapatite nanopowder. 2008;202:536–42.
[129] Bogdanoviciene I, Beganskiene A, Tõnsuaadu K, Glaser J, Meyer HJ, Kareiva A. Calcium hydroxyapatite, Ca10(PO4)6(OH)2 ceramics prepared by aqueous sol–gel processing. Materials Research Bulletin. 2006;41:1754-62.
[130] Engin A, Girgin İ. Synthesis of hydroxyapatite by using calcium carbonate and phosphoric acid in various water-ethanol solvent systems. Central European Journal of Chemistry. 2009;7:745-51.
[131] Chen J, Wang Y, Chen X, Ren L, Lai C, He W, et al. A simple sol-gel technique for synthesis of nanostructured hydroxyapatite, tricalcium phosphate and biphasic powders. Materials Letters. 2011;65:1923-6.
[132] Gopi D, Govindaraju K, Victor C, Kavitha L, Rajendiran N. Spectroscopic investigations of nanohydroxyapatite powders synthesized by conventional and ultrasonic coupled sol–gel routes. Spectrochim Acta A: Mol Biomol Spectrosc. 2008;70:1243-5.
[133] Wang P, Li C, Gong H, Jiang X, Wang H, Li K. Effects of synthesis conditions on the morphology of hydroxyapatite nanoparticles produced by wet chemical process. Powder Technology - POWDER TECHNOL. 2010;203:315-21.
[134] Ferraz MP, Monteiro FJ, Manuel CM. Hydroxyapatite nanoparticles: A review of preparation methodologies. J Appl Biomater Biomech. 2004;2:74-80.
[135] Guo X, Yan H, Zhao S, Li Z, Li Y, Liang X. Effect of calcining temperature on particle size of hydroxyapatite synthesized by solid-state reaction at room temperature. 2013;24:1034–8.
[136] Pramanik S, Agarwal A, Rai K, Garg A. Development of high strength hydroxyapatite by solid-state-sintering process. 2007;33:419–26.
[137] Zhang C, Yang J, Quan Z, Yang P, Li C, Hou Z, et al. Hydroxyapatite nano-and microcrystals with multiform morphologies: controllable synthesis andluminescence properties. Cryst Growth Des. 2009;9:2725–33.
[138] Zhang H-b, Zhou K-c, Li Z-y, Huang S-p, Zhao Y-z. Morphologies of hydroxyapatite nanoparticles adjusted by organic additives in hydrothermal synthesis. Journal of Central South University of Technology. 2009;16:871-5.
[139] Nathanael AJ, Han SS, Oh TH. Polymer-Assisted Hydrothermal Synthesis of Hierarchically Arranged Hydroxyapatite Nanoceramic. Journal of Nanomaterials. 2013;2013:1-8.

[140] Wang A, Yin H, Liu D, Wu H, Ren M, Jiang T, et al. Size-controlled synthesis of hydroxyapatite nanorods in the presence of organic modifiers. 2007;61:2084–8.
[141] Wang X, Zhuang J, Peng Q, Li Y. Liquid–solid–solution synthesis of biomedical hydroxyapatite nanorods. Adv Mater. 2006;18:2031–4.
[142] Bose S, Dasgupta S, Tarafder S, Bandyopadhyay A. Microwave processed nanocrystalline hydroxyapatite: Simultaneous enhancement of mechanical and biological properties. Acta Biomater. 2010;6:3782-90.
[143] Dasgupta S, Tarafder S, Bandyopadhyay A, Bose S. Effect of grain size on mechanical, surface and biological properties of microwave sintered hydroxyapatite. 2013;33:2846–54.
[144] Fang Y, Agrawal DK, Roy DM, Roy R. Microwave sintering of hydroxyapatite ceramics. Journal of Materials Research. 1994;9:180-7.
[145] Tarafder S, Balla VK, Davies NM, Bandyopadhyay A, Bose S. Microwave-sintered 3D printed tricalcium phosphate scaffolds for bone tissue engineering. Journal of Tissue Engineering and Regenerative Medicine. 2013;7:631-41.
[146] Sanosh KP, Chu M-C, Balakrishnan A, Kim TN, Cho S-J. Utilization of biowaste eggshells to synthesize nanocrystalline hydroxyapatite powders. Materials Letters. 2009;63:2100-2.
[147] Giraldo-Betancur AL, Espinosa-Arbelaez DG, Real-López Ad, Millan-Malo BM, Rivera-Muñoz EM, Gutierrez-Cortez E, et al. Comparison of physicochemical properties of bio and commercial hydroxyapatite. Current Applied Physics. 2013;13:1383-90.
[148] Wu S, Tsou H, Hsu H, Hsu S, Liou S, Ho W. A hydrothermal synthesis of eggshell and fruit waste extract to produce nanosized hydroxyapatite. 2013;39:8183–8.
[149] Gergely G, Wéber F, Lukács I, Tóth AL, Horváth ZE, Mihály J, et al. Preparation and characterization of hydroxyapatite from eggshell. Ceramics International. 2010;36:803-6.
[150] Gergely G, Wéber F, Lukács I, Illés L, Tóth A, Horváth Z, et al. Nano-hydroxyapatite preparation from biogenic raw materials. Central European Journal of Chemistry. 2010;8:375-81.
[151] Siva Rama Krishna D, Siddharthan A, Seshadri SK, Sampath Kumar TS. A novel route for synthesis of nanocrystalline hydroxyapatite from eggshell waste. Journal of Materials Science: Materials in Medicine. 2007;18:1735-43.
[152] K. P, A. B, S. R. Development of calcium phosphate based apatite from hen's eggshell. Bulletin of Materials Science. 2005;28:115-9.
[153] Xu Y, Wang D, Yang L, Tang H. Hydrothermal conversion of coral into hydroxyapatite. Materials Characterization. 2001;47:83-7.
[154] Wu S-C, Hsu H-C, Wu Y-N, Ho W-F. Hydroxyapatite synthesized from oyster shell powders by ball milling and heat treatment. Materials Characterization. 2011;62:1180-7.
[155] M.K. H, Muzafar C, A.E. T. Natural Bioceramics Bone Graft: A Comparative Study of Calcite Hydroxyapatite, Gypsum Hydroxyapatit, Bovine Hydroxyapatite and Cuttlefish Shell Hydroxyapatite. Proceedings of the Asia Pacific Industrial Engineering & Management Systems Conference 2012: V. Kachitvichyanukul, H.T. Luong, and R. Pitakaso Eds.; 2012. p. 1137-46.
[156] Boutinguiza M, J. P, Comesaña R, Lusquiños F, Carlos A, León B. Biological hydroxyapatite obtained from fish bones. 2012;32:478–86.
[157] Huang Y-C, Hsiao P-C, Chai H-J. Hydroxyapatite extracted from fish scale: Effects on MG63 osteoblast-like cells. 2011;37:1825–31.

[158] Supova M, Martynkova GS, Sucharda Z. Bioapatite made from chicken femur bone. Ceramics Silikaty. 2011;55:256-60.
[159] Ooi CY, Hamdi M, Ramesh S. Properties of Hydroxyapatite Produced by Annealing of Bovine Bon. Ceramics International. 2007;33:1171-7.
[160] Shaltout AA, Allam MA, Moharram MA. FTIR spectroscopic, thermal and XRD characterization of hydroxyapatite from new natural sources. Spectrochim Acta A Mol Biomol Spectrosc. 2011;83:56-60.
[161] Nayar S, Guha A. Waste utilization for the controlled synthesis of nanosized hydroxyapatite. Materials Science and Engineering: C. 2009;29:1326-9.
[162] Oppenheimer AJ, Tong L, Buchman SR. Craniofacial Bone Grafting: Wolff's Law Revisited. Craniomaxillofac Trauma Reconstr. 2008;1:49-61.
[163] Kolk A, Handschel J, Drescher W, Rothamel D, Kloss F, Blessmann M, et al. Current trends and future perspectives of bone substitute materials - from space holders to innovative biomaterials. J Craniomaxillofac Surg. 2012;40:706-18.
[164] Sen MK, Miclau T. Autologous iliac crest bone graft: should it still be the gold standard for treating nonunions? Injury. 2007;38 Suppl 1:S75-80.
[165] Rupprecht S, Petrovic L, Burchhardt B, Wiltfang J, Neukam FW, Schlegel KA. Antibiotic-containing collagen for the treatment of bone defects. J Biomed Mater Res B Appl Biomater. 2007;83:314-9.
[166] Fischer J, Kolk A, Wolfart S, Pautke C, Warnke PH, Plank C, et al. Future of local bone regeneration - Protein versus gene therapy. J Craniomaxillofac Surg. 2011;39:54-64.
[167] Maus U, Andereya S, Gravius S, Ohnsorge JA, Niedhart C, Siebert CH. BMP-2 incorporated in a tricalcium phosphate bone substitute enhances bone remodeling in sheep. J Biomater Appl. 2008;22:559-76.
[168] Smeets R, Maciejewski O, Gerressen M, Spiekermann H, Hanisch O, Riediger D, et al. Impact of rhBMP-2 on regeneration of buccal alveolar defects during the osseointegration of transgingival inserted implants. Oral Surg Oral Med Oral Pathol Oral Radiol Endod. 2009;108:e3-e12.
[169] Handschel J, Berr K, Depprich R, Naujoks C, Kubler NR, Meyer U, et al. Compatibility of embryonic stem cells with biomaterials. J Biomater Appl. 2009;23:549-60.
[170] Naujoks C, Langenbach F, Berr K, Depprich R, Kubler N, Meyer U, et al. Biocompatibility of osteogenic predifferentiated human cord blood stem cells with biomaterials and the influence of the biomaterial on the process of differentiation. J Biomater Appl. 2011;25:497-512.
[171] Bauer TW, Geesink RC, Zimmerman R, McMahon JT. Hydroxyapatite-coated femoral stems. Histological analysis of components retrieved at autopsy. J Bone Joint Surg Am. 1991;73:1439-52.
[172] Poinern GE, Brundavanam RK, Mondinos N, Jiang ZT. Synthesis and characterisation of nanohydroxyapatite using an ultrasound assisted method. Ultrason Sonochem. 2009;16:469-74.
[173] Huang J, Best SM, Bonfield W, Brooks RA, Rushton N, Jayasinghe SN, et al. In vitro assessment of the biological response to nano-sized hydroxyapatite. J Mater Sci Mater Med. 2004;15:441-5.
[174] LeGeros RZ. Biodegradation and bioresorption of calcium phosphate ceramics. Clin Mater. 1993;14:65-88.
[175] Stupp SI, Ciegler GW. Organoapatites: materials for artificial bone. I. Synthesis and microstructure. J Biomed Mater Res. 1992;26:169-83.

[176] Orlovskii VP, Komlev VS, Barinov SM. Hydroxyapatite and Hydroxyapatite-Based Ceramics. Inorganic Materials. 2002;38:973-84.
[177] Suchanek W, Yoshimura M. Processing and properties of hydroxyapatite-based biomaterials for use as hard tissue replacement implants. Journal of Materials Research. 1998;13:94-117.
[178] de Putter C, de Groot K, Smitt PAES. Transmucosal implants of dense hydroxylapatite. The Journal of prosthetic dentistry. 1983;49:87-95.
[179] Denissen HW, Groot Kd. Immediate dental root implants from synthetic dense calcium hydroxylapatite. The Journal of prosthetic dentistry. 1979;42:551-6.
[180] De Lange GL, De Putter C, De Groot K, Burger EH. A clinical, radiographic, and histological evaluation of permucosal dental implants of dense hydroxylapatite in dogs. J Dent Res. 1989;68:509-18.
[181] Ogiso M, Yamashita Y, Matsumoto T. The process of physical weakening and dissolution of the HA-coated implant in bone and soft tissue. J Dent Res. 1998;77:1426-34.
[182] Driessens F, R V. Relation between Physico - Chemical Solubility and Biodegrability of Calcium Phosphates. In: de Putter C dLG, de Groot K, Lee AJC, editor. Implant materials in biofunction Advances in Biomaterials. Amsterdam: Elsevier; 1998. p. 48-52.
[183] Bell L, Mika H, BJ K. Synthetic hydroxyapatite-solubility product and stoichiometry of dissolution. 1978;23:329–36.
[184] Gross KA, Berndt CC. Thermal processing of hydroxyapatite for coating production. Journal of Biomedical Materials Research. 1998;39:580-7.
[185] Kuroda K, Okido M. Hydroxyapatite Coating of Titanium Implants Using Hydroprocessing and Evaluation of Their Osteoconductivity. Bioinorg Chem Appl. 2012;2012:1-7.
[186] Lazic S, Zec S, Miljevic N, Milojnic S. The effect of Temperature on the Properties of Hydroxyapatite Precipitated from Calcium Hydroxide and Phosphoric Acid. 2001:13-22.
[187] Gayathri S, Lakshminarayanan R, Weaver JC, Morse DE, Kini RM, Valiyaveettil S. In vitro study of magnesium-calcite biomineralization in the skeletal materials of the seastar Pisaster giganteus. Chemistry. 2007;13:3262-8.
[188] Gunasekaran S, Anbalagan G, Pandi S. Raman and infrared spectra of carbonates of calcite structure. Journal of Raman Spectroscopy. 2006;37:892-9.
[189] Gunasekaran S, Anbalagan G. Spectroscopic characterization of natural calcite minerals. Spectrochim Acta A Mol Biomol Spectrosc. 2007;68:656-64.
[190] Rodrigues CVM, Serricella P, Linhares ABR, Guerdes RM, Borojevic R, Rossi MA, et al. Characterization of a bovine collagen–hydroxyapatite composite scaffold for bone tissue engineering. Biomaterials. 2003;24:4987-97.
[191] Gadaleta SJ, Camacho NP, Mendelsohn R, Boskey AL. Fourier transform infrared microscopy of calcified turkey leg tendon. Calcif Tissue Int. 1996;58:17-23.
[192] Landi E, Logroscino G, Proietti L, Tampieri A, Sandri M, Sprio S. Biomimetic Mg-substituted hydroxyapatite: from synthesis to in vivo behaviour. J Mater Sci Mater Med. 2008;19:239-47.
[193] Gibson IR, Bonfield W. Novel synthesis and characterization of an AB-type carbonate-substituted hydroxyapatite. J Biomed Mater Res. 2002;59:697-708.
[194] Zairin N. Nanohydroxyapatite Application to Osteoporosis Management. Journal of Osteoporosis. 2013;2013.
[195] Pouliot Y, Landry J, Giasson J. Induction of calcium phosphate precipitation in sweet whey permeate. Lait. 1991;71:313-20.

[196] Diallo-Garcia S, Laurencin D, Krafft J-M, Casale S, Smith ME, Lauron-Pernot H, et al. Influence of Magnesium Substitution on the Basic Properties of Hydroxyapatites. The Journal of Physical Chemistry C. 2011;115:24317-27.
[197] Kohutová A, Honcová P, Svoboda L, Bezdička P, Maříková M. Structural characterization and thermal behaviour of biological hydroxyapatite. Journal of Thermal Analysis and Calorimetry. 2012;108:163-70.
[198] Suchanek WL, Byrappa K, Shuk P, Riman RE, Janas VF, TenHuisen KS. Preparation of magnesium-substituted hydroxyapatite powders by the mechanochemical-hydrothermal method. Biomaterials. 2004;25:4647-57.
[199] Ou-Yang H, Paschalis EP, Boskey AL, Mendelsohn R. Two-dimensional vibrational correlation spectroscopy of in vitro hydroxyapatite maturation. Biopolymers. 2000;57:129-39.
[200] Koutsopoulos S. Synthesis and characterization of hydroxyapatite crystals: a review study on the analytical methods. J Biomed Mater Res. 2002;62:600-12.
[201] Mir M, Leite FL, Herrmann Junior PSdP, Pissetti FL, Rossi AM, Moreira EL, et al. XRD, AFM, IR and TGA study of nanostructured hydroxyapatite. Materials Research. 2012;15:622-7.
[202] Thulin J, Andrushaitis A. The Baltic Sea: Its Past, Present and Future. Religion, Science and the Environment Symposium V on the Baltic Sea2003.
[203] Schwarzer K. Field trip along the Baltic Sea coastline. The 3rd joint IGCP588 / INQUA 1001 conference. Christian-Albrechts-University Kiel2012.
[204] Schwarzer K, Ricklefs K, Bartholomä A, Zeiler M. Geological development of the North Sea and the Baltic Sea. Die Küste. 2008;74:1-17.
[205] Seifert TT, F., Kayser B. A high resolution Spherical Grid topography oft the Baltic Sea – 2nd edition. Baltic Science Congress, Stockholm 25 – 29, November2001.
[206] Corell H, Döös K. Difference in Particle Transport Between Two Coastal Areas in the Baltic Sea Investigated with High-Resolution Trajectory Modeling. AMBIO. 2013;42:455-63.
[207] Kamba AS, Ismail M, Ibrahim T, Zakaria Z. Synthesis and characterisation of calcium carbonate aragonite nanocrystals from cockle shell powder (anadara granosa). J Nanomaterials. 2013;2013 1-9.
[208] Wang Y, Moo YX, Chen C, Gunawan P, Xu R. Fast precipitation of uniform CaCO3 nanospheres and their transformation to hollow hydroxyapatite nanospheres. J Colloid Interface Sci. 2010;352:393-400.
[209] Linga Raju C, Narasimhulu KV, Gopal NO, Rao JL, Reddy BCV. Electron paramagnetic resonance, optical and infrared spectral studies on the marine mussel Arca burnesi shells. Journal of Molecular Structure. 2002;608:201-11.
[210] Vongsavat V, Winotai P, Meejoo S. Phase transitions of natural corals monitored by ESR spectroscopy. Nuclear Instruments and Methods in Physics Research B. 2006;243:167-73.
[211] Cheng B, Cai W, Yu J. DNA-mediated morphosynthesis of calcium carbonate particles. J Colloid Interface Sci. 2010;352:43-9.
[212] Reyes-Gasga J, Martinez-Pineiro EL, Rodriguez-Alvarez G, Tiznado-Orozco GE, Garcia-Garcia R, Bres EF. XRD and FTIR crystallinity indices in sound human tooth enamel and synthetic hydroxyapatite. Mater Sci Eng C Mater Biol Appl. 2013;33:4568-74.
[213] Le NTV, Richardson DR. Iron chelators with high antiproliferative activity up-regulate the expression of a growth inhibitory and metastasis suppressor gene: a link between iron metabolism and proliferation. Blood. 2004;104:2967-75.

[214] Jain TK, Reddy MK, Morales MA, Leslie-Pelecky DL, Labhasetwar V. Biodistribution, clearance, and biocompatibility of iron oxide magnetic nanoparticles in rats. Mol Pharm. 2008;5:316-27.
[215] Prijic S, Scancar J, Romih R, Cemazar M, Bregar VB, Znidarsic A, et al. Increased cellular uptake of biocompatible superparamagnetic iron oxide nanoparticles into malignant cells by an external magnetic field. J Membr Biol. 2010;236:167-79.
[216] Sun C, Du K, Fang C, Bhattarai N, Veiseh O, Kievit F, et al. PEG-mediated synthesis of highly dispersive multifunctional superparamagnetic nanoparticles: their physicochemical properties and function in vivo. ACS Nano. 2010;4:2402-10.
[217] Ajeesh M, Francis BF, Annie J, Harikrishna Varma PR. Nano iron oxide-hydroxyapatite composite ceramics with enhanced radiopacity. J Mater Sci Mater Med. 2010;21:1427-34.
[218] Motoyama J, Yamashita N, Morino T, Tanaka M, Kobayashi T, Honda H. Hyperthermic treatment of DMBA-induced rat mammary cancer using magnetic nanoparticles. Biomagn Res Technol. 2008;6:1-6.
[219] Kalambur VS, Han B, Hammer BE, Shield TW, Bischof JC. In vitro characterization of movement, heating and visualization of magnetic nanoparticles for biomedical applications. Nanotechnology. 2005;16:1221-33.
[220] Mornet S, Vasseur S, Grasset F, Duguet E. Magnetic nanoparticle design for medical diagnosis and therapy. Journal of Materials Chemistry. 2004;14:2161-75.
[221] Amirfazli A. Nanomedicine: magnetic nanoparticles hit the target. Nat Nanotechnol. England2007. p. 467-8.
[222] Buyukhatipoglu K, Chang R, Sun W, Clyne AM. Bioprinted nanoparticles for tissue engineering applications. Tissue Eng Part C Methods. 2010;16:631-42.
[223] Kim K, Fisher JP. Nanoparticle technology in bone tissue engineering. J Drug Target. 2007;15:241-52.
[224] Abraham R, Walton J, Russell L, Wolman R, Wardley-Smith B, Green JR, et al. Dietary determinants of post-menopausal bone loss at the lumbar spine: a possible beneficial effect of iron. Osteoporos Int. 2006;17:1165-73.
[225] Harris MM, Houtkooper LB, Stanford VA, Parkhill C, Weber JL, Flint-Wagner H, et al. Dietary iron is associated with bone mineral density in healthy postmenopausal women. J Nutr. 2003;133:3598-602.
[226] Parelman M, Stoecker B, Baker A, Medeiros D. Iron restriction negatively affects bone in female rats and mineralization of hFOB osteoblast cells. Exp Biol Med (Maywood). 2006;231:378-86.
[227] Pareta RA, Taylor E, Webster TJ. Increased osteoblast density in the presence of novel calcium phosphate coated magnetic nanoparticles. Nanotechnology. 2008;19:265101.
[228] Kanchana P, Lavanya N, Sekar C. Development of amperometric L-tyrosine sensor based on Fe-doped hydroxyapatite nanoparticles. Mater Sci Eng C Mater Biol Appl. 2014;35:85-91.
[229] Khachani M, Kacimi M, Ensuque A, Piquemal J-Y, Connan C, Bozon-Verduraz F, et al. Iron–calcium–hydroxyapatite catalysts: Iron speciation and comparative performances in butan-2-ol conversion and propane oxidative dehydrogenation. Applied Catalysis A: General. 2010;388:113-23.